Seton Hall University

eRepository @ Seton Hall

Fluorescence-Based Techniques for the Identification of Small Biomolecules

Charnette Frederic
charnette.frederic@student.shu.edu

Fluorescence-Based Techniques for the Identification of Small Biomolecules

Charnette Frederic

A thesis submitted in conformity with the requirements for the degree of Doctor of Philosophy.

Seton Hall University

Department of Chemistry and Biochemistry

South Orange, NJ

2024

Abstract

Understanding fluorescence-based methods for detecting small biomolecules is a crucial area of focus in research investigations. Our studies focused on the challenge in two parts: Non-intrinsic fluorescence and intrinsic fluorescence. For studies on Non-intrinsic fluorescence, Rifampicin (Rif), an antibiotic harnessed for treating diverse bacterial infections, including tuberculosis (TB), serves as a focal point. Leveraging the Systematic Evolution of Ligands by Exponential Enrichment (SELEX) process, aptamers emerged from the nonspecific 40-mer Deoxyribonucleic Acid (DNA) library to interact with its target, Rif. During each SELEX cycle, the recovered nucleotides underwent amplification via Polymerase Chain Reaction (PCR) until the most selective aptamers were found. The core objectives of this study encompassed the discovery of aptamers targeting Rifampicin and the comprehension of their binding efficacy to Rif.

For intrinsic small-molecule fluorescence, photo-switchable molecules were explored to investigate the interaction between the azobenzene moiety and neighboring aromatic amino acids tryptophan. Under 365 nm irradiation, the photo-switching behavior favored a singular isomer, which is red-shifted or visibly fluorescent. This is the first evidence to suggest that primary protein structure could affect photo-switch activity. The insights from this investigation can potentially advance the understanding of photo-switch molecules within biomolecules.

Keywords: Aptamers, Rifampicin, SELEX, Azobenzene, Tryptophan, Intrinsic, non-intrinsic, peptide, photocontrol

Acknowledgments

I want to express my gratitude to the many individuals who have supported me throughout my Ph.D. journey. Without their help, encouragement, and guidance, I would not have been able to complete this project. First and foremost, I would like to thank my advisor, Dr. Gregory Wiedman, for his unwavering support, guidance, and mentorship. His expertise, feedback, and encouragement have been invaluable to me throughout my research. His dedication to my success has been instrumental in completing my Ph.D.

I would also like to thank the members of 3B Lab for their insightful comments and suggestions on my work. Their expertise and feedback have been essential to the success of this project. The collaborative environment fostered in the lab allowed me to learn and grow. I am also grateful to the staff and faculty of the Chemistry and Biochemistry Department of Seton Hall University for their support and resources, which have made this research possible. I would like to acknowledge the research that Dr. Cristina Ventura did in the lab, which inspired me to come up with valuable data.

I would like to thank my family and friends for their encouragement and support throughout this journey. Their support and love have kept me motivated and focused on my goals. I want to thank my dad and mom, who believe in education and instilled this value within me. I am grateful to my son, Ben, for being a constant source of inspiration and motivation throughout my Ph.D. journey. As a mother, it was important for me to show him that with hard work and persistence, anything is possible. I often shared my struggles and triumphs with him. I want to express my gratitude to my husband, Betissan, who has constantly supported me throughout this journey.

Table of Contents

List of Figures

Content   **Page**

Appendix A. SELEX Data Figures

Appendix B. Additional peptides Figures

List of Tables

Appendix A. SELEX Data Tables

Appendix B. Additional Peptides Tables

Abbreviations

Abbreviation	Meaning
A	3'-deoxyadenine
Å	Angstroms
ACN	Acetonitrile
AmB	Amphotericin B
AW	L-alanyl-L-tryptophan
AZ	4-(phenylidazenyl)(benzoyl)-L-alanine
BSA	Bovine Serum Albumin
DCC	Dicyclohexylcarbodiimide
DCM	Dichloromethane
DIEA	N,N-diisopropylethylamine
DMF	N,N-Dimethylformamide
DMSO	Dimethyl Sulfoxide
DNA	Deoxyribonucleic acid
dsDNA	Double-stranded DNA
EDTA	Ethylene diamine tetraacetic acid
ELISA	Enzyme-Linked Immunosorbent Assay
EtBr	Ethidium bromide
FA	Formic acid
FITC	Fluorescein isothiocyanate
FMOC	9-fluorenylmethyloxycarbonyl
GO	Graphene Oxide
HCl	Hydrochloric acid
HCTU	Hexafluorophosphate Cyanuric acid Tetramethyl Uronium
HIV	Human Immunodeficiency Virus
HPLC	High pressure liquid chromatography
ICT	Intramolecular charge transfer
IDT	Integrated DNA Technologies
Kd	Dissociation constant
LC-MS/MS	Liquid Chromatography-Mass Spectrometry

NMR	Nuclear Magnetic Resonance
MeOH	Methanol
M. tuberculosis	Mycobacterium tuberculosis
MIC	Minimum inhibitory concentration
MSD	Mass Selective Detector
m/z	Mass to charge ratio
N_2	Nitrogen gas
nm	Nanometers
NMR	Nuclear Magnetic Resonance
ODS	Octadecyl Silane
PCR	Polymerase Chain Reaction
PDA	Photo Diode Array
PET	Photoinduced electron transfer
pH	Potential of hydrogen
QCM	Quartz crystal microbalance
qPCR	Quantitative Polymerase Chain Reaction
RFU	Relative Fluorescence Unit
Rif	Rifampicin
Rif_3_Fluor	Fluorescein isothiocyanate labeled Rifampicin
RNA	Ribonucleic acid
rpm	Revolutions per minute
SARS-CoV-2	Severe Acute Respiratory Syndrome Coronavirus 2
SELEX	Systematic Evolution of Ligands by Exponential Enrichment
S.O.C.	Super Optimal Broth with Catabolite
SPPS	Solid-phase peptide synthesis
SPR	Surface plasmon resonance
ssDNA	Single-stranded deoxyribonucleic acid
T	3'-thymine
TB	Tuberculosis
TBE	Tris-Borate-EDTA
TDM	Therapeutic Drug Monitoring

TES	Triethoxysilane
TFA	Trifluoroacetic Acid
TOPO TA	Thymine Overhangs and Tailing Addition, the PCR product is treated with Taq DNA polymerase with 3'-deoxyadenine (A), and the vector used contains complementary 3'-thymine (T) overhangs
UV	Ultraviolet
UV-VIS	Ultra-violet visible spectroscopy
V	Volt
v/v	Volume/volume
W	Tryptophan
WZ	4-(phenylidazenyl)(benzoyl)-L-tryptophan
Z	4-(Phenylazo)benzoic acid
$\epsilon\lambda$	Extinction coefficient

Chapter 1. Introduction

1.1. Non-Intrinsic Fluorescence

Non-intrinsic fluorescence involves the use of fluorescent markers or probes that are introduced into the biological system. These markers can be organic dyes, quantum dots, or other fluorophores. When exposed to specific wavelengths of light, these markers absorb photons and re-emit them at longer wavelengths, producing fluorescence[1]. The optical characteristics of organic dyes arise from conjugated π-electron systems within their molecular structures[2]. This conjugation involves alternating single and double bonds along the carbon backbone, creating a delocalized electron system. This arrangement leads to distinctive electronic transitions that give rise to the absorption and emission of light. The presence of functional groups attached to the conjugated π-electron systems in organic dyes can substantially impact their optical properties[3]. Additionally, this functional group introduces the potential for free rotation around single bonds, and this dynamic molecular motion has a distinct impact on the emission behavior of these dyes.

Modification of the molecular structure of organic dyes enables the tuning of their absorption and emission wavelengths. This tunability is achieved by altering the length of the conjugated system, introducing different functional groups, or changing the overall chemical structure[4]. As a result, a diverse range of colors can be obtained, allowing for the customization of dyes to match the specific requirements of various applications. These dyes' absorption and emission wavelengths can be tuned by modifying their molecular structure, allowing for a broad spectrum of colors. Non-intrinsic fluorescence dyes were examined to enhance our comprehension of aptamers. They are short, single-stranded nucleic acid molecules that bind to specific target molecules with high affinity and specificity, similar to antibodies. One of these investigated dyes was OliGreen.

Over the years, a significant effort has been made to develop non-isotopic labeling methods as alternatives to radioactive labels in deoxyribonucleic acid (DNA) probe-based assays[5]. OliGreen dye is a proprietary nucleic acid-binding dye developed by Molecular Probes, a division of Thermo Fisher Scientific. OliGreen, utilized in molecular biology and nucleic acid research, exhibits a distinctive selectivity for single-stranded DNA (ssDNA)[6]. OliGreen dye is known for its sensitivity and high fluorescence, making it suitable for various assays, including quantification of Polymerase Chain Reaction (PCR) or Quantitative Polymerase Chain Reaction (qPCR) products, DNA concentration measurement, and nucleic acid staining[7–9].

One characteristic of OliGreen dye is its non-intrinsic fluorescence, which exhibits enhanced fluorescence upon binding to DNA[10]. This feature facilitates the detection of nucleic acids, making it a valuable tool in various applications. OliGreen dye is employed in conjunction with fluorescence-based instruments, such as a fluorometer, to measure the fluorescence intensity emitted by the dye when bound to DNA. it exhibits fluorescence emission at approximately 525 nm when excited at 480 nm in the presence of ssDNA sequences rich in thymine (T) or guanine (G) bases[11]. The resulting fluorescence signal is then correlated with the concentration of DNA in the sample.

1.2. Fluorescently Labeled Aptamers

Aptamers are short, single-stranded DNA or RNA molecules selected in vitro for their high affinity and specificity toward a target molecule. The process of Systematic Evolution of Ligands by EXponential enrichment (SELEX) enables the generation of aptamers that can bind to a diverse array of targets, ranging from small molecules to proteins[12]. Initially, a pool of 40-mer ssDNA molecules is obtained. This pool undergoes binding and selection with the target molecule,

Rifampicin (Rif), where sequences that bind to the target are retained while non-binding sequences are removed. The bound aptamers are then isolated and amplified through PCR technique, generating an enriched pool for subsequent rounds. Successive rounds of selection further enhance the affinity and specificity of the aptamers by increasing selection stringency using Amphotericin B (AmB). After multiple rounds, individual aptamer sequences are identified, characterized, and used for further evaluation. The principles underlying aptamer technology form the foundation for the design and application of fluorescently labeled aptamers. Fluorescently labeled aptamers leverage various labeling strategies to integrate fluorophores without compromising their binding affinity[13]. These strategies include direct chemical conjugation, where fluorophores are attached to specific positions on the aptamer sequence, and indirect labeling of the modified nucleotides[14].

Fluorescently labeled aptamers can selectively recognize and bind to specific biomolecules, including proteins, nucleic acids, and small molecules. This specificity forms the basis for sensitive biosensors, where the binding event triggers a fluorescence signal. The high specificity of aptamers ensures minimal interference from nonspecific molecules, enhancing the accuracy and reliability of biosensing platforms[15]. The binding properties of fluorescently labeled aptamers make them well-suited for point-of-care diagnostics. These aptamer-based assays can be designed for on-site testing, providing real-time results without sophisticated laboratory equipment. An effective selection strategy becomes necessary to optimize aptamer screening[16]. As a result, a thorough analysis of critical elements within the SELEX process encompasses aspects like the design of the initial library, screening procedures, and post-screening steps, such as truncation and modification. This examination aims to identify potential challenges at each stage of SELEX.

Since the discovery of azobenzene's isomerization in 1937, it has emerged as a highly promising and versatile compound, showcasing tremendous potential across a spectrum of applications[17]. Azobenzene serves as a building block for light-driven molecular configurations, where controlled motion or mechanical responses are induced by light. Researchers have created photoresponsive switches by integrating azobenzene units into the architecture of molecular structures. These light-driven molecular structures have implications for nanotechnology and the development of responsive materials[18]. Azobenzene has the capacity for reversible cis–trans isomerization when subjected to photo-irradiation at specific wavelengths[19]. This inherent ability makes azobenzene an invaluable tool in molecular structures, thereby enabling a myriad of practical applications[20].

Upon irradiation, the azobenzene molecule undergoes an exciting transformation, transitioning from its stable ground state to an unstable excited state. Azobenzene switches between the thermodynamically stable trans-state and the less stable cis-state. This reversible photoisomerization is the foundation for designing molecular switches, enabling control over molecular configurations with light stimuli. This process involves releasing energy, a phenomenon that paves the way for a return to the ground state through various intricate mechanisms. These mechanisms include excitation formation, intramolecular rotation of single bonds, internal transformation, intramolecular charge transfer (ICT), photoinduced electron transfer (PET), and photoinduced proton transfer, among other non-radiative transitions[18,21]. The culmination of these dynamic processes results in the emission of fluorescence or phosphorescence.

1.3. Intrinsic Fluorescence

Intrinsic fluorescence is the natural fluorescence exhibited by certain molecules, particularly biomolecules such as proteins, without adding external fluorophores. This

phenomenon arises from the inherent fluorescence properties of certain aromatic amino acid residues, such as tryptophan, tyrosine, and phenylalanine. Intrinsic fluorescence is commonly observed in biomolecules due to aromatic amino acids[22]. Tryptophan is especially important in this context because it has an indole ring that exhibits strong intrinsic fluorescence when exposed to ultraviolet (UV) light[23]. Its indole ring contains a conjugated of double bonds, allowing it to absorb UV light at wavelengths around 280 nanometers (nm)[24], and providing valuable insights into the structure and dynamics of biomolecules[25]. Therefore, tryptophan fluorescence is characterized by an emission peak around 350-355 nm upon excitation at approximately 280 nm[26].

Rather than relying on external fluorophores or nanomaterial probes, the intrinsic fluorescence of biomolecules can be harnessed for the straightforward and non-destructive identification of biological materials[27]. Unique photophysical properties of fluorescent amino acids make it possible to track protein-protein interactions and observe high-resolution nanoscopic events.[28] This intrinsic fluorescence is highly sensitive to the tryptophan microenvironment within a protein[29]. Factors such as solvent exposure, local pH, and interactions with neighboring amino acid residues can influence the fluorescence intensity and emission spectrum[30]. Tryptophan fluorescence's intensity and spectral characteristics are highly sensitive to its local environment, making it a valuable probe for monitoring conformational changes, ligand binding, and interactions within proteins[31][32]. As a result, intrinsic fluorescence is a valuable tool for probing the structural and environmental changes in biomolecules[33].

The fluorescence of tryptophan has been extensively used in studying protein structure and folding[34]. By monitoring changes in tryptophan fluorescence spectra, researchers gain insights into alterations in the microenvironment around tryptophan residues, providing information about protein conformation, stability, and folding kinetics[35]. This has proven particularly valuable in

understanding the dynamics of biomolecular processes[36]. Tryptophan fluorescence is sensitive to the binding of ligands or the occurrence of molecular interactions. Changes in fluorescence intensity, peak wavelength, or fluorescence anisotropy indicate ligand binding or alterations in the protein's environment. This property has been widely exploited to study enzyme-substrate interactions, receptor-ligand binding, and other biomolecular interactions[37].

1.4. Purpose of Study

This study explores the dual facets of fluorescence, unraveling the principles and applications of both intrinsic fluorescence found in biomolecules and the non-intrinsic fluorescence exhibited by photoresponsive molecules such as azobenzene. The investigation spans from understanding the innate fluorescence of biomolecules to engineering molecular switches and responsive materials using azobenzene. Consequently, for Aim 1, we utilized the SELEX process to develop a Rif-binding aptamer. For Aim 2, we conducted testing and validation of the Rif-binding aptamer, and for Aim 3, we synthesized a visibly fluorescent peptide using azobenzene and the aromatic amino acid tryptophan. By bridging these realms, we seek to understand synergies that could open new avenues for advanced sensing, imaging, and materials science applications.

Exploring non-intrinsic and intrinsic fluorescence captures the journey of photoresponsive molecules, revealing a dynamic interplay between natural and engineered fluorescence. Intrinsic fluorescence, an inherent characteristic of biomolecules like aromatic amino acids and fluorescent proteins, serves as a luminescent signature within living systems, providing a means to unravel the intricacies of molecular structures and interactions. Chapter 2 explored the modulation of absorption and emission wavelengths of dyes through modifications in their molecular structure, enabling a diverse range of colors. The focus was on non-intrinsic fluorescence dyes to deepen our understanding of aptamers. Within this exploration, special attention was given to examining

OliGreen as one of the investigated dyes. The SELEX process progressed through multiple rounds as the aptamer pool became enriched with sequences that exhibited a higher affinity for the target, Rifampicin. The aptamers obtained demonstrate characteristics that make them potential candidates for further analysis and set the stage for a more comprehensive exploration of their potential applications in scientific and medical contexts in Chapter 3. On the other hand, azobenzene, a synthetic molecule, introduces an intriguing twist to this narrative by showcasing non-intrinsic fluorescence through its remarkable reversible cis-trans isomerization induced by light. This unique property positions azobenzene as a molecular switch, where the molecule toggles between two distinct conformations in response to specific wavelengths of light. Chapter 4 examined the structure and function of peptides regulated by azobenzene. This exploration aims to understand how amino acids, such as tryptophan, interact and impact the isomerization of a photoswitchable molecule. The journey through this exploration is grounded in the desire to uncover the full spectrum of possibilities that emerge when non-intrinsic and intrinsic fluorescence converge with the unique characteristics of azobenzene.

Chapter 2. Development of Rifampicin-Binding Aptamers

2.1   Abstract

Rifampicin (Rif) is an antibiotic known for its effectiveness against bacterial strains, with an emphasis on combatting Mycobacterium tuberculosis. It is widely prescribed to patients globally. Despite its widespread use, challenges persist in accurately detecting and quantifying Rifampicin in biological samples. The strengths and limitations of existing analytical methods, including immunoassays and chromatographic techniques, were evaluated. Advanced alternatives such as Liquid Chromatography-Mass Spectrometry (LC-MS/MS) and the GeneXpert molecular diagnostic platform are examined, along with the microbiological assay using rifampicin-infused agar plates. Recognizing the drawbacks of current methods, this study proposed exploring aptamer development via the SELEX method. The role of Therapeutic Drug Monitoring (TDM) in optimizing individualized drug therapies, especially for hydrophobic drugs like Rifampicin, is emphasized. The detailed SELEX process offers a potential solution to streamline Rifampicin monitoring.

2.2   Introduction

Rifampicin (Rif) demonstrates broad-spectrum efficacy, particularly against Mycobacterium tuberculosis. Despite its effectiveness, challenges remain in detecting and quantifying Rifampicin in biological samples[38]. This introduction provides an overview of Rifampicin's significance, its mechanism of action, and the emergence of drug resistance[39]. Current analytical methods, including immunoassays and chromatographic techniques, are outlined, each presenting strengths and limitations. Advanced technologies such as LC-MS/MS, the GeneXpert molecular diagnostic platform, and the microbiological assay using rifampicin-infused agar plates

are introduced[40–42]. Recognizing the need for improved methods, the study proposed exploring aptamer development through the SELEX method, which emphasized the role of Therapeutic Drug Monitoring (TDM) in optimizing drug therapies, especially for hydrophobic drugs, Rif.

2.3   Rifampicin

Rifampicin is an essential antibiotic against many bacterial species. It is particularly effective against Gram-positive bacteria such as Mycobacterium tuberculosis, the causative agent of tuberculosis[43]. Rif is also used to treat infections caused by other bacteria, including Staphylococcus aureus, Streptococcus pneumoniae, and Neisseria meningitidis[44]. As shown in Figure 1[45], the molecular structure of Rifampicin is classified as a bactericidal antibiotic; it kills bacteria rather than just inhibits their growth. Its mechanism of action involves binding to the beta subunit of bacterial RNA polymerase, a crucial enzyme involved in transcription[46]. Rifampicin's binding to RNA polymerase inhibits transcription, leading to the cessation of bacterial RNA synthesis and, consequently, the death of the bacteria.

In addition to its role in treating tuberculosis, rifampicin has clinical applications in treating other bacterial infections. It is frequently used with other antibiotics to treat complicated skin and soft tissue infections caused by Staphylococcus aureus[47]. Rifampicin is used in the prophylactic treatment of meningococcal carriers and in treating infections caused by Nocardia, Legionella, and Brucella species. Despite its effectiveness, rifampicin is associated with the development of drug resistance, particularly in tuberculosis[48]. This has led to the development of combination therapies involving rifampicin and other antibiotics to help prevent the emergence of resistance. Rifampicin is generally well-tolerated, but like all antibiotics, it can cause side effects such as gastrointestinal upset, skin rash, and hepatotoxicity[49].

Absolute stereochemistry shown
E/Z labels describe double bond geometry
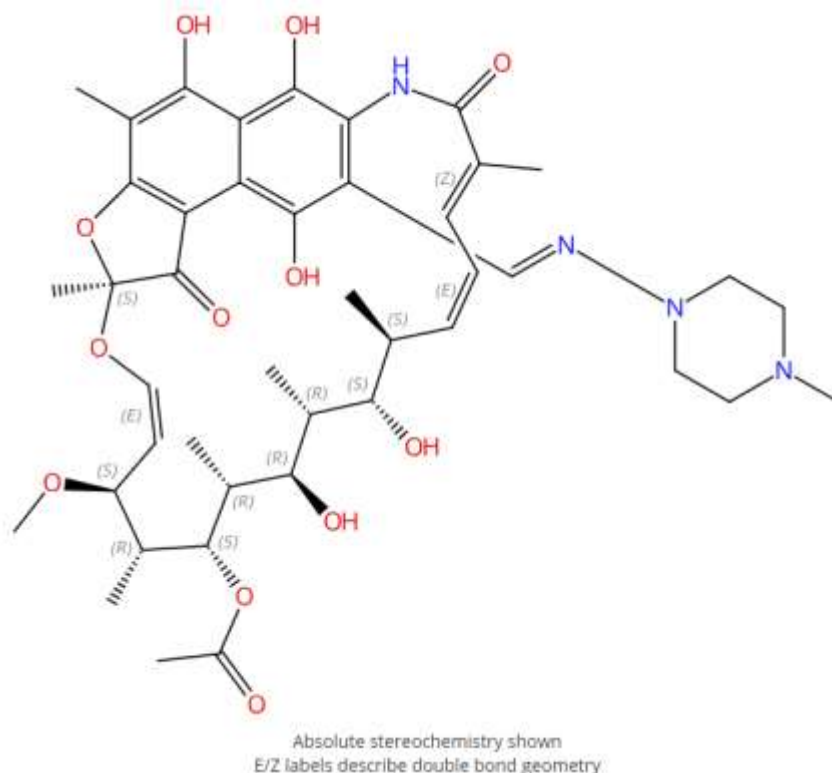
Figure 1. Rifampicin structure generated using SciFinder

2.4   Rifampicin: Detection and Quantification

The detection and quantification of rifampicin in biological samples can be challenging due to the limitations of the current analytical methods used for its analysis. The most used rifampicin detection and quantification methods include immunoassays, chromatographic techniques, molecular diagnostic platforms, and microculture assays. While these methods have their strengths, they also have several limitations. Immunoassays, including enzyme-linked immunosorbent assays (ELISA), are valuable clinical and pharmaceutical analysis tools, particularly for detecting drugs like rifampicin. These assays offer a combination of simplicity and high sensitivity, making them attractive for various medical diagnostics and research applications[50]. They can detect target molecules, rifampicin, at very low concentrations in complex biological matrices. This high sensitivity is crucial for monitoring drug levels in patient

26

samples, where even trace amounts can be diagnostically relevant. The assay format typically involves the immobilization of an antigen, rifampicin on a solid support, adding a specific antibody, and the subsequent detection of the antibody-antigen complex. This process reduces the need for highly specialized training, making immunoassays accessible to more users[51].

However, Immunoassays rely on the specific binding of antibodies to the target molecule, which is usually an antigen or analyte of interest. As a result, antibodies can sometimes cross-react with structurally related compounds that share similarities with the target molecule. Rifampicin, for instance, has structural analogs or metabolites that may trigger cross-reactivity in the assay. Cross-reactivity can lead to false-positive results, indicating the presence of the target molecule when it may not be present in sufficient quantities. This can concern clinical diagnostics and drug monitoring, where accurate measurements are critical for patient care and therapeutic decision-making. In clinical settings, patients are often taking multiple medications, and their biological samples may contain a variety of drugs and their metabolites. Immunoassays are vulnerable to interference from these coexisting substances, which can impact the assay's accuracy. Biological samples, such as blood or urine, are complex matrices containing proteins, lipids, salts, and other components.[51] These matrix effects can interfere with the assay, affecting the binding of antibodies and the accuracy of the results. Therefore, understanding the potential sources of error in immunoassays is crucial for ensuring accurate and reliable clinical diagnostics and drug monitoring results and the need for novel TDM.

Chromatographic techniques, such as high-pressure liquid chromatography (HPLC), are considered the standard for quantifying rifampicin due to their high selectivity and sensitivity[52]. Rifampicin is a complex drug, often present at low concentrations in biological samples, and its accurate quantification is important in various clinical and pharmaceutical applications. HPLC is

known for its selectivity, which enables it to separate and quantify analytes in complex mixtures. This is particularly advantageous in clinical and pharmaceutical settings where samples often contain myriad compounds, including metabolites and co-administered drugs. HPLC's ability to distinguish rifampicin from other compounds in the sample is essential for accurate quantification. Selectivity is achieved through the choice of appropriate stationary phase and mobile phase, as well as by optimizing the chromatographic conditions. In the case of rifampicin, its structural specificity can be exploited, making HPLC a well-suited technique for its quantification. HPLC's precision and accuracy are vital in clinical and pharmaceutical contexts. It provides reproducible results, which are essential for monitoring drug levels over time and making informed therapeutic decisions. Using internal standards can further enhance the accuracy of Rifampicin's quantification[53].

While HPLC techniques offer numerous advantages, they are not without their drawbacks. These drawbacks include the time-consuming nature of the analysis, complex sample preparation procedures, high costs, and the need for specialized equipment and trained personnel. The HPLC's process involves several steps, such as sample preparation, equilibrating the column, sample injection, separation, and data analysis. This time investment can be a constraint in situations requiring rapid results, such as emergency clinical diagnostics. The chromatographic method's complexity and the need for calibration and quality control can extend the analysis time further. Chromatographic techniques can be expensive to implement and maintain. The equipment, including the HPLC system and associated accessories, can be a significant investment. This cost can be a barrier to smaller laboratories or research facilities with limited budgets. Consumables, such as columns and solvents, also contribute to ongoing operational costs. Regular maintenance and calibration are necessary to ensure the accuracy and reliability of results. Effective utilization

of chromatographic techniques demands a high level of training and expertise. This includes understanding chromatography principles, method development, instrument operation, troubleshooting, and data interpretation[54].

Liquid Chromatography-Mass Spectrometry (LC-MS/MS) is a highly sophisticated technique for quantitative analysis. It combines liquid chromatography with mass spectrometry to separate, identify, and quantify rifampicin in complex samples[55]. LC-MS/MS offers exceptional sensitivity, specificity, and the ability to analyze multiple compounds simultaneously. It is commonly used in research and clinical laboratories for pharmacokinetic studies and drug monitoring. Proper maintenance, calibration, and troubleshooting can ensure accurate and reproducible results. Operators must be trained to handle and maintain these complex systems, which can be costly.

Developing LC-MS/MS methods can be time-consuming and intricate process [55]. It involves optimizing various parameters, such as the mobile phase, column selection, ionization source, and mass spectrometric parameters. The ability to fine-tune these parameters for different analytes and matrices is a skill that requires experience and expertise[56]. The data generated by LC-MS/MS can be massive and complex. Analyzing and interpreting this data necessitates using specialized software and a deep understanding of mass spectrometry principles. Identification and quantification of compounds often involve complex data processing algorithms, which require additional expertise.   Many real-world samples contain matrix components that can interfere with the analysis, leading to ion suppression or enhancement. Mitigating these matrix effects through proper sample preparation can be complex, and it may require additional cleanup steps or the use of isotopically labeled internal standards.

GeneXpert is a molecular diagnostic platform with a single cartridge-based assay to detect either Tuberculosis (TB), Human Immunodeficiency Virus (HIV), or Severe Acute Respiratory Syndrome Coronavirus 2 (SARS-CoV-2). This equipment can rapidly and accurately detect Mycobacterium tuberculosis (M. tuberculosis) and assess rifampicin resistance, a key aspect of tuberculosis management[57]. This system utilizes real-time polymerase chain reaction (PCR) technology to amplify specific DNA segments and detect gene sequences associated with rifampicin resistance[58]. One of the primary advantages of the GeneXpert platform is its speed. Traditional culture-based methods for tuberculosis diagnosis can take several weeks to yield results. In contrast, GeneXpert can provide a definitive diagnosis within hours, dramatically reducing the time from patient presentation to treatment initiation[59]. GeneXpert is designed to be user-friendly and can be operated by individuals with varying levels of laboratory experience. It automates the entire diagnostic process, from DNA extraction to result interpretation, minimizing the risk of human error. GeneXpert identifies the presence of M. tuberculosis and determines whether it carries mutations associated with rifampicin resistance.

GeneXpert is adaptable in various healthcare settings, including remote or resource-limited areas. This flexibility is especially valuable in regions with high tuberculosis prevalence, where timely diagnosis and treatment are critical. Rapid diagnosis using GeneXpert enhances public health efforts and improves individual patient care. It allows for the timely initiation of the appropriate treatment regimen, minimizing the risk of disease progression and complications. The deployment of GeneXpert has significantly impacted global tuberculosis control efforts[60]. Its speed and accuracy have been instrumental in the early diagnosis of tuberculosis cases, even in challenging environments.

While GeneXpert is a versatile diagnostic platform with numerous advantages, it is essential to acknowledge its limitations and disadvantages. GeneXpert systems and associated consumables, including test cartridges and reagents, can be relatively expensive. This cost can be a significant barrier to adoption in resource-constrained healthcare settings, particularly in low- and middle-income countries where tuberculosis is prevalent. GeneXpert systems require a consistent power supply, which can be problematic in regions with unreliable electricity. Power outages can disrupt testing, leading to delays and potential data loss. The number of modules limits the instrument's capacity, which can be a drawback when dealing with a high volume of samples. Running multiple tests in parallel may be challenging for laboratories with a substantial workload. The time required to process samples on a GeneXpert system can be a limiting factor for high-throughput laboratories. Despite its speed compared to traditional methods, the analysis time for multiple samples may still be significant when a large number of tests are needed. GeneXpert cartridges are designed for specific tests, and customization is limited. This lack of flexibility can be a drawback for laboratories that need to adapt or expand their test menu based on changing diagnostic needs. GeneXpert instruments require regular maintenance to ensure their accuracy and reliability. Maintenance and servicing can be costly and require specialized personnel or manufacturer contracts. While GeneXpert is designed to be user-friendly, it still requires training and competency to operate effectively. Adequate training is essential to ensure the correct use of the system and the accurate interpretation of results.

The microbiological assay using a paper disk or agar plate infused with rifampicin is a classic and effective method for evaluating the presence and potency of this antibiotic against susceptible bacterial strains. This assay, often referred to as the "antibiotic susceptibility test" or "disk diffusion test," plays a crucial role in antimicrobial susceptibility testing and clinical

microbiology[61]. In this assay, an agar plate is infused with a known concentration of rifampicin. The rifampicin solution is evenly distributed onto the disk or poured onto the surface of the agar plate. Bacterial strains being tested for their susceptibility to rifampicin are inoculated onto the surface of a culture medium within a petri dish. This medium typically contains essential nutrients to support bacterial growth. The petri dish, with the infused agar plate and inoculated bacterial strains, is incubated under controlled conditions. This allows the bacterial strains to grow and form a visible bacterial lawn on the agar surface. Rifampicin, imbued in the agar plate, diffuses outward into the surrounding agar. The diffusion rate depends on the solubility and concentration of rifampicin in the imbued material. The presence of the drug inhibits bacterial strains sensitive to rifampicin. As the antibiotic diffuses into the agar, it creates a concentration gradient. Bacterial growth is prevented in areas where the rifampicin concentration is above the minimum inhibitory concentration (MIC)[62]. This forms a clear zone around the agar plate, known as the "zone of inhibition." The size of the zone of inhibition is measured in millimeters using a calibrated ruler or calipers. A larger zone of inhibition indicates that the bacterial strain is more susceptible to rifampicin, while a smaller or absent zone suggests resistance[63].

Clinical laboratories and healthcare providers use standardized guidelines to interpret the zone sizes and determine whether the bacterial strain is susceptible, intermediate, or resistant to rifampicin. These interpretations are based on established breakpoints and epidemiological data[64]. The results of this assay help guide the selection of appropriate antibiotic therapy for infections caused by specific bacterial strains. If a bacterial strain is susceptible to rifampicin, it can be effectively treated with this antibiotic. In contrast, resistance may necessitate the use of alternative antibiotics. To ensure the reliability of the assay, laboratories employ quality control measures,

including using reference strains with known susceptibility profiles and performing regular checks of the assay's accuracy.

The microbiological assay using rifampicin-infused agar plates is a relatively simple and cost-effective method for assessing the susceptibility of bacterial strains to this antibiotic. However, it has certain limitations, including a lack of precision compared to more advanced methods[65]. While it is user-friendly, it lacks the precision and accuracy offered by more advanced and instrumental methods, such as liquid chromatography-mass spectrometry (LC-MS) or molecular diagnostics like GeneXpert. The microbiological assay determines whether a bacterial strain is susceptible, intermediate, or resistant to rifampicin based on the size of the zone of inhibition. However, it doesn't yield specific concentration values. This lack of quantitative data can limit its utility when precise MIC values are required for treatment decision-making. The measurement of the zone of inhibition can be subjective and may vary between operators or laboratories. Variability in interpretation can impact the consistency of results, potentially leading to inconclusive or inconsistent findings. The range of rifampicin concentrations achieved using imbued agar plates is relatively narrow. This may limit the assay's ability to detect subtle differences in susceptibility among bacterial strains, especially when working with strains on the borderline between susceptible and resistant. Some bacterial resistance mechanisms may not be accurately detected using the microbiological assay alone. For instance, certain resistance mechanisms may confer resistance even in a visible zone of inhibition.

The selection of a method for analyzing rifampicin depends on various factors, each of which carries its own set of advantages and limitations. Many analytical methods, especially those based on traditional assays or chromatography, may have a detection limit above which they cannot reliably quantify rifampicin. This limitation can be problematic when attempting to detect the drug

in biological fluids, such as blood or urine, where concentrations may be low, especially in patients on therapy. This research study focuses on developing a new analytical method that can overcome these limitations, improve the sensitivity and specificity of rifampicin detection, and reduce the time and cost of analysis.

The proposal to develop single-stranded DNA-based aptamers for Rif (rifampicin) using the Systematic Evolution of Ligands by EXponential Enrichment (SELEX) method is a promising approach that can address some of the challenges associated with current methods for Rif detection and quantification. SELEX is a well-established and highly versatile technique for selecting aptamers, short, single-stranded DNA or RNA molecules capable of binding to specific target molecules with high affinity and specificity[66]. Aptamers have some advantages over antibodies because they are easier to synthesize and reconstitute after denaturation and storage.

2.5   Therapeutic Drug Monitoring

Individualized drug therapies for patients using Therapeutic Drug Monitoring (TDM) have been a cornerstone of pharmacotherapy since the early 1970s[67]. To ensure the consistent and accurate use of TDM in clinical practice, it is crucial to define the term precisely. The International Association for Therapeutic Drug Monitoring and Clinical Toxicology provides a widely accepted definition: "the measurement of a parameter that, with the appropriate interpretation, will directly influence drug prescribing procedures"[68]. As a result, TDM plays a vital role in understanding drug efficacy and potential toxicity in individual patients. TDM is essential for precise drug dosage adjustments, combating antimicrobial resistance, and addressing drug interactions, including those with food[69]. This definition underscores the practical utility of TDM in guiding clinical decision-making and emphasizes its role in delivering safe and effective drug therapies. It aids in optimizing drug effectiveness, minimizing toxicity, and ensuring personalized treatments. TDM has found

applications in diverse medical fields, including oncology, psychiatry, infectious diseases, and more.

TDM helps clinicians strike a delicate balance between therapeutic efficacy and potential toxicity. By monitoring drug concentrations in a patient's bloodstream, physicians can fine-tune the drug dosage to ensure it remains within the therapeutic range, where it is most effective while avoiding harmful side effects. This is especially crucial for medications with a narrow therapeutic index, where small deviations in dosage can lead to severe consequences. Every individual responds differently to medications due to variations in factors like metabolism, genetics, and underlying health conditions. TDM enables the tailoring of drug therapies to each patient's specific needs. By tracking drug levels over time, healthcare professionals can adjust treatment plans to match the unique pharmacokinetics of an individual, resulting in more precise and effective care.

The rise of antimicrobial resistance is a global health concern[64]. TDM plays a pivotal role in managing antibiotic treatments by ensuring the antibiotic concentration remains above the minimum inhibitory concentration (MIC) for the pathogen. This helps prevent the development of resistant strains and ensures that patients receive the most effective antibiotics for their infections. TDM is essential when patients take multiple medications or have dietary restrictions. It assists in identifying potential drug interactions, allowing for dose adjustments or alternative medication choices to mitigate adverse effects or compromised drug efficacy. This is particularly important in elderly patients or those with chronic diseases who often have complex medication regimens.

Monitoring drug therapy, especially for hydrophobic drugs like Rif, presents unique challenges due to their complex pharmacokinetics and potential for toxicity. With its extensive molecular structure and diverse pharmacological effects, Rifampicin is a prime example of a drug that requires careful monitoring in clinical practice. Rifampicin is a complex molecule with a

35

molecular weight of 822.94 g/mol. Its chemical structure, 5,6,9,17,19,21-hexahydroxy-23-methoxy-2,4,12,16,18,20,22-heptamethyl-8-[N-(4-methyl-1-piperazinyl)formimidoyl]-2,7-(epoxypentadeca [1,11,13]trienimino)-naphtho[2,1-b]furan-1,11(2 H)-dione 21-acetate (C43H58N4O12), is highly hydrophobic, making its solubility in aqueous solutions limited. This hydrophobic nature can affect its absorption, distribution, metabolism, and elimination within the body, necessitating specialized monitoring methods.

Rifampicin has a reputation for causing hepatic, renal, hematological disorders, and convulsions[70]. These adverse effects stem from its ability to inhibit DNA-dependent RNA polymerase activity and form a stable complex with the enzyme. As a result, monitoring Rif's serum levels is critical to prevent or detect these toxicities promptly. The hydrophobic nature of Rifampicin makes traditional analytical methods, such as Liquid chromatography techniques, mass spectrometry, or immunoassays, less straightforward. These methods often require complex sample preparation and extraction procedures to quantify Rifampicin levels in biological samples accurately. The hypothesis is to develop point-of-care testing devices that provide rapid, on-site Rifampicin level measurements. These devices aim to streamline the monitoring process and improve accessibility, particularly in resource-limited settings.

2.6   Aptamer

Aptamers, derived from the Latin word "aptus" meaning "to fit", and the Greek word "meros" meaning "Particle", are short, single-stranded Deoxyribonucleic acid (ssDNA) or Ribonucleic acid (RNA) molecules that exhibit high affinity and specificity for binding to various target molecules[71]. Aptamers are typically ranging from 20 to 60 nucleotides in length that can bind to specific target molecules. They are often referred to as chemical antibodies due to their ability to recognize and bind to target molecules in a manner that binds to antigens[72].

Aptamers are generated through the Systematic Evolution of Ligands by Exponential Enrichment (SELEX). In SELEX, a pool of random oligonucleotides is subjected to iterative rounds of selection and amplification. During each round, the oligonucleotides that bind most tightly to the target molecule of interest are selected, amplified, and used as the starting material for the next round[73–75]. Through this iterative process, the pool of oligonucleotides gradually evolves to contain aptamers with high affinity and specificity for the target molecule.

Aptamers' binding specificity arises from their unique three-dimensional structures, formed through intramolecular interactions within the single-stranded nucleic acid sequences[76]. This structural diversity allows aptamers to bind to targets, including small molecules, proteins, peptides, nucleic acids, and whole cells.

In 1990, Professor Larry Gold and Craig Tuerk introduced the SELEX process at the University of Colorado[74]. This innovative technique allowed the systematic evolution of ligands by iteratively selecting and amplifying nucleic acid sequences that bind tightly to specific target molecules. The initial experiment's results demonstrated the remarkable versatility of SELEX in generating nucleic acid ligands with high affinity and specificity, opening new possibilities for molecular diagnostic platforms and targeting[77].

Aptamers offer several advantages over traditional antibodies as molecular recognition elements. They can be generated against targets that are difficult to immunize against, such as small molecules or toxic compounds. Aptamers can also be chemically synthesized, which allows for easy modification and optimization of their properties. Moreover, aptamers can exhibit high stability, withstanding various temperatures and pH conditions[78].

The unique properties of aptamers have led to their application in various fields, including diagnostics, therapeutics, and biosensing. They can be used as sensing probes to detect and

quantify target molecules in complex samples, such as blood or environmental samples[79]. Aptamers also have potential as therapeutic agents, as they can interfere with specific molecular interactions or pathways in diseases, offering an alternative to traditional small molecule drugs or antibodies[80].

2.7   Methods

2.7.1   Rif-labeled beads and Unlabeled Control Beads

To prepare the Rif-labeled beads, the solid support (beads) was activated to enable the covalent attachment of Rifampicin. The activation process involved forming an active ester group on the bead surface, which reacted with Rifampicin. The goal was to create a functionalized surface on the beads for subsequent binding of Rifampicin[81]. The activation mixture, Rif-labeled beads, was prepared by measuring the 4-Nitrophenol and Dicyclohexylcarbodiimide (DCC) in N,N-Dimethylformamide (DMF). The DCC activated the beads' surface by reacting with the 4-Nitrophenol. The activated beads underwent incubation with Rifampicin, and we hypothesized that these activated beads covalently bind to the activated sites on the bead surface, potentially involving secondary or tertiary amine or amide interactions, as illustrated in Figure 2. To stop the labeling reaction and remove any unbound Rifampicin, the beads were quenched by adding methylamine and DMF. The quenching step deactivated any unreacted activated sites on the beads. The beads were washed with DMF and 20% glycerol. The final step involves measuring the bead capacity using the nanodrop spectrophotometer at 405nm.

Figure 2. Schematic of Rif-Labeled Beads

Unlabeled beads were prepared in a manner consistent with the Rifampicin-labeled beads and utilized as control beads. They aimed to monitor non-specific binding, evaluate the specificity of chosen aptamers, and confirm that binding was specific to the target rather than a consequence of interactions with the bead material. The control beads were used alongside the Rif-labeled beads during the SELEX process. If aptamers show minimal or no binding to the control beads, their binding to the Rif-labeled beads is primarily target-specific and not influenced by interactions with the bead material.

2.7.2   SELEX Process

The SELEX process commenced with incubating a pool of random-sequence 40-mer single-stranded DNA molecules, with the target molecule, Rif-labeled beads, and the unlabeled beads as the control in SELEX buffer (140 mM sodium chloride, 2 mM potassium chloride, 5 mM magnesium chloride, 2 mM calcium chloride, 0.05% Tween in 20 mM pH 7.4 Tris buffer), which is shown in Figure 3. The beads were washed with SELEX buffer. To release the DNA from the column, 20 µL of autoclaved water was added, the mixture was heated at 95°C for 2 minutes, then promptly centrifuged. The resulting 20 µL solution was transferred to a new Eppendorf tube, and

a final centrifugation step was performed. The recovered DNA was purified using a Zymo Research DNA preparation column. The recovered DNA was amplified under the following conditions: an initial round at 95°C for 5 minutes, followed by 15 cycles of 95°C for 0.30 minutes, 50°C for 0.30 minutes, and 72°C for 1 minute. Subsequently, the process concluded with a final extension at 72°C for 5 minutes. The samples were treated with exonuclease and incubated at 37°C for 30 min. This mixture was purified using a Zymo column, and the output was checked for absorbance at 260 nm using the Nanodrop spectrophotometer. If the yield was less than 10 ng/µL for Labeled-Rif, an additional PCR was conducted as described above, substituting 10 cycles for the 15 cycles. Further rounds of SELEX included the following modifications: for rounds 4 through 6, 20 µL of 20 pmol Rif was used instead of water to release the DNA. For rounds 7 through 11, an additional competitive wash, 20 µL of 20 pmol Amphotericin B (AmB) used to incubate with Rif-labeled beads and Unlabeled beads.

Figure 3. The SELEX scheme to create the Rif-Labeled aptamers.

2.7.3 Gel Electrophoresis

DNA library, Labeled-Rif beads, and Unlabeled Control beads after PCR amplification were tested via electrophoresis separation. A 15% agarose gel was prepared using Tris-borate-EDTA (TBE) buffer as the running medium. The agarose powder was weighed, and the gel solution was created by dissolving the agarose in TBE buffer and heating until complete dissolution using the microwave. Ethidium bromide (EtBr) was added to the warm agarose solution. The gel was cast with a comb inserted to create wells for loading DNA samples. Before loading, DNA samples were mixed with DNA loading dye for visualization during electrophoresis. The gel was then placed in the electrophoresis tank filled with 1X TBE buffer, and DNA samples and a molecular weight marker were loaded into the wells. The electrophoresis was run at 120 V (volt) until the DNA bands had migrated sufficiently. Subsequently, the gel was visualized under UV light, and the bands were documented.

2.8   Results and Discussion

2.8.1 SELEX Process Summary

Table 1 shows the PCR output measured using the Nanodrop Spectrophotometer for each round conducted in the SELEX process. This table captures the results obtained from the SELEX rounds, providing an overview of the progression of aptamer selection. The data includes concentrations for Unlabeled Beads (Counter-SELEX), representing the control group designed to ensure specificity in the selection process. The concentrations of labeled Rifampicin (SELEX) are documented, showing the enrichment of sequences that exhibit binding affinity to the target molecule. Modifications for bead selectivity are highlighted, offering insights into the strategies employed to enhance the selectivity and specificity of the aptamer pool.

Table 1. A breakdown of DNA concentrations for each SELEX round - Unlabeled Beads (Counter-SELEX), labeled Rifampicin (SELEX), and the modification for bead selectivity.

Labeled-Rif (ng/µL)	Unlabeled Control (ng/µL)	Rounds	Modification
48.2	50.3	1	Water
72.4	82	2	Water
68.8	81.1	3	Water
28.3	46.9	4	Rif
67.8	50	5	Rif
43.1	84.6	6	Rif
58.4	57.7	7	AmB
76.1	48.7	8	AmB
56.5	2.3	9	AmB
35.5	4	10	AmB
32.7	33.8	11	AmB

The bar graph in Figure 4 visually represents the results obtained from the SELEX rounds, offering the progression of aptamer selection. Notably, Rounds 9 and 10 exhibit a higher degree of selectivity for the labeled beads when compared to the unlabeled control beads. The observation that Rounds 9 and 10 are more selective for the labeled beads than the unlabeled control beads is a significant finding for further analysis. It suggests that the SELEX process has been successful in developing aptamers with an increased specificity for Rif. This increased selectivity in Rounds 9 and 10 is indicative of the aptamers' enhanced ability to distinguish and preferentially bind to Rif. These rounds represent a stage where aptamers with the desired specificity have been enriched.
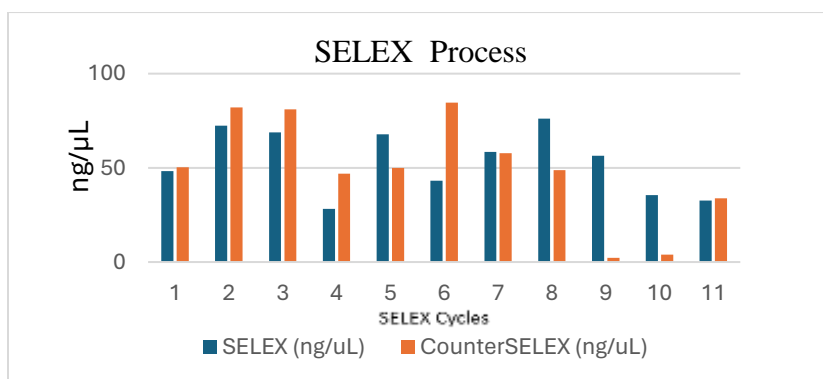
Figure 4. Results obtained from SELEX process.

2.8.2 Gel Electrophoresis Results

Based on the results shown in Table 1, round 2 and round 6 unlabeled beads were used to verify the DNA amplification experiment during the SELEX process. The assessment of DNA size is an important step in molecular biology and aptamer selection processes. Agarose gel electrophoresis was the technique used to separate DNA molecules based on their size. It assesses the size and integrity of DNA samples, including aptamers and amplified DNA from SELEX rounds[82]. A 0.1 µM concentration of the 40-mer library was analyzed to serve as a reference to assess the size and integrity of the aptamer sequence. Additionally, amplified products from unlabeled rounds 2 and 6 were assessed. These samples represent the progress in SELEX rounds and the enrichment of aptamer sequences over time. Figure 5 presents the results of the agarose gel electrophoresis. We evaluated the DNA samples' quality and confirmed that the amplification process was carried out successfully.

The presence of one (1) band in the lane corresponding to the aptamer indicates that the 40-Mer library sequence is intact and present at the expected size. This verifies the quality and stability of the initial aptamer. In contrast, the presence of two (2) bands in the lanes for the amplified rounds (rounds 2 and 6) suggests that the DNA from these rounds has been successfully amplified. The appearance of multiple bands is attributed to the presence of various DNA sequences, which is expected as SELEX is an iterative process that diversifies aptamer sequences over rounds.

The presence of multiple bands in the lanes for amplified rounds is a positive outcome. It confirms that DNA amplification was performed effectively, enriching aptamer sequences with each successive SELEX round. The analysis presented in Figure 5 is essential for validating the

progress of the SELEX process. The visual confirmation of aptamer amplification at different rounds is a key milestone in demonstrating that the SELEX procedure is evolving aptamers with potentially higher affinity for the target molecule, Rifampicin.

Figure 5. Gel Electrophoresis result showed well 1 with 40-mer DNA aptamer with a single strand, while wells 2 and 3 for rounds 2 and 6 showed double bands of DNA.

After completing all the SELEX rounds and analyzing the data, Figure 6 represents the outcomes of rounds 9, 10, and 11 following the amplification process. Round 10 was chosen for cloning using the TOPO TA Cloning vendor protocol (Invitrogen/Life Technologies, USA). The selection of a specific round is a crucial decision in the SELEX process. Round 10 was selected because it demonstrated significant improvements in DNA profile and concentration compared to other amplified rounds. It is the juncture where the most promising aptamers are singled out for further development. This choice evaluates multiple factors, including the aptamers' binding characteristics and overall performance. By selecting Round 10, there was a strong indication that the aptamers generated in this round have the most promising potential for further development.
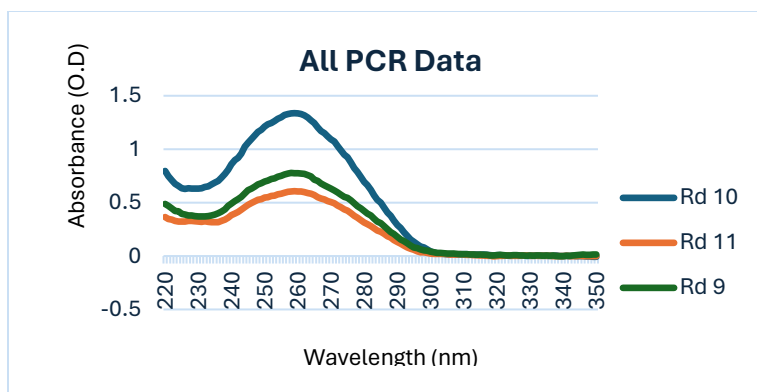
Figure 6. Graph of DNA Concentration after round 9, 10, and 11 amplifications.

These results reflected the SELEX process that progressed through multiple rounds as the aptamer pool became enriched with sequences that exhibited a higher affinity for the target. Among the last three rounds of the SELEX process, the Round 10 profile stands out as promising. This particular round's profile demonstrates characteristics that make it a potential candidate for further analysis. Therefore, the observed results underscore the SELEX process's success in enriching the aptamer pool and pinpointing the Round 10 profile, setting the stage for a more comprehensive exploration of its potential applications.

2.9   Conclusion

Rifampicin's pivotal role in combating bacterial infections underscores the urgency of addressing challenges in its accurate detection and quantification. Assessing existing analytical methods sheds light on their strengths and limitations. Advanced technologies offer promising alternatives, including LC-MS/MS, the GeneXpert platform, and the microbiological assay. The study proposed a forward-looking approach through aptamer development via the SELEX method, envisioning a transformative impact on Rifampicin monitoring. Emphasis is placed on the indispensable role of Therapeutic Drug Monitoring in tailoring drug therapies, particularly for

hydrophobic drugs like Rifampicin. Further research will be done to innovate analytical methods, enhance sensitivity, and contribute to monitoring antimicrobial resistance.

Chapter 3. Aptamer's Sequences

3.1   Abstract

In this Chapter, we aim to characterize the aptamer structure. The cloning process of Round 10 aptamer was done by utilizing the TOPO TA Cloning kit. The procedure involved combining the PCR product with the TOPO vector and cloning and heat-shock treatment of competent E. coli cells. Successful cloning was verified through a quantitative assessment of DNA concentration data, showcasing DNA amplification in the colonies. Gel electrophoresis confirmed the cloning process. High-throughput sequencing and structural predictions revealed the genetic makeup of colonies, providing insights into aptamer sequences and potential folding patterns. Aptamer Rif_3 demonstrated promising results in binding assays, showing specificity for labeled-Rif beads. Competitive experiments with Amphotericin B (AmB) indicated the aptamer's detachment, suggesting a potential stronger affinity for AmB compared to Rif. The study concluded by emphasizing that Non-intrinsic fluorescence, illustrated through Oligreen dye, facilitated sensitive detection of nucleic acids in the binding assays.

3.2   Introduction

Aptamers recognize and bind to their targets by adopting 3-dimensional shapes and participating in diverse physiochemical interactions, mirroring the mechanisms observed in antibody binding. These interactions include hydrophobic, electrostatic, hydrogen bonding, van der Waals forces, base stacking, and shape complementarity. Due to their intrinsic flexibility and limited steric hindrance, aptamers, as functional nucleic acid molecules, exhibit a proficient capacity to recognize biomolecules effortlessly[83]. In binding assays, Aptamer Rif_3 exhibited promising results. The specificity observed in the binding interactions underscores the selectivity

of Aptamer Rif_3 towards the designated target, emphasizing its efficacy in recognizing and binding to the labeled-Rif beads. The success of Aptamer Rif_3 in these binding assays highlights its functional competence and positions it as a promising candidate for further exploration.

3.3   Methods

3.3.1 Cloning process

In accordance with the Invitrogen/Life Technologies vendor protocol, the TOPO TA Cloning was prepared using the specified reagents as follows: 1 µL of Fresh Round 10 PCR product, 1 µL of Salt Solution, 3 µL of Water, and 1 µL of TOPO® vector, resulting in a final volume of 6 µL. The reaction mixture was gently mixed and incubated at room temperature for 5 minutes. Subsequently, 2 µL of the TOPO Cloning reaction from the previous step was added to a vial containing One Shot chemically competent E. coli, and the mixture was gently mixed without pipetting up and down. The vial was incubated on ice for 15 minutes, followed by a 30-second heat shock at 42°C using a heat block. The tubes were immediately transferred to ice, and 250 µL of room temperature Super Optimal Broth with Catabolite (S.O.C.) medium was added. The capped tubes were shaken horizontally (200 rpm) at 37°C for 1 hour. To initiate colony growth, 10 µL and 50 µL of the solution were spread onto pre-warmed plates. Additionally, a third plate was created by spreading 100 µL of the solution. The plates were incubated at 37°C overnight. Colonies were harvested by scooping out colonies into 100 µL of water.

3.3.2 PCR method

To amplify the harvested DNA fragments, PCR method was employed utilizing specific reagents. The reaction mixture consisted of 5 µL of dNTPs, 5 µL of PCR buffer, 1 µL each of M13

Forward and Reverse Primers, 36.5 µL of water, 1 µL of the sample, and 0.5 µL of rTaq polymerase. The PCR protocol involved an initial denaturation step at 95°C for 5 minutes, followed by cycling conditions including denaturation at 95°C for 1 minute, annealing at 54°C for 1.5 minutes, and extension at 72°C for 1 minute. This cycle repeated 34 times, with a final extension at 72°C for 1 minute. Subsequently, the samples underwent cleanup using the Zymo kit. The concentration of amplified DNA was assessed using the Nanodrop, and the PCR products were further analyzed through gel electrophoresis.

3.3.3 Spectrochemistry method

The absorbances of amplified DNA samples were measured using a NanoDrop 1000 Spectrophotometer (Thermo Scientific). For each sample, 2 µL was loaded onto the spectrophotometer, and the absorbance was recorded across the spectrum ranging from 220nm to 750nm. The NanoDrop 1000 Spectrophotometer utilized for this analysis is equipped with a 1mm path length, ensuring accurate measurements, and operated using software version 3.8.1 for data analysis and interpretation.

3.3.4 Gel Electrophoresis

DNA bands for round 10's first seven (7) colonies were tested via electrophoresis separation. A 15% agarose gel was prepared using Tris-borate-EDTA (TBE) buffer as the running medium. The agarose powder was weighed, and the gel solution was created by dissolving the agarose in TBE buffer and heating until complete dissolution using the microwave. Ethidium bromide (EtBr) was added to the warm agarose solution. The gel was cast with a comb inserted to create wells for loading DNA samples. Prior to loading, DNA samples were mixed with DNA loading dye for visualization during electrophoresis. The gel was then placed in the electrophoresis

tank filled with 1X TBE buffer, and DNA samples and a molecular weight marker were loaded into the wells. The electrophoresis was run at 120 V volt until the DNA bands had migrated sufficiently. Subsequently, the gel was visualized under UV light, and the bands were documented.

3.3.5   Spectrofluorometer Method

To conduct spectrofluorometer analysis, a 10 mg/mL of graphene solution was prepared by weighing 1.81 mg and adding 181 μL of 1X SELEX buffer. Then, 10 μL of the diluted fluor apt 3 was added to a tube along with 10 μL of the 10 mg/mL graphene solution. The mixture was then incubated for 30 minutes at room temperature. Afterward, the solution was washed twice with 100 μL of 1X SELEX buffer and subsequently resuspended in 1 mL of SELEX buffer. The solution was then divided into nine (9) wells, with 100 μL each. Rifampicin and Amphotericin B solutions, both at a concentration of 1 mM in 1% DMSO, were prepared, along with a 1% water/DMSO solution by adding 10 μL of DMSO to 990 μL of water. Triplicates of 1 μL of rifampicin, amphotericin B, and water/DMSO were added to the wells. Kinetic readings were taken at 0, 15, 30, 45, and 60 minutes using a microplate reader equipped with a Tecan 96 transparent plate. Fluorescence intensity was measured with an excitation wavelength of 494 nm and an emission wavelength of 525 nm, using a bandwidth of 5 nm.

3.4   Results and Discussion

The cloning process of the Round 10 aptamer, specifically selected due to its elevated DNA concentration and profile, as depicted in the measurements shown in Figure 5, involved several steps to ensure amplification and isolation. This selection process ensured that only colonies containing the desired aptamer sequence were chosen for further analysis. E. coli was incubated as a control. However, since it lacked ampicillin resistance, no growth was observed, as depicted

in Figure 7. Once identified, the colonies were carefully harvested from the plate by scooping and

transferring them into 100 µL of water. This step ensured the preservation of the colonies and their

associated DNA content for subsequent amplification.
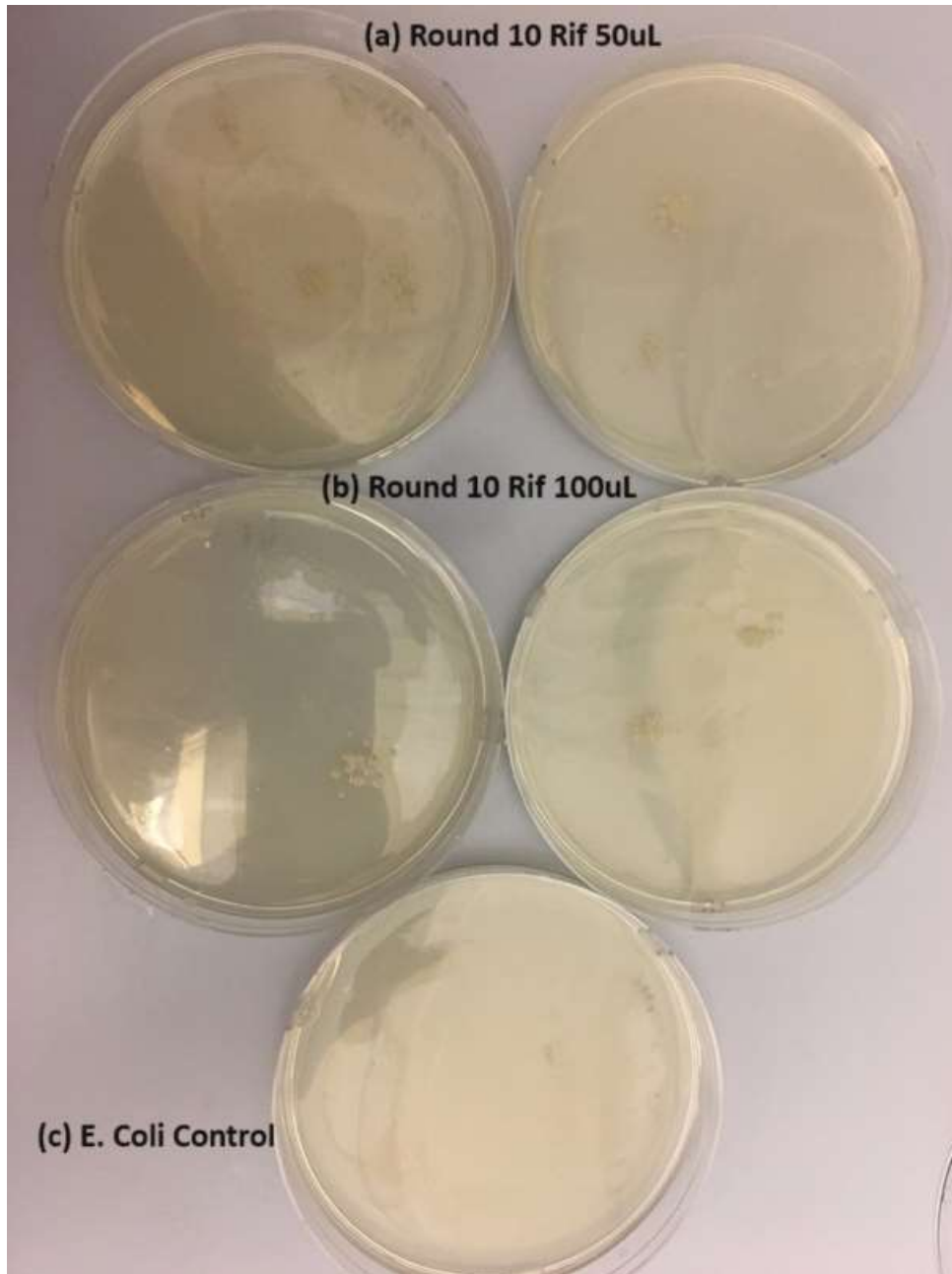
Figure 7. (a) The growth observed for Round 10 Rif at a volume of 50 µL in duplicate, (b) The growth for Round 10 Rif at a volume of 100 µL in duplicate, and (c) The absence of growth observed for the E. coli control.

The harvested colonies underwent amplification using the polymerase chain reaction (PCR) method. Through PCR amplification, the DNA from the harvested colonies was exponentially multiplied, resulting in a significant increase in the quantity of the Round 10 aptamer sequence. Figure 8 presents information regarding the DNA concentration of colonies derived from the cloning process. This figure provided a quantitative assessment of the success of the cloning procedure, offering insights into the yield and concentration of the DNA obtained from each colony. The DNA concentration data was valuable in evaluating the efficiency of the cloning process and provided a basis for comparing different colonies.
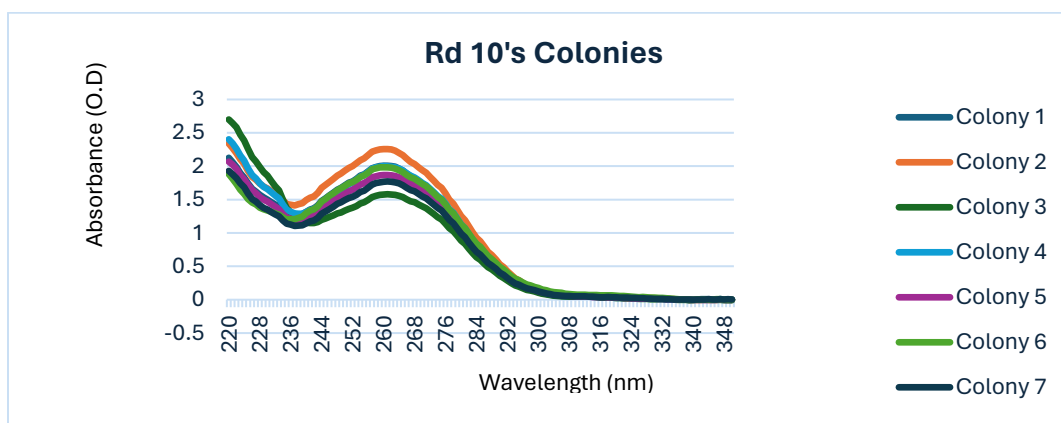
Figure 8. Absorbance of DNA Concentration for round 10's seven colonies after cloning.

Gel electrophoresis allowed the visualization and analysis of nucleic acids based on size and structure. Figure 9 illustrates the distinctive bands corresponding to ssDNA generated from each colony in this context. The fact that each colony displayed a single band in the gel electrophoresis results is a significant indicator of the success of the cloning process. A single band suggests the production of a specific and uniform DNA product, reinforcing the reliability and specificity of aptamer cloning.

Figure 9. DNA band for round 10's first 7 colonies using Gel Electrophoresis

The investigation into the genetic makeup of the colonies involved obtaining the reverse complementary sequences, which were sent to GENEWIZ for sequencing analysis. Knowing the forward primer M13 region on the vector (TAGGGAAGAGAAGGACATATGAT TTGACTAGTACATGACCACTTGA), reverse primer M13 region on the vector (ATCATATGTCCTTCTCTTCCCTA TCAAGTGGTCATGTACTAGTCAA), and knowing the EcoR1 sequences near the PCR product, the sequences for each colony were analyzed. Based on the predicted structures, colonies 3, 4, 7, and 12 were selected and sent to be synthesized by Integrated DNA Technologies (IDT) Company for further analysis.

The DNA sequences were entered into the University of Rochester Structure Prediction Tools to gain further insights into the structural characteristics of the aptamers[84]. These tools are designed to predict the secondary structure of nucleic acids based on their primary sequence. DNA was specified as the type of nucleic acid, and a temperature of 298K, along with other default parameters, was employed. The secondary structure prediction provided an understanding of the aptamer sequences' potential folding patterns and conformational dynamics. This predictive approach aids in revealing the three-dimensional arrangement of the nucleotides, providing information about the aptamers' structural properties and potential functional domains, as shown in Figure 10.

(a) Colony 2.
CAGCACAC<u>TACCAT</u>ACTACCCCCTACCTCACGCCCCCGCC
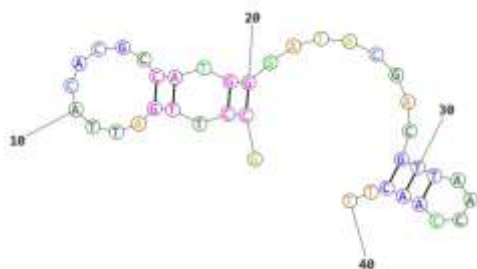
(b) Colony 3.
GCCTTGATT<u>ACAC</u>GCCATGGGATACGACGTT<u>AACCAA</u>CTT
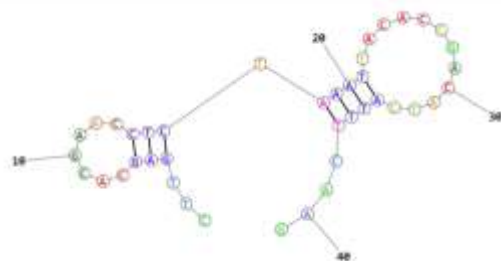
(c) Colony 4.
CTTGAGCACG<u>AACCTC</u>TAAATTACACCGACATCATTTCAAG
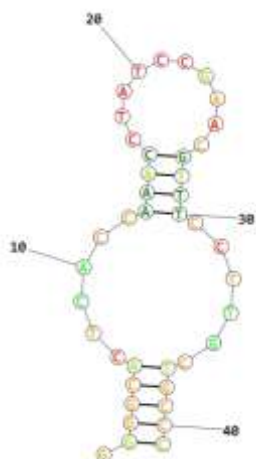
(d) Colony 5.
 GGGGCACTCACCA<u>AAACCTA</u>TCCGAACGTTTCCTTGCTGCCC
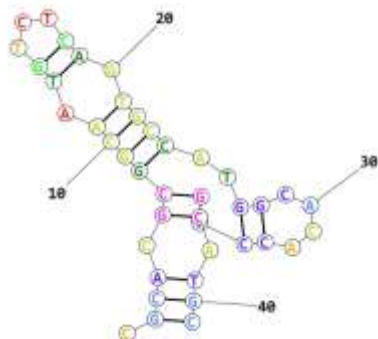
(e) Colony 6.
 CGCACGCGGCAATGTCTCAGTGCCATGGC<u>ACAC</u>CTGCATGC
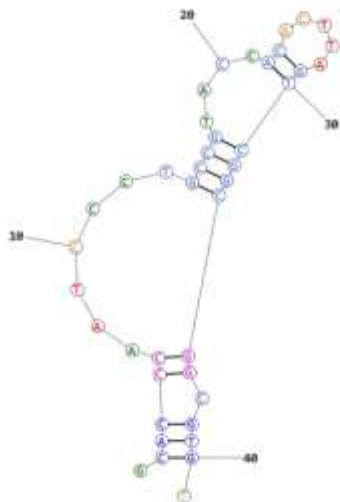
(f) Colony 7.
 GCACCCAATCCCTGCCGTACC<u>ACAC</u>TTAGTCGGCGGCGTGT
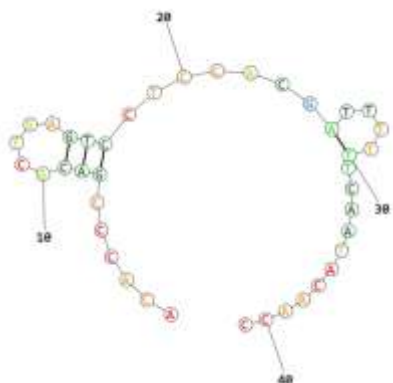
(g) Colony 8.
  <u>ACAC</u>CCGACGCTGAGTCCTCCACGATTTTTTCAATACAACC

(h) Colony 9.
  GACC<u>ACAC</u>ACCACCCCGCCGAAATTTACCCCGACAGGTTTG
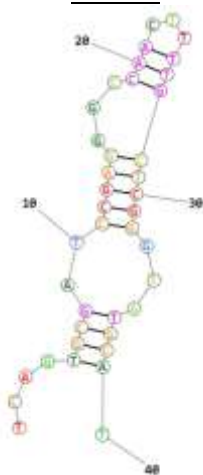
(i) Colony 10.
  TCAGTGCGATCCGAGGGCCA<u>AC</u>TTTTGCTCGGGTATGCAT
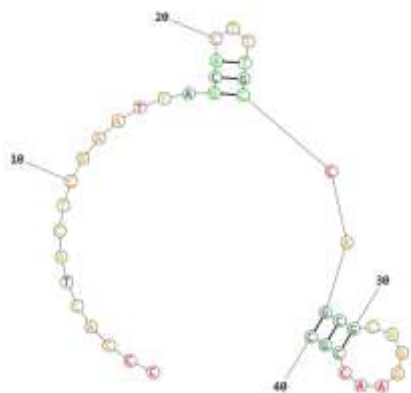
(j) Colony 11.
    CCC<u>ACTAC</u>TCGAATTAGCACTTTGCCAGCGCAGGAACCGC
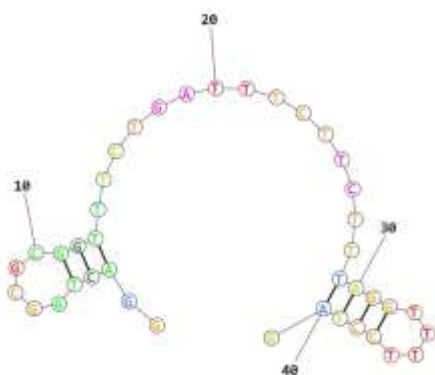
(k) Colony 12.
    GGACTGGCGCGGTTTCTGATTTCTTCTTTAGGTT<u>TTCCTAG</u>

Figure 10. DNA sequences from colonies (a) to (k) showcase the predicted secondary structure of the aptamers acquired through cloning.

Figure 10 visually represents the predicted secondary structure of the aptamer sequences obtained from the cloning process. The figures depict the aptamer sequences' potential folding patterns and structural arrangements. Visualizing the secondary structure offers a glimpse into the potential three-dimensional conformation of the aptamer, allowing the identification of regions of stability and flexibility. The binding properties of aptamers, along with their biological impact, are significantly influenced by their spatial conformation, primarily delineated by the pattern of base pairs formed within the nucleic acid sequence[85]. This secondary structure provides insights

into the aptamer's ability to interact with its target molecule and perform its intended function. At its core, the secondary structure comprises various elements, including stems, inner loops, bulges, and hairpins, which collectively contribute to the overall three-dimensional arrangement of the aptamer. These structural motifs play the roles in determining the stability, specificity, and affinity of the aptamer-target interaction[86]. Colonies 2, 8, 11, and 12 exhibit pseudoknot structural motifs, whereas colonies 3, 4, 5, 6, 7, 9, and 10 predominantly display main structural elements such as stems, inner loops, bulges, and hairpins. Figure 11 offers insights into the spatial arrangement and organization of the aptamer's nucleotide sequences for colony 3. For instance, stems form through the pairing of complementary nucleotides, providing structural rigidity and stability to the aptamer. On the other hand, inner loops and bulges introduce flexibility and structural diversity, allowing the aptamer to adapt to different target conformations. Additionally, hairpins contribute to the overall folding of the aptamer and can serve as recognition sites for target binding[87]. Understanding the interplay between these secondary structure elements is central to explaining the functional mechanisms of aptamers and optimizing their performance for various applications.
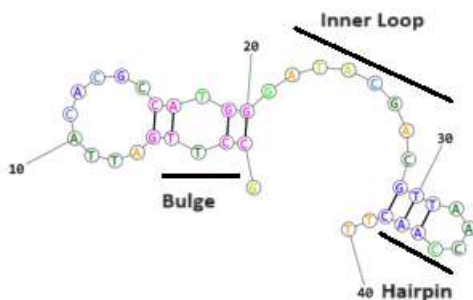
Figure 11. The secondary structure of the aptamer from Colony 3 sequences highlights its structural elements, including the inner loop, bulge, and hairpin.

The binding assays for the obtained aptamers constituted a valuable phase of the experimental analysis. Among these aptamers, Aptamer Rif_3 emerged as particularly noteworthy

due to its promising results. To measure fluorescence intensity, these assays involved utilizing the Tecan Spark Plate reader with specified parameters, including a wavelength excitation of 480 nm and a wavelength emission of 520 nm.
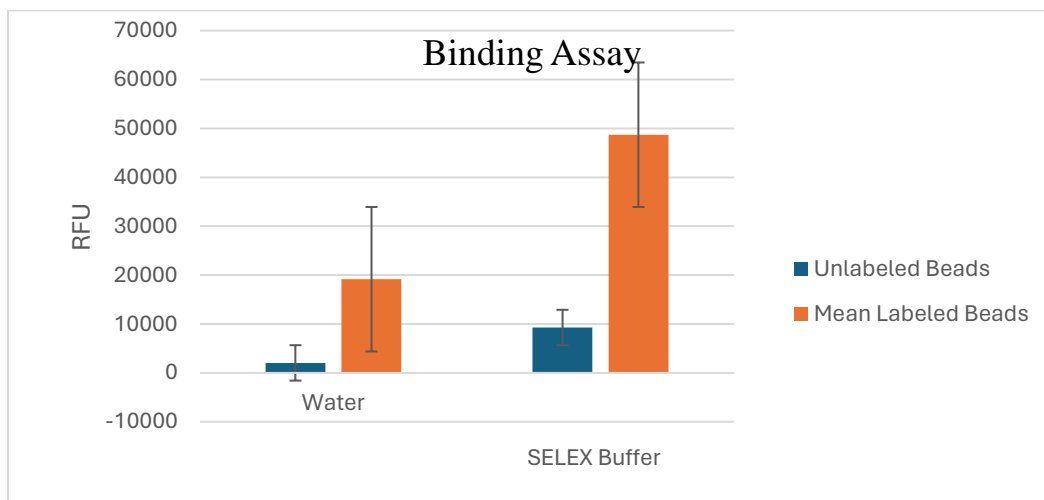
Figure 12. Graphed data for Aptamer Rif_3, n=3. The aptamer showed selectivity for labeled beads when compared to the control, the unlabeled beads.

The comparison between labeled and unlabeled beads and the evaluation of the Relative Fluorescence Unit (RFU) in water versus 1X SELEX buffer allowed for an assessment of the binding specificity of the aptamers. Remarkably, Aptamer Rif_3 exhibited distinct and favorable outcomes, as shown in Figure 12. The data revealed that the SELEX buffer generated a higher RFU compared to water, indicating that the aptamer had an elevated affinity for the target in the presence of the SELEX buffer. Moreover, the labeled beads, serving as the target, demonstrated a higher RFU than the unlabeled beads, reinforcing the aptamer's capacity for specific and robust binding interactions. The performance of Aptamer Rif_3 in these binding assays is indicative of its heightened specificity for the labeled beads, suggesting a strong and selective binding affinity

for the intended target. These promising results of Aptamer Rif_3 in the binding assays mark an advancement in more targeted assays.

Building on the promising results, an investigation was conducted to explore the influence of the competitive drug Amphotericin B (AmB) on the aptamers. This executed experiment was performed in triplicate to ensure data reliability. The aptamers were subjected to specific treatments and interactions with labeled beads, followed by subsequent steps involving exposure to Rif or AmB solutions. The outcomes were assessed by measuring Relative Fluorescence Units (RFU) in the supernatant, with the addition of Oligreen dye, known for its non-intrinsic fluorescence. Figure 13 visually presents the overall results, offering insights into the impact of AmB on the aptamers and underscoring the significance of Oligreen dye in facilitating data interpretation. These findings contribute to our understanding of competitive dynamics in drug-binding research.
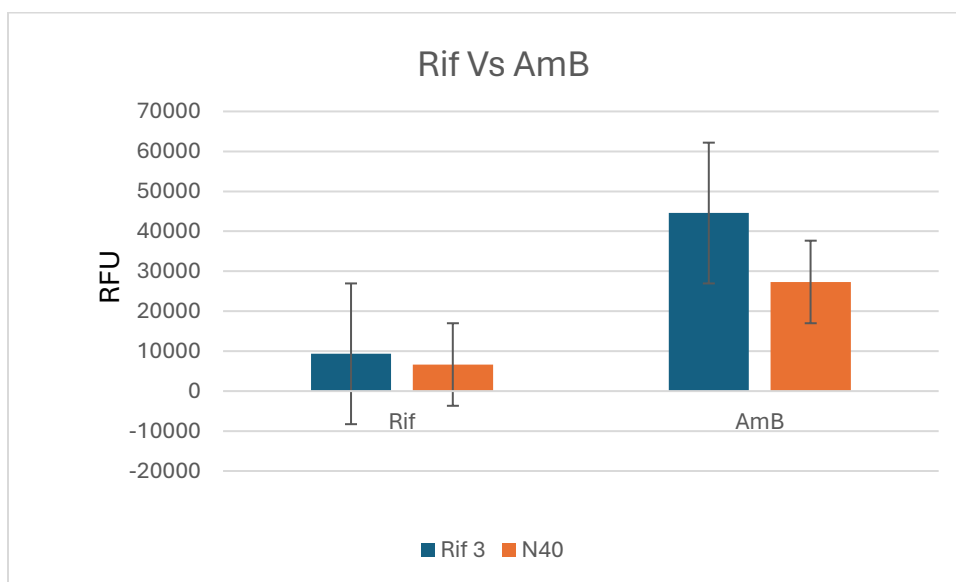
Figure 13. Graphed data for aptamer Rif_3 and nonselective aptamer N40 when competitor AmB was introduced in the experiment, n=3.

The findings revealed that, in both instances, the aptamer demonstrated detachment from the beads, with the Rif_3 aptamer exhibiting more detachment compared to the non-specific N40

library. Interestingly, Amphotericin B (AmB) induced a higher RFU compared to Rifampicin (Rif). This observation suggests that, in a solution, AmB might have a stronger binding affinity to the aptamer. Further experiments are necessary to validate this observation conclusively. Nonetheless, the insights from the outcomes presented in Figure 13 offer an understanding of the competitive dynamics between AmB and the lead aptamer.

Graphene oxide (GO) is a graphene derivative with unique properties that enable interaction via π-π stacking and hydrophobic interactions between the bases and GO[88]. This facilitates strong adsorption of single-stranded DNA (ssDNA) onto the surface of GO. Additionally, the phosphate skeleton of DNA provides protective effects on base pairs. Consequently, GO exhibits weak adsorption on double-stranded DNA (dsDNA)[89]. This study detected aptamers based on GO using a fluorescence detection method. Aptamers are modified with fluorescence groups. The fluorescence of the aptamer is quenched due to the fluorescence quenching effect of GO in the absence of the target. However, when the aptamers bind to the target, they dissociate from the surface of GO, leading to fluorescence recovery. Therefore, the presence of the target was detected by the change in fluorescent signal.

The Fluorescein isothiocyanate (FITC) labeled aptamer Rif_3 (Rif_3_fluor) was purchased to perform the GO assays. Using the Tecan Microplate Reader, the plate was read at T=0, T=15, T=30, and T=60 minutes at fluorescence intensity, wavelength excitation 494 nm, Wavelength emission 525 nm, and Bandwidth 5. The blank wells remained relatively constant, while the Rif and the AmB changed slightly over time.

The graphene assay was repeated using 1µL of 10mg/mL graphene instead of 10µL of 10mg/mL graphene and 1µL of Aptamer Rif_3_Fluor in one assay and another assay using 1µL of 10mg/mL graphene and 10µL of fluorophore Aptamer Rif_3_Fluor. Figure 14 shows the results

obtained. There is no clear difference between Rif and AmB selectivity, while 1% DMSO and blank wells showed no selectivity.
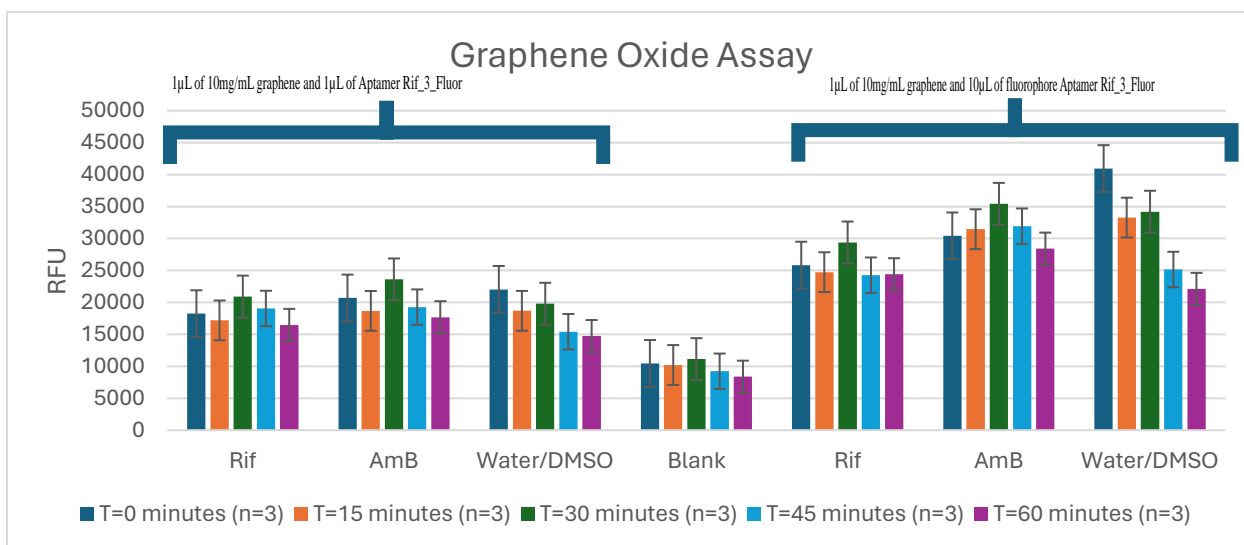
Figure 14. The average of graphene assay's results. 1µL of 10mg/mL graphene and 1µL of Aptamer Rif_3_Fluor. 1µL of 10mg/mL graphene and 10µL of fluorophore Aptamer Rif_3_Fluor

Based on the preliminary results, further analysis is needed to understand the aptamer interaction on GO. Because minor to no change was observed for the aptamer Rif_3_Fluor when the Rif was added compared to when AmB was added.

Circular Dichroism (CD) spectroscopy experiments were conducted to investigate structural changes and folding of aptamers in the presence of graphene and Rif. Certain molecules possess chiral or secondary structures detectable by CD spectroscopy. Based on the sequences obtained, secondary structures potentially interact with the drug of interest, Rif. CD spectra of the obtained rounds were analyzed, as shown in Figure 15, to understand the folded DNA, utilizing a wavelength range from 320 nm to 200 nm. Notably, molecules such as amino acid residues, sugars, proteins, and nucleic acids absorb left and right circularly polarized light differently due to

asymmetric carbons[90]. We hypothesize that binding to the target molecule could induce changes in the aptamer's secondary structure. In the presence of graphene, as shown in Figure 16, the CD spectra changed for Aptamer sequences GCCTTGATTACACGCCATGGGA TACGACGTTAACCAACTT, indicating graphene's influence in the experiment.
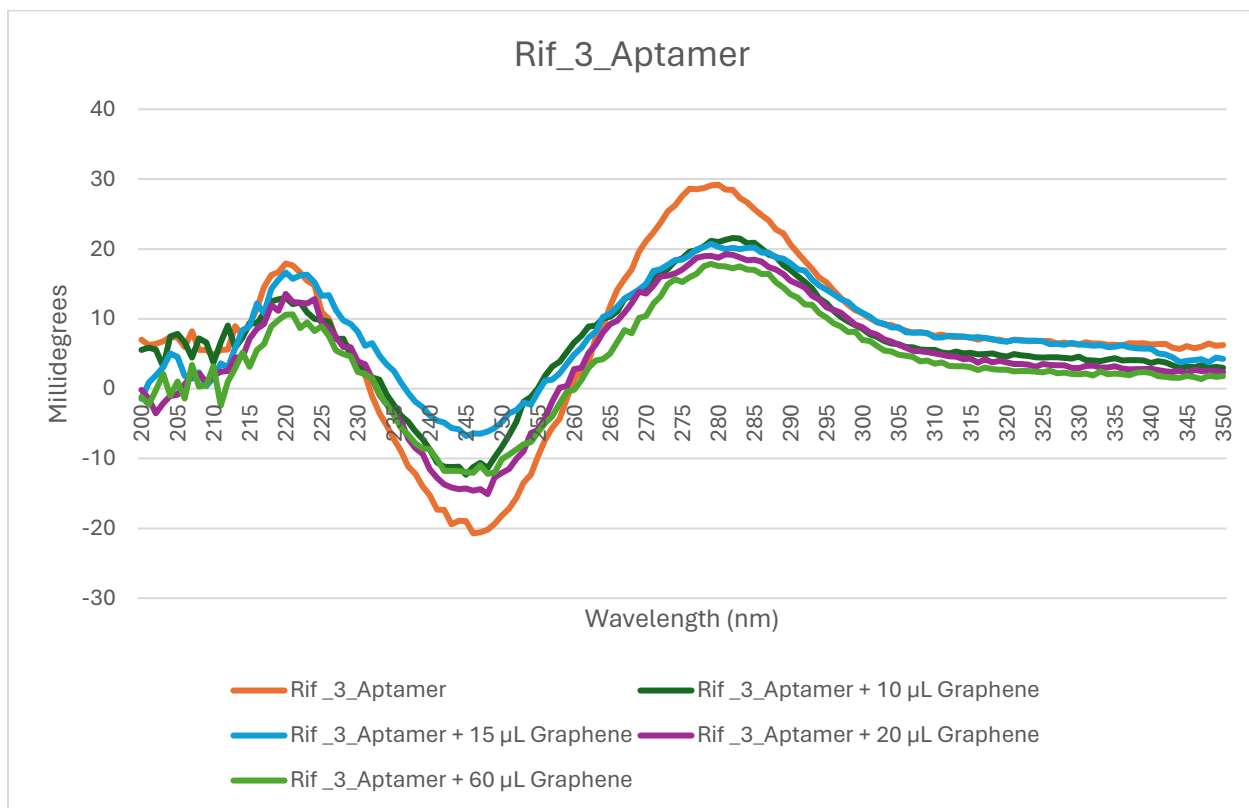
Figure 15. CD spectroscopy experiments investigating structural alterations and folding dynamics of Rif_3_Aptamer in the presence of graphene at concentrations ranging from 0 µL to 60 µL (0 µL, 10 µL, 15 µl, 20 µl, and 60 µL.

3.7   Conclusion

This study demonstrates the cloning process of the Round 10 aptamer and the aptamer characterization. The DNA concentration data, gel electrophoresis results, and structural predictions explain the cloned aptamers' efficiency and specificity. Aptamer Rif_3's performance in binding assays highlights its potential for targeted applications. The competitive experiments

with Amphotericin B offer intriguing insights into the aptamer's detachment dynamics, suggesting a stronger binding affinity for AmB. The study underscores the importance of non-intrinsic fluorescence in probing structural and environmental changes in biomolecules, contributing to the broader understanding of aptamer structure-function relationships and competitive dynamics in drug-binding research.

Chapter 4. Interaction of azobenzene moiety on the aromatic amino acid tryptophan

4.1   Abstract

Photocontrol is known to regulate biological processes and demonstrates efficacy in manipulating biomolecular structures. Among diverse photoswitchable compounds, azobenzene moieties have emerged as particularly versatile. Their widespread utilization in controlling biomolecular structures is attributed to the intrinsic connection between the azobenzene structure and the electron density distribution of the bonds, which significantly contributes to the isomerization of the molecule. The cis and trans states of azobenzene exhibit geometrical alterations when exposed to light. This unique property induces conformational changes capable of modifying the structure of proteins or ligands, consequently influencing the protein's binding site. Despite the considerable progress in understanding the impact of azobenzene on biomolecular structures, there remains a gap in knowledge regarding its interaction with aromatic amino acids, especially when they are near the azobenzene moiety. While previous studies have explored the broader implications of azobenzene-induced conformational changes, the specific effects on aromatic amino acids have not been comprehensively investigated. This work aims to address this gap by presenting a preliminary examination of the intricate interplay between azobenzene and aromatic amino acids. By investigating this, we seek to unravel potential nuances in the interaction dynamics that may arise when aromatic amino acids are near the azobenzene moiety. The findings of this study could offer valuable insights into the broader applications and implications of azobenzene-driven photocontrol in biological systems.

4.2   Introduction

At room temperature, the azobenzene chromophore exhibits a natural nonfluorescent behavior in solution, a characteristic widely documented in the literature, with only a few noteworthy exceptions[91]. One such exception involves the incorporation of azobenzene into a bilayer structure, where a distinct fluorescence emission was observed. This phenomenon was attributed to excited states of azobenzene moieties, representing a unique circumstance that deviates from the general nonfluorescent nature of azobenzene in aqueous solution[92].

This fluorescence emission was associated with specific changes in absorption characteristics, notably a decrease in absorption intensity around 365 nm resulting from the $\pi \rightarrow \pi^*$ transition and a simultaneous increase in absorption intensity around 465 nm due to the $n \rightarrow \pi^*$ transition[93]. These alterations in absorption properties provided insights into the reversible trans-cis isomerization processes induced by photochemical stimuli, a feature that has been extensively studied, particularly in substituting azobenzene amino acid derivatives for proline residues in melittin[94].

Despite the research on azobenzene's behavior in various contexts, exploring azobenzene moiety-coupled with aromatic amino acids has been relatively limited[95]. This study aimed to provide understanding by synthesizing a combination of tryptophan (W), a naturally fluorescent amino acid, and 4-(Phenylazo)benzoic acid (Z) using Fmoc solid-phase peptide synthesis (SPPS). This synthesis was undertaken to investigate the intriguing effects of the photoswitchable molecule, azobenzene, and its potential interference with the isomerizing state of the chromophore[96].

The hypothesis guiding this investigation suggested that the combination of tryptophan and 4-(Phenylazo)benzoic acid would yield a molecule with unique optical characteristics, given the

inherent fluorescence of tryptophan and the photoswitchable nature of azobenzene. To assess the intrinsic characteristics of the synthesized peptide, absorbance measurements were employed to determine the molar extinction coefficient in understanding the optical behavior of the compound[97].

4.3   Aromatic Amino Acid and Azobenzene Interaction

Tryptophan is one of the twenty (20) standard amino acids that constitute the building blocks of proteins. Tryptophan plays a crucial role in various physiological processes and serves as a precursor for synthesizing important biomolecules[98]. Tryptophan has a complex chemical structure featuring a heterocyclic aromatic ring. The indole ring is a distinctive tryptophan component responsible for many of its unique properties. The aromatic side chain contributes to the hydrophobicity of tryptophan and plays a significant role in protein folding and stability[99]. Its presence in proteins contributes to their overall structure and function. Tryptophan is unique among amino acids because it possesses intrinsic fluorescence. The indole ring absorbs ultraviolet light and emits fluorescence, making it a valuable probe in studies of protein structure and dynamics[100]. This aromatic nature allows tryptophan to absorb ultraviolet (UV) light with a peak absorption wavelength of around 280 nanometers, making it highly responsive to UV radiation.

The absorption of UV light by the indole ring leads to the excitation of electrons to higher energy levels. Subsequently, as these electrons return to their ground state, they emit fluorescence. This phenomenon is particularly valuable in biochemical and biophysical studies, as it provides a natural and intrinsic fluorescent probe for investigating the structure and dynamics of proteins[101]. In this research study, the intrinsic fluorescence of tryptophan was leveraged as a tool to probe the microenvironment of amino acids within peptides. The intensity and wavelength of the emitted fluorescence were influenced by the local environment surrounding the tryptophan residue. Factors

such as solvent accessibility, neighboring amino acids, and switchable molecule, such as azobenzene modulated the fluorescence properties of tryptophan.

It is widely recognized that photocontrol is an effective way to regulate biological processes. Azobenzene moieties have emerged as versatile structures with photo-switchable properties, making them valuable compounds[102]. They find extensive use in controlling biomolecular structures, owing to the correlation between the azobenzene structure and the electron density distribution of the bonds involved in the molecule's isomerization. The exposure of azobenzene to light induces significant geometrical alterations between its cis and trans states[103]. Previous research indicates that the conformational changes observed are substantial enough to impact the structure of proteins or ligands, thereby influencing the binding site of the protein[104]. However, exploring this phenomenon in the presence of aromatic amino acids near the azobenzene moiety remains incomplete. The present work examined the interaction between azobenzene and aromatic amino acids[96].

Previous investigations extensively substituted azobenzene amino acid derivatives for proline residues in melittin[94]. However, limited attention has been given to studying azobenzene moiety coupled with aromatic amino acids. In this research, we synthesized a hybrid peptide incorporating tryptophan (W) and 4-(Phenylazo)benzoic acid (Z) using FMOC solid-phase peptide synthesis (SPPS). This study sought to understand the interaction between the azobenzene moiety and the aromatic amino acid tryptophan.

4.4   Methods

4.4.1   Peptides Synthesis

The peptides were synthesized using tryptophan (W), 4-(phenylazo) benzoic acid (Z), and Alanine (A) to create WZ, AW, and AZ using solid support Wang resin (100–200 mesh) along with

standard solid phase peptide synthesis techniques[105]. The protection scheme utilized FMOC as the protecting group. The amino acid was coupled to preloaded Wang resin with the appropriate amino acid 100–200 mesh before proceeding to the deprotection. This was done using 3:3:6:1 molar ratios of amino acid: HCTU: DIEA: Resin for 1 h. After this coupling, the resin was washed with DMF, Methanol, and DCM three times. A solution of 10% piperidine in dimethylformamide (DMF) (v/v) was then used to deprotect the amino acid on resin with an incubation time of 20 min. The protecting group (FMOC) is removed from the growing peptide with the piperidine solution[106]. The coupling was monitored using a qualitative Kaiser Test. This test revealed successful coupling as clear/colorless beads, and each amino acid was coupled successfully. A final deprotection was prepared. Peptides were cleaved using a mixture of 95% TFA, 2.5% TES, and 2.5% water (v/v/v) for 2 h. The resulting solution was collected in a falcon tube. A steady stream of N_2 gas was used to evaporate the liquid. The remaining dried material was diluted to 10 mL in 10% acetic acid in water (v/v). The samples were frozen in the -80ºC freezer, lyophilized, and stored for further purification.

4.4.2 Purification

A Varian Prep Star chromatographic system (Palo Alto, CA) was used to purify the peptides. The Samples were diluted to 5 mL in 50% acetonitrile in water (v/v) with 0.1% formic acid (FA) buffer to make a 5 mg/mL concentration. The mixture was filtered through 0.45 mm filter and sonicated to remove air bubbles. The 5 mL filtrate was loaded into a 10 mL injection loop. The preparatory column was a Phenomenex Luna C18 column (250 × 21 mm, 10 μm, 100 Å). A 5 mL per minute flow rate was used at a gradient of 5-95% acetonitrile (ACN) with 0.1% FA. The 220 nm and 280 nm channels were used to monitor and detect the sample via dual channel detectors. Fractions were collected in 50 mL falcon tubes, and the volumes were reduced to 10-

20mL on a roto-evaporator. Solutions were frozen in the –80°C freezer. The synthesized peptides were lyophilized to dry powder and characterized.

High-performance liquid chromatography (HPLC) Shimadzu Nexera-i LC2040c device equipped with a photodiode array detector (PDA) was used to determine the purity of crude and purified peptides. A Phenomenex Hypersil 5 μm ODS (C18) 120Å, 125 x 4 mm LC Column was utilized as the stationary phase to determine the purity of the peptides. A 1 mg/mL peptide concentrations were produced in 50% ACN containing 0.1% FA and 50% water containing 0.1% FA. Experiments were conducted using a flow rate of 1 mL/min and injection volumes of 10 μL. A gradient of mobile phase 5–95%, water containing 0.1% FA, and ACN containing 0.1% FA. The data was gathered using the PDA detector with a spectral window ranging from 200 to 456 nm. The percent purity was determined at 220 nm, 280nm, and 320 nm using the area under the curve of peaks in the chromatograms.

4.4.3 Mass characterization

Peptides were analyzed with a Hewlett Packard 1100 MSD Electrospray Mass Spectrometer to determine their properties. After producing peptides at a concentration of 1 mg/mL in 50% ACN containing 0.1% FA and 50% water containing 0.1% FA. Flow rates of 0.5 mL/min were used for direct injections of 10 μL. Chemstation software was utilized for peak deconvolution.

4.4.4 Spectrochemistry

A NanoDrop 1000 Spectrophotometer (Thermo Scientific) was used to measure the absorbances of the synthesized dipeptides. The samples were diluted using various solvents depending on the experiment. UV light was used to irradiate the peptides depending on the

experiments. This was accomplished with a Blak-Ray UV Lamp, 366 nm wavelength, 115 V, 60 Hz, 0.16 amps, manufactured by UVP Inc. of Upland, California, and the blue (visible) light at 465 nm wavelength. The samples were tested using the spectrum, 220nm-750nm. The NanoDrop 1000 Spectrophotometer is equipped with a 1mm path length and operating software 1000 version 3.8.1 for data analysis.

The Beer-Lamber law was utilized to calculate the extinction coefficients of the peptides:

$$\text{Equation 1: } \epsilon_\lambda = A /(b * c)$$

Where A = absorbance value, ϵ_λ = wavelength-dependent molar absorptivity coefficient or extinction coefficient with units of /M/Cm, b = the path length in centimeters, c = analyte concentration in moles/liter or molarity (M)[97]. Peptide measurements were evaluated using the Tecan Spark plate reader. Depending on the experiment, different solvents and parameters were used. The samples were analyzed using parameters of excitation wavelength of 280 nm, excitation bandwidth of 5 nm, emission wavelength start of 300 nm, emission wavelength end of 600 nm, and emission bandwidth of 5 nm. The purified peptides were analyzed using parameters of excitation wavelength 365 nm, excitation bandwidth 5 nm, emission wavelength start 380-600 nm, and emission bandwidth 5 nm. The purified peptides were analyzed using the parameters used: excitation wavelength start 280 nm, excitation wavelength start 380 nm, excitation bandwidth 5 nm, emission wavelength 400 nm, and Emission bandwidth 5 nm. A 3D scan was performed using the following parameters: excitation wavelength starts 280-380nm, excitation bandwidth 5 nm, emission wavelength 400-600 nm, and Emission bandwidth 5 nm.

4.5   Results and Discussion

### 4.5.1   Design of Azobenzene-amino acid conjugates

Azobenzene and several of its derivatives undergo reversible changes from the typically more stable trans-form to the less stable cis-form upon exposure to Ultraviolet light, resulting in a wavelength-dependent photostationary structure.[107,108] Red-shifted azobenzenes tend to undergo rapid cis-to-trans conversions.   The conformational modification generated by isomerization of azobenezene derivatives has been used to regulate the biological characteristics of numerous systems.[109,110] As part of this research into 4-(Phenylazo)benzoic acid behavior, several peptides were synthesized and characterized, as shown in Figure 16, as the hypothetically most likely thermostable forms. Given the apparent significance of these molecules, these peptides, 4-(phenylidazenyl)(benzoyl)-L-tryptophan   (WZ),   L-alanyl-L-tryptophan   (AW),   and   4-(phenylidazenyl)(benzoyl)-L-alanine (AZ), were developed to determine if conjugation to aromatic amino acids can alter the photophysical properties of azobenzene and azobenzene derivatives.
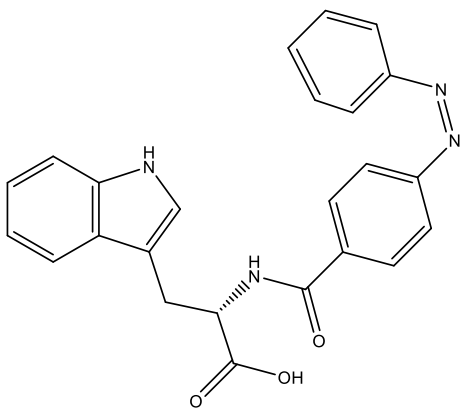
(a) (4-(phenylidazenyl)(benzoyl)-L-tryptophan (WZ)
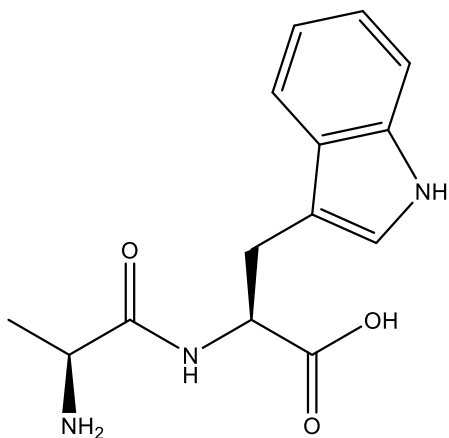
(b) L-alanyl-L-tryptophan (AW)
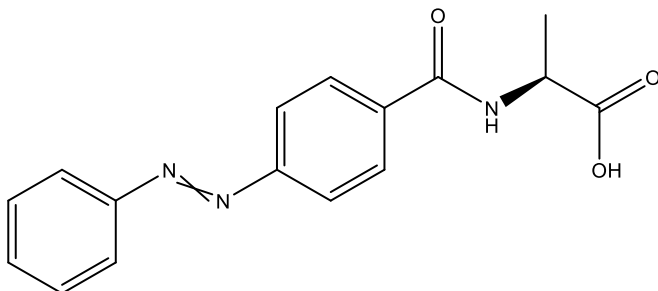
(c) 4-(phenylidazenyl)(benzoyl)-L-alanine (AZ)

Figure 16. Structure of the peptides (a) (Z)-(4-(phenylidazenyl)(benzoyl)-L-tryptophan (WZ), (b) L-alanyl-L-tryptophan (AW), and (c) 4-(phenylidazenyl)(benzoyl)-L-alanine (AZ).

Purification and characterization were performed for each peptide, namely WZ with an expected weight of 412.15 g/mol, AW with an expected weight of 275.13 g/mol, and AZ with an expected weight of 297.11 g/mol. Each purified peptide was subjected to characterization processes using mass spectrometry, which provided molecular weight information and structural insights, as shown in Figure 17. Furthermore, HPLC was employed to assess the purity of the peptides. HPLC analysis allowed for separating individual components within the peptide samples based on their respective retention times, providing a quantitative purity assessment. The obtained results revealed that the purity of each peptide exceeded 85%.
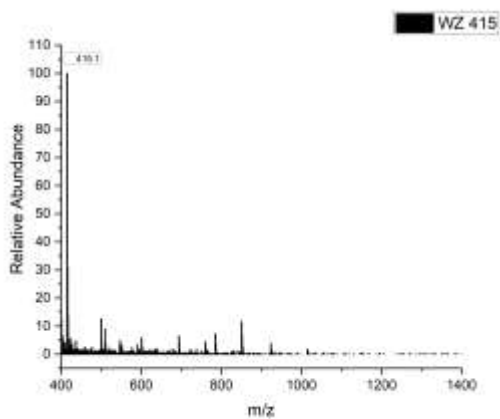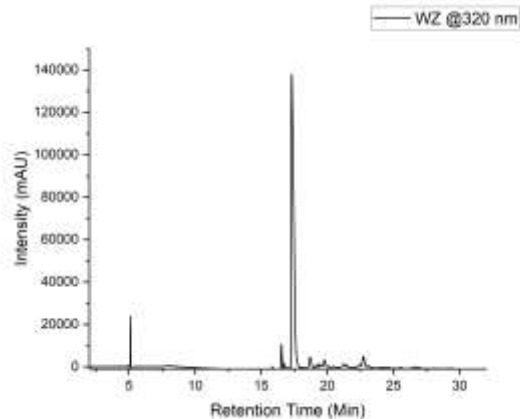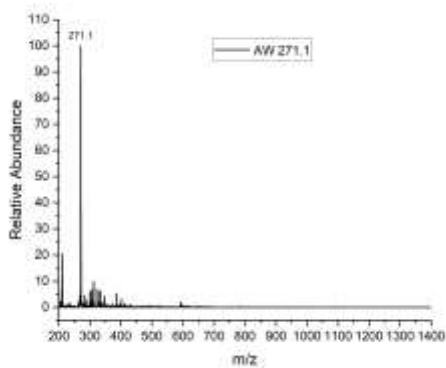
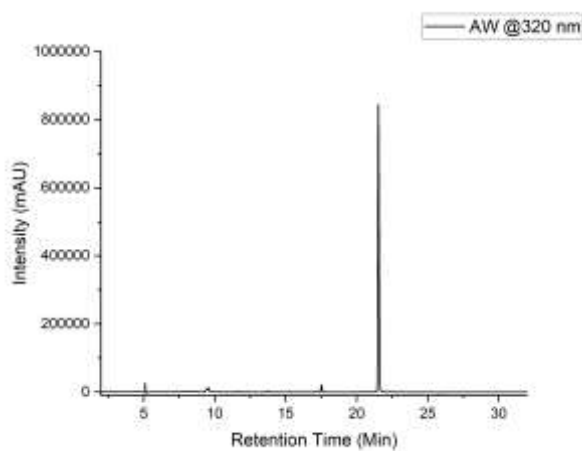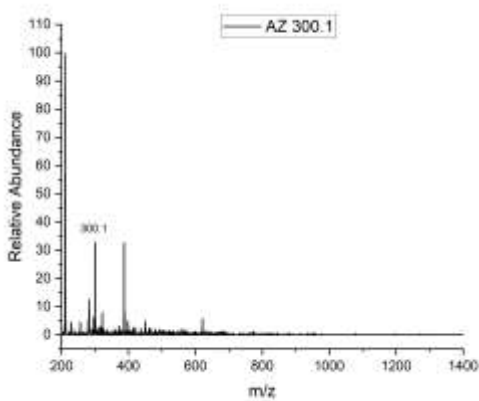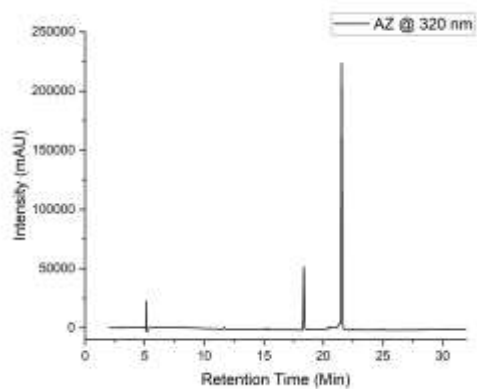**Figure 17.** Mass spectrometry data showing the molecular weight and structural characterization of peptides WZ (a1), AW (b1), and AZ (c1). HPLC chromatograms demonstrate the separation and purity assessment of peptides WZ (a2), AW (b2), and AZ (c2).

4.5.2   Photophysical Properties of the Azobenzene-amino acid conjugates

The combination of peptides in this study, particularly the specific sequence of amino acids in WZ, appeared to induce a molecular structure that distinctly interacts with UV light. This interaction results in visible fluorescence emission and is characterized by a shift towards longer wavelengths (red-shifted), as shown in Figure 18. Under UV irradiation, the synthesized peptides exhibited a visually discernible fluorescence compared to counterparts AZ and AW. This phenomenon highlighted the development of a molecule with unique and intriguing optical characteristics.
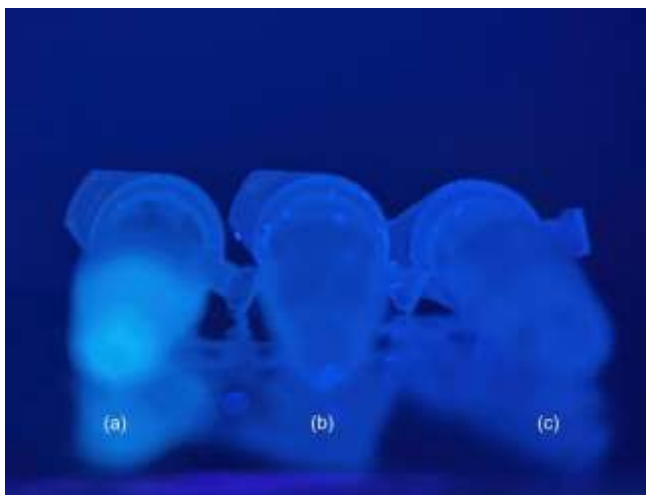
Figure 18. The synthesized peptides irradiated with UV light, (a) WZ exhibits visible red-shifted fluorescence when compared to (b) AZ and (c) AW.

Determination of the concentration of the aqueous samples was performed by measuring their absorbance in the near-ultraviolet region using a spectrophotometer. The control Tryptophan was diluted at various concentrations and scanned from 220 to 750 nm. At each dilution, the maximum absorbance (O.D) at 280 nm for Tryptophan was selected to calculate the extinction coefficient, as shown in Figure 19 using the Equation 1. The average extinction coefficient was

5714 /M/Cm when the control, Tryptophan, was dissolved in 50% acetonitrile. This determined average extinction coefficient for the Tryptophan is comparable to Mach et al. at 5540 /M/Cm.[111] The maximum absorbance versus the concentration was plotted, and the R squared was greater than 0.99.
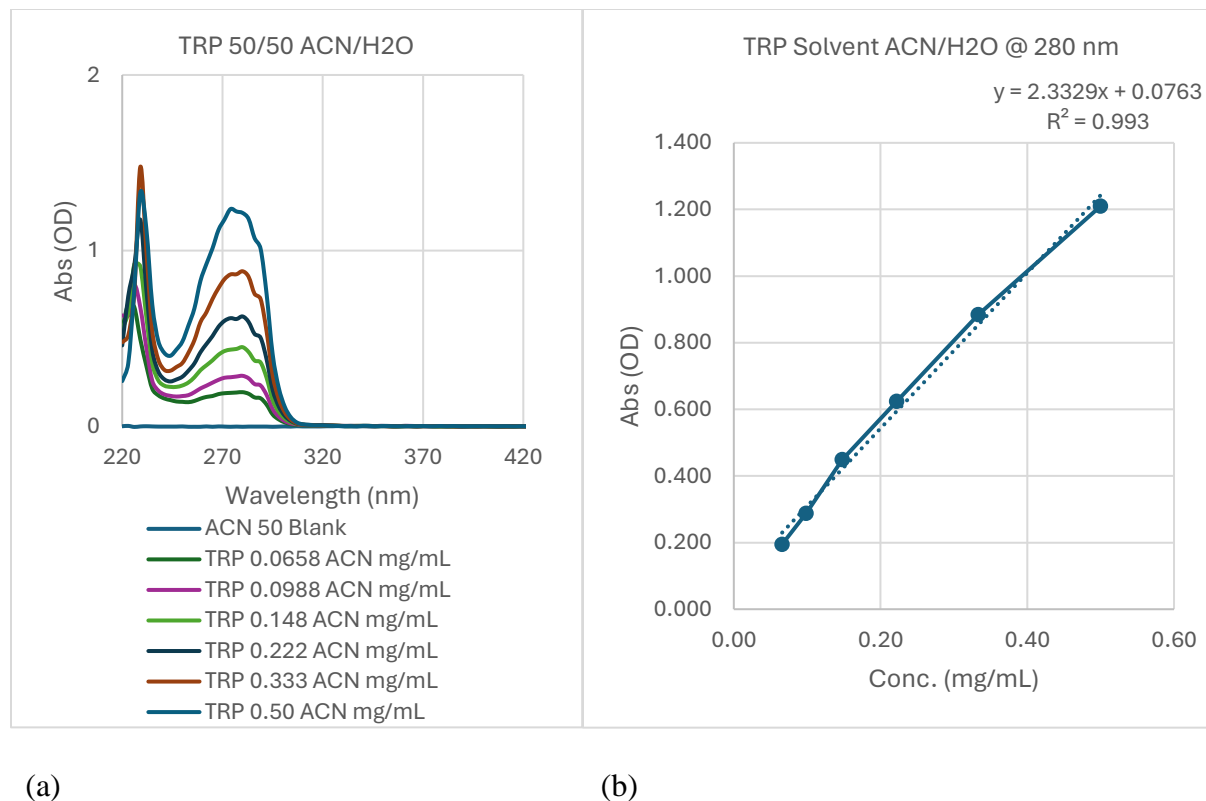
Figure 19. The absorbance of various concentrations versus the scanned wavelength in (a) and the linear curve of maximum absorbance versus the concentrations in (b).

The overall extinction coefficient for the synthesized peptides was determined, as shown in Figure 20. For the synthesized peptides, the various concentrations were irradiated for 10 minutes using Ultraviolet light, and the absorbance of the samples was measured. The measurements were repeated after incubating the samples using visible light. The maximum

absorbance versus the concentration was plotted, and the R squared for each plot was greater than 0.99.
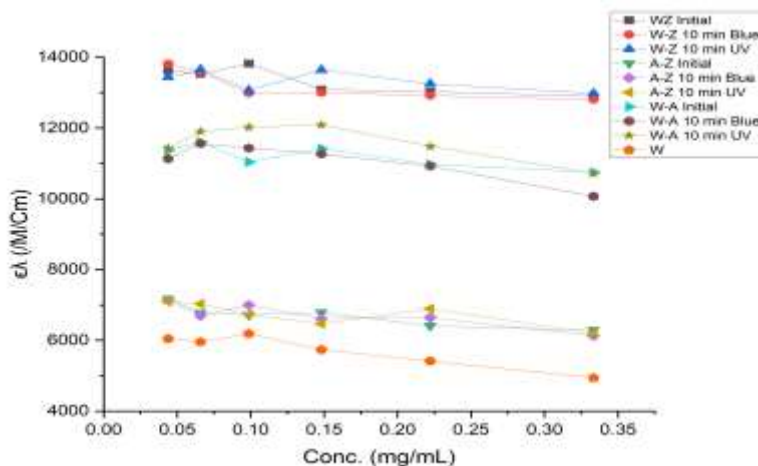
Figure 20. The graph of the Extinction coefficients versus the concentration for the synthesized peptides at initial state, after incubating for 10 minutes with visible light, 465 nm, and after irradiating for 10 minutes with UV light, 366 nm.

Based on the data, the initial Extinction coefficients are comparable when the samples are irradiated with UV and visible light, as shown in Table 2. The azobenzene within the peptide, WZ, remained the same when incubated with either visible or ultraviolet light, as depicted in Figure 21.

Table 2. The average Extinction Coefficient is shown for the peptides at their respective maximum absorbance wavelength.

Samples	Average $\epsilon\lambda$ ($M^{-1}cm^{-1}$)	Wavelength (nm)
W	5714	280
WZ Initial	13331	
WZ 10 min Vis	13186	280
WZ 10 min UV	13339	
AZ Initial	6693	
AZ 10 min Vis	6701	274
AZ 10 min UV	6735	
AW Initial	11194	
AW 10 min Vis	11066	265
AW 10 min UV	11608	

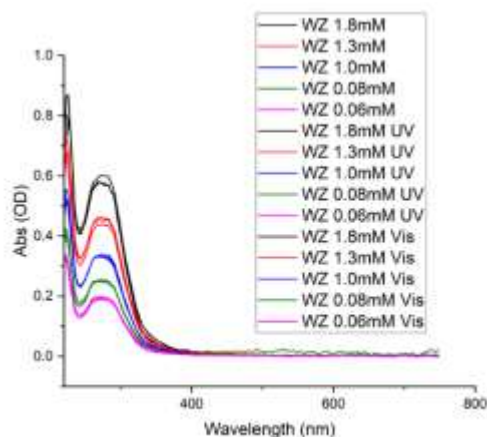**Figure 21.** The graph of absorbance measurements for WZ at various concentrations. The samples were irradiated for 10 minutes using UV light and incubated using visible light.

The fluorescence intensity of light-induced isomerization was measured for the synthesized peptides. All purified samples were serially diluted at various absorbances. Using the following parameters on the spectrofluorometer: excitation at 365 nm and emission wavelength 380-600 nm, the samples were measured using a 96-well black plate. The samples were irradiated with 366 nm light. When exposed to visible or ultraviolet light, the azobenzene in the WZ peptide showed no noticeable change in spectra, as seen in Figure 22. When the WZ sample is excited at 365 nm from the plate reader, the sample emits maximum Relative Fluorescence Unit (RFU) at around 475 nm. Statistical analysis of the RFU values, as illustrated in Figure 23, indicated a variation in RFU for the peptide. However, the wavelength corresponding to the maximum RFU demonstrated no statistically significant difference (ANOVA, $p > 0.05$) for the samples.
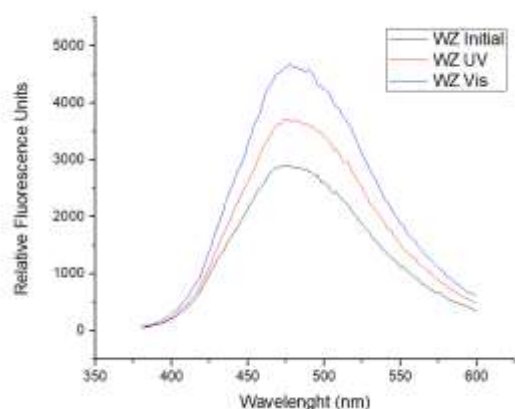
Figure 22. Representative traces of peptide fluorescence with UV and visible light exposure. The peptide maximum fluorescence was determined initially after irradiating at 366nm light (UV) and after relaxation in visible light (Vis).
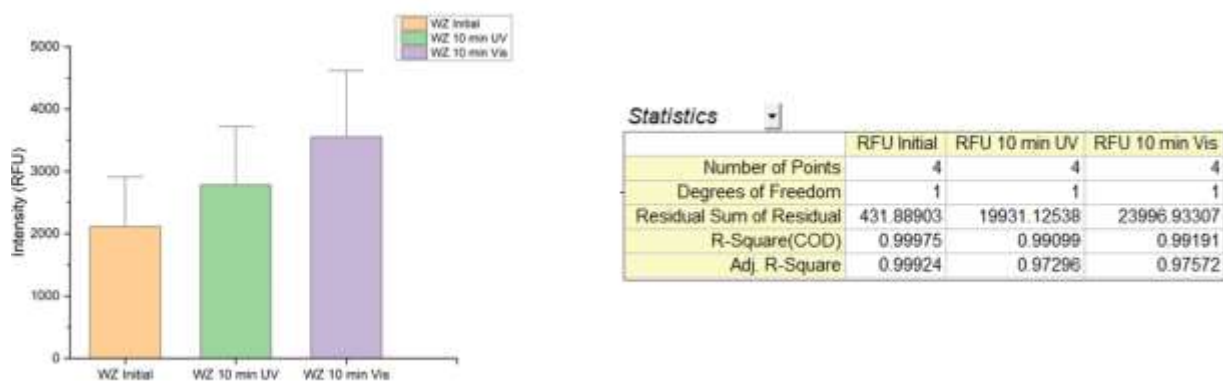

Statistics ▾			
	RFU Initial	RFU 10 min UV	RFU 10 min Vis
Number of Points	4	4	4
Degrees of Freedom	1	1	1
Residual Sum of Residual	431.88903	19931.12538	23996.93307
R-Square(COD)	0.99975	0.99099	0.99191
Adj. R-Square	0.99924	0.97296	0.97572

Figure 23. Statistical analysis of WZ, including the initial condition, irradiated for 10 minutes with UV light and incubated for 10 minutes with visible light, n=4.

Other researchers have investigated the aggregation characteristics of photoresponsive azobenzene-containing compounds.[112,113] In high concentrations or aggregation, fluorophores exhibit strong intermolecular $\pi \rightarrow \pi$ interactions, resulting in either weak emissions or non-emission in aggregates. To study this effect, the visibly fluorescent materials, WZ, were serially diluted, and the visibly fluorescent, red-shifted were observed when irradiated using the UV light at various concentrations, as shown in Figure 24. The persistence of fluorescence at low concentrations suggests that this is not merely an aggregation effect. To further prove this point, the WZ peptide

was denatured by adding 2 μL of concentrated Hydrochloric acid (HCl). The red-shifted peptide

was no longer visibly fluorescent, and the RFU intensity was significantly reduced when excited

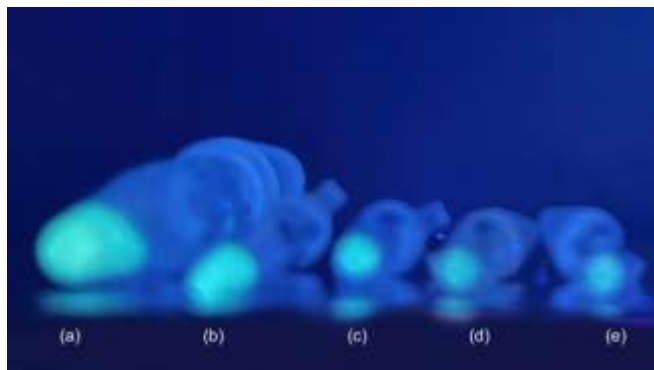at 365 nm with an emission 380 nm to 600 nm, as shown in Figure 25.

Figure 24. Serially diluted peptides under UV light. The serially diluted WZ peptides exhibited red-shifted characteristics irrespective of concentration (a) 1.8mM, (b) 1.3mM, (c) 1.0mM, (d) 0.08 mM, and (e) 0.06 mM.
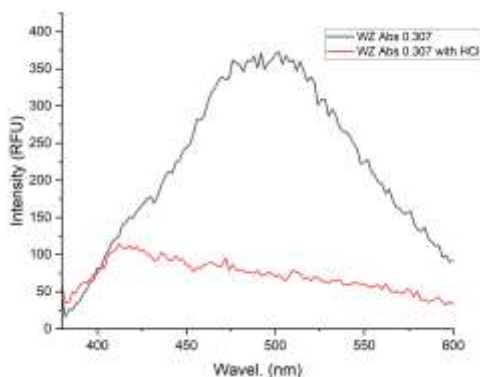
Figure 25. The peptide bond was cleaved using HCl. Upon cleavage, the peptides were no longer visibly fluorescent, and the fluorescence intensity decreased between 450 nm and 550 nm.

The Stokes shift is the difference in wavelength between the spectral position of the first

absorption band's maximum and the fluorescence emission's maximum. Small Stokes shift limits

the range of applications and is especially problematic for uses.[114] In this research study, the

peptides were subjected to a 3D fluorescence scan, excitation wavelength 280 nm to 380 nm,

emission wavelength 400 nm to 600 nm as shown in Figure 26, and the stokes shifts were

calculated as seen in Table 3 by identifying the point of maximal RFU and subtracting the excitation wavelength from the emission wavelength. The peptides exhibited an apparent Stokes shift much higher than the tryptophan-alanine or the azobenzene-alanine complex. This again highlighted that proximity to an aromatic amino acid can lead to unusual photochemical properties.

Table 3. The approximate Stokes Shift for the peptides

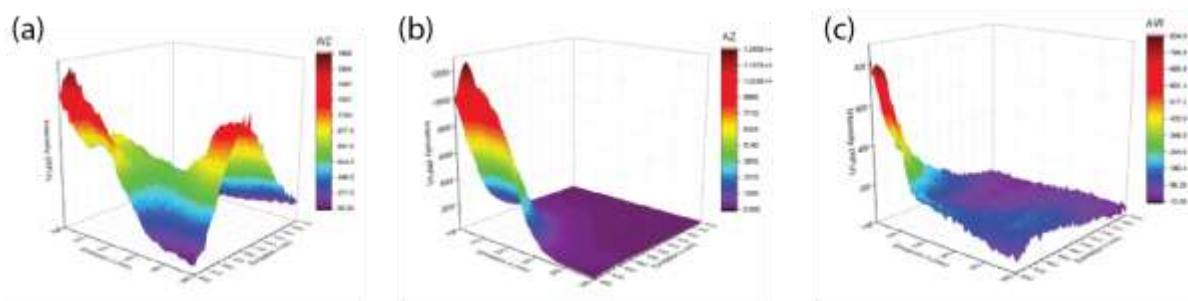| Peptide	Emission λ (nm)	Excitation λ (nm)	Max intensity	Stokes Shift
WZ	408	288	6783	120
AW	304	268	12862	36
AZ	310	268	6509	42

Figure 26. 3D fluorescence scanned of the synthesized peptides WZ (a), AZ (b), AW (c).

4.6   Conclusion

The structure and function of a peptide can be successfully regulated by molecules like azobenzene if an appropriate motif is designed. It is, therefore, crucial to comprehend how amino acids like tryptophan interact and influence the isomerization of a photoswitchable molecule. It may even be possible to eventually incorporate this moiety into larger protein structures either by post-translational chemical modification or through tRNA engineering.[115,116] Previous studies have shown that azobenzene can impact the structure of peptides in various ways. It is known that peptides stapled with azobenzene on side groups can control peptide alpha-helical function.[117] Azobenzene derivatives have also been shown to modulate the structure of nominally beta-sheet

peptides.[118] Again, these experiments rely on isomerization to influence secondary structural changes in peptides. Azobenzene has also found use with other biological or bio-inspired molecules, including nanoparticles, liposomal vesicles, and hydrogels, wherein isomerization has been used to trigger drug release.[119–121] Our research study revealed that the WZ peptide was visibly fluorescent, red-shifted, and did not appear to exhibit spectral changes when irradiated with Ultraviolet light. It, therefore, means that any molecules containing tryptophan may exhibit altered activity if the azobenzene molecule is close to the tryptophan moiety. This phenomenon was further evaluated as the serially diluted materials spectrofluorometer results indicate that the fluorescence is not caused by intermolecular π–π stacking but rather by the aromatic ring's influence on the 4-(Phenylazo)benzoic acid molecule. Overall, researchers may find it necessary to reconsider the placement of an azobenzene next to an aromatic amino acid, as this may impact the photoswitching properties of the molecule.

Chapter 5. Future Studies

5.1   Non-Intrinsic Fluorescence

One of our major research aims was to characterize and optimize aptamer sequences for enhanced selectivity compared to control beads and the competitor reagent AmB. Spectral analysis provided insights into the secondary structure of the aptamers and revealed changes upon the addition of graphene. Optimization efforts focused on improving binding capabilities relative to AmB. Furthermore, our investigation extended to exploring the potential of a photo-switchable molecule to regulate protein structure and function, with findings indicating that the WZ peptide exhibited visible fluorescence and a red-shifted preference for the cis isomer when exposed to ultraviolet light. Spectrofluorometer analysis of serially diluted materials suggested that the fluorescence was influenced by the aromatic ring's effect on the 4-(PhenylAzo)benzoic Acid molecule, rather than intermolecular $\pi-\pi$ stacking, emphasizing the importance of understanding molecular interactions for future applications.

Future studies should examine full-length aptamers, incorporating an analysis of the primers employed during the SELEX process. The investigation aims to discern whether the loss of selectivity observed in previous experiments might be attributed to specific characteristics within the full-length aptamers. The hypothesis guiding these future inquiries revolves around the potential advantages conferred by full-length aptamers. It is postulated that these longer sequences may exhibit intricate secondary structures that could contribute to heightened specificity, enhanced affinity, and increased selectivity specifically tailored to the target drug, Rif[122].

A comprehensive analysis of the full-length aptamers, including an exploration of their secondary structures, can be done to substantiate this hypothesis. Techniques such as

bioinformatics tools, enzymatic probing assays, and structural prediction algorithms could be employed to unravel the intricate folding patterns of these aptamers. Furthermore, comparisons between the secondary structures of full-length aptamers and their truncated counterparts can provide valuable insights into the role of these structures in enhancing selectivity.

This proposed avenue of research aligns with previous studies highlighting the importance of secondary structures in aptamers' functionality and specificity[123]. By elucidating the impact of full-length sequences and primers on the structural aspects of aptamers, future investigations could contribute to refining the SELEX process. The ultimate goal is to optimize aptamer design, ensuring that these molecular recognition elements exhibit better selectivity, specificity, and affinity for Rifampicin, thereby advancing their potential application in analytical and diagnostic settings.

Future studies should focus on understanding the binding kinetics of aptamers to their target molecule, Rif, by determining dissociation constants (Kd values). Furthermore, these experiments can incorporate investigations into the impact of Bovine Serum Albumin (BSA) on the aptamer-Rif interactions, aiming to ascertain whether protein binding induces noteworthy alterations in the dissociation constants.   Future studies could employ advanced biophysical techniques such as surface plasmon resonance (SPR), quartz crystal microbalance (QCM), or other suitable methods to determine the dissociation constants for the aptamer-Rif interactions. This analysis will be used to understand the strength and specificity of the binding between the aptamers and Rif.

5.2   Influence of BSA on Binding Dynamics for Rifampicin and Rifabutin

To mimic physiological conditions more accurately, the impact of protein binding, specifically BSA, on the aptamer-Rif interactions could be investigated. By introducing BSA into

the experimental setup, researchers can assess whether the presence of proteins in a complex biological milieu affects the dissociation constants. This step is given that biological samples often contain a myriad of proteins that could potentially influence the binding characteristics of aptamers. Statistical analyses could be applied to discern any significant differences in dissociation constants between experiments conducted with and without BSA. The inclusion of BSA in the experiments not only serves as a model protein but also adds a layer of physiological relevance. This is particularly important in the context of developing aptamers for applications such as diagnostics or therapeutics, where interactions with proteins in biological samples are inevitable.

Future work as depicted in Appendix A, the SELEX process can include rifabutin, an antibiotic with structural differences from rifampicin, such as the presence of a secondary amine in addition to the amide group. Rifabutin is commonly used against mycobacterial infections, and conducting the SELEX process for this compound aims to generate new aptamers specific to rifabutin. Running the SELEX process for both rifampicin and rifabutin concurrently could yield potential aptamers with high affinity and selectivity, thereby optimizing a simpler TDM approach for these antibiotics.

5.3   Intrinsic Fluorescence

To gain insight into the intrinsic characteristics of tryptophan and the understanding of azobenzene, future studies will employ the application of Nuclear Magnetic Resonance (NMR) spectroscopy as a tool for analysis of the peptides, enabling the determination of their composition, purity, and detailed molecular structure. The preliminary investigation of proton interactions using peptides WZ and WAZ was conducted on NMR spectroscopy, as illustrated in Appendix B. My interest in utilizing alanine as a spacer between tryptophan and azobenzene to explore the visibly

fluorescent (red-shifted) phenomenon led to preliminary research. The findings revealed that peptides with six alanine spacers exhibited visible fluorescence, as depicted in Appendix B. Additionally, investigations into the quantum yield of the materials will offer insights into the efficiency of the fluorophore in converting excitation light into fluorescence, which is essential for optimizing fluorescent properties and applications. Furthermore, there is a need to understand the photophysical mechanism underlying the favored cis isomerization over trans isomerization. Unraveling the intricacies of this phenomenon will provide understanding regarding molecular dynamics and could potentially unlock novel avenues for controlled molecular switching and regulation. Incorporating these approaches into future research might advance our comprehension of molecular interactions and pave the way for innovative applications in various fields.

5.4   Conclusion

Our research aimed to characterize and optimize aptamer sequences for enhanced selectivity compared to control beads and the competitor reagent AmB. Spectral analysis provided valuable insights into the secondary structure of the aptamers. Optimization efforts focused on enhancing binding capabilities relative to AmB, while also exploring the potential of a photo-switchable molecule, exemplified by the WZ peptide, to regulate protein structure and function. Spectrofluorometer analysis of serially diluted materials shed light on the influence of aromatic rings on the isomerization's stability. Future studies should look into the characterization of full-length aptamers and their secondary structures, employing advanced techniques such as NMR spectroscopy and bioinformatics tools. Furthermore, investigations into binding kinetics and the impact of Bovine Serum Albumin (BSA) on aptamer interactions with Rifampicin (Rif) will be used to understand their functionality in complex biological environments. Additionally, understanding the intrinsic characteristics of tryptophan through exploring the photophysical

mechanism underlying isomerization will pave the way for innovative applications in various fields. Overall, incorporating these approaches into future research can advance our understanding of molecular interactions and enhance the development of aptamers and photo-switchable molecules for diverse applications.

References

(1) Watanabe, S. Fluorophores: Characterization, Synthesis and Applications. *Nova Science Publishers, Inc.*, 2013.

(2) Traven, V. F.; Cheptsov, D. A.; Lodeiro, C. Control of Fluorescence of Organic Dyes in the Solid-State by Supramolecular Interactions. *J Fluoresc* **2023**, *33* (3), 799–847, https://doi.org/10.1007/s10895-022-03056-4.

(3) Ntziachristos, V. Fluorescence Molecular Imaging. *Annu Rev Biomed Eng* **2006**, *8* (1), 1–33, https://doi.org/10.1146/annurev.bioeng.8.061505.095831.

(4) Yang, Z.; Cao, J.; He, Y.; Yang, J. H.; Kim, T.; Peng, X.; Kim, J. S. Macro-/Micro-Environment-Sensitive Chemosensing and Biological Imaging. *Chem. Soc. Rev.* **2014**, *43* (13), 4563–4601, https://doi.org/10.1039/C4CS00051J.

(5) Mansfield, E. S.; Worley, J. M.; McKenzie, S. E.; Surrey, S.; Rappaport, E.; Fortina, P. Nucleic Acid Detection Using Non-Radioactive Labelling Methods. *Mol Cell Probes* **1995**, *9* (3), 145–156, https://doi.org/10.1006/mcpr.1995.0023.

(6) Zhang, J.; Liang, D.; He, W.; Wan, F.; Ying, Q.; Chu, B. Fast Separation of Single-Stranded Oligonucleotides by Capillary Electrophoresis Using OliGreen® as Fluorescence Inducing Agent. *Electrophoresis* **2005**, *26* (23), 4449–445, https://doi.org/10.1002/elps.200500099.

(7) Standley, S. M.; Mende, I.; Goh, S. L.; Kwon, Y. J.; Beaudette, T. T.; Engleman, E. G.; Fréchet, J. M. J. Incorporation of CpG Oligonucleotide Ligand into Protein-Loaded Particle Vaccines Promotes Antigen-Specific CD8 T-Cell Immunity. *Bioconjug Chem* **2007**, *18* (1), 77–83, https://doi.org/10.1021/bc060165i.

(8) Xu, L.; He, X.-Y.; Liu, B.-Y.; Xu, C.; Ai, S.-L.; Zhuo, R.-X.; Cheng, S.-X. Aptamer-Functionalized Albumin-Based Nanoparticles for Targeted Drug Delivery. *Colloids Surf B Biointerfaces* **2018**, *171*, 24–30, https://doi.org/10.1016/j.colsurfb.2018.07.008.

(9) Reyderman, L.; Stavchansky, S. Quantitative Determination of Short Single-Stranded Oligonucleotides from Blood Plasma Using Capillary Electrophoresis with Laser-Induced Fluorescence. *Anal Chem* **1997**, *69* (16), 3218–3222, https://doi.org/10.1021/ac970280+.

(10) Zhou, X.; Wang, C.; Wu, L.; Wei, W.; Liu, S. An OliGreen-Responsive Fluorescence Sensor for Sensitive Detection of Organophosphorus Pesticide Based on Its Specific Selectivity towards T-Hg2+-T DNA Structure. *Spectrochim Acta A Mol Biomol Spectrosc* **2021**, *247*, 119155, https://doi.org/10.1016/j.saa.2020.119155.

(11) Zhou, X.; Wang, C.; Wu, L.; Wei, W.; Liu, S. An OliGreen-Responsive Fluorescence Sensor for Sensitive Detection of Organophosphorus Pesticide Based on Its Specific Selectivity towards T-Hg2+-T DNA Structure. *Spectrochim Acta A Mol Biomol Spectrosc* **2021**, *247*, 119155, https://doi.org/10.1016/j.saa.2020.119155.

(12) Zhu, C.; Feng, Z.; Qin, H.; Chen, L.; Yan, M.; Li, L.; Qu, F. Recent Progress of SELEX Methods for Screening Nucleic Acid Aptamers. *Talanta* **2024**, *266*, 124998, https://doi.org/10.1016/j.talanta.2023.124998.

(13) Wu, Y. X.; Kwon, Y. J. Aptamers: The "Evolution" of SELEX. *Methods* **2016**, *106*, 21–28, https://doi.org/10.1016/j.ymeth.2016.04.020.

(14) Tan, Y.; Ma, L.; Yang, X.; Cheng, Q.-N.; Wu, J.-F. Current Status and Challenges of Aptamers Screening and Optimization. *Comb Chem High Throughput Screen* **2023**, *26* (6), 1067–1082, https://doi.org/10.2174/1386207325666220501170846.

(15) Ellington, A. D.; Szostak, J. W. Selection in Vitro of Single-Stranded DNA Molecules That Fold into Specific Ligand-Binding Structures. *Nature* **1992**, *355* (6363), 850–852, https://doi.org/10.1038/355850a0.

(16) Ellington, A. D.; Szostak, J. W. Selection in Vitro of Single-Stranded DNA Molecules That Fold into Specific Ligand-Binding Structures. *Nature* **1992**, *355* (6363), 850–852, https://doi.org/10.1038/355850a0.

(17) Hartley, G. S. The Cis-Form of Azobenzene. *Nature* **1937**, *140* (3537), 281–281, https://doi.org/10.1038/140281a0.

(18) Xue, L.; Pan, Y.; Zhang, S.; Chen, Y.; Yu, H.; Yang, Y.; Mo, L.; Sun, Z.; Li, L.; Yang, H. Fluorescent Azobenzene-Containing Compounds: From Structure to Mechanism. *Crystals (Basel)* **2021**, *11* (7), 840, https://doi.org/10.3390/cryst11070840.

(19) Rau, H. Spectroscopic Properties of Organic Azo Compounds. *Angewandte Chemie International Edition in English* **1973**, *12* (3), 224–235, https://doi.org/10.1002/anie.197302241.

(20) Zhong, H.-Y.; Chen, L.; Yang, R.; Meng, Z.-Y.; Ding, X.-M.; Liu, X.-F.; Wang, Y.-Z. Azobenzene-Containing Liquid Crystalline Polyester with π–π Interactions: Diverse Thermo- and Photo-Responsive Behaviours. *J Mater Chem C Mater* **2017**, *5* (13), 3306–3314, https://doi.org/10.1039/C6TC05493E.

(21) Zhu, M.; Zhou, H. Azobenzene-Based Small Molecular Photoswitches for Protein Modulation. *Org Biomol Chem* **2018**, *16* (44), 8434–8445, https://doi.org/10.1039/C8OB02157K.

(22) Mendive-Tapia, L.; Subiros-Funosas, R.; Zhao, C.; Albericio, F.; Read, N. D.; Lavilla, R.; Vendrell, M. Preparation of a Trp-BODIPY Fluorogenic Amino Acid to Label Peptides for Enhanced Live-Cell Fluorescence Imaging. *Nat Protoc* **2017**, *12* (8), 1588–1619, https://doi.org/10.1038/nprot.2017.048.

(23) Winnicka, E.; Kańska, M. Synthesis of L-Tryptophan Labeled with Hydrogen Isotopes in the Indole Ring. *J Radioanal Nucl Chem* **2009**, *279* (2), 675–678, https://doi.org/10.1007/s10967-007-7310-8.

(24) Richard J. Sundberg. *Indoles, Best Synthetic Methods*; Academic Press, London, **1996**.

(25) Urbaneja, M. A.; Rivas, S.; Carrascosa, J. L.; Valpuesta, J. M. An Intrinsic-tryptophan-fluorescence Study of Phage Φ29 Connector/Nucleic Acid Interactions. *Eur J Biochem* **1994**, *225* (2), 747–753, https://doi.org/10.1111/j.1432-1033.1994.00747.x.

(26) Khokhar, V.; Guha, A.; Dhawan, S.; Trivedi, S.; Haridas, V.; Pandey, S. Spectroscopic Investigation of Linear and Branched Tryptophan-Containing Peptides. *J Photochem Photobiol A Chem* **2019**, *372*, 186–195, https://doi.org/10.1016/j.jphotochem.2018.11.022.

(27) Sementa, D.; Dave, D.; Fisher, R. S.; Wang, T.; Elbaum-Garfinkle, S.; Ulijn, R. V. Sequence-Tunable Phase Behavior and Intrinsic Fluorescence in Dynamically Interacting Peptides. *Angewandte Chemie International Edition* **2023**, *62* (50), https://doi.org/10.1002/anie.202311479.

(28) Verma, R.; Pyreddy, S.; Redmond, C. E.; Qazi, F.; Khalid, A.; O'Brien-Simpson, N. M.; Shukla, R.; Tomljenovic-Hanic, S. Detection and Identification of Amino Acids and Proteins Using Their Intrinsic Fluorescence in the Visible Light Spectrum. *Anal Chim Acta* **2023**, *1282*, 341925, https://doi.org/10.1016/j.aca.2023.341925.

(29) Waner, M. J.; Ellis, G.; Graeca, M.; Ieraci, N.; Morell, C.; Murphy, A.; Mascotti, D. P. Avidin Cooperative Allosterism upon Binding Biotin Observed by Differential Changes in Intrinsic Fluorescence. *Biochem Biophys Rep* **2023**, *36*, 101554, https://doi.org/10.1016/j.bbrep.2023.101554.

(30) Tevonyan, L. L.; Beniaminov, A. D.; Kaluzhny, D. N. Quenching of G4-DNA Intrinsic Fluorescence by Ligands. *European Biophysics Journal* **2024**, https://doi.org/10.1007/s00249-023-01696-3.

(31) Verheyden, S.; Sillen, A.; Gils, A.; Declerck, P. J.; Engelborghs, Y. Tryptophan Properties in Fluorescence and Functional Stability of Plasminogen Activator Inhibitor 1. *Biophys J* **2003**, *85* (1), 501–510, https://doi.org/10.1016/S0006-3495(03)74495-6.

(32) Ladokhin, A. S.; Jayasinghe, S.; White, S. H. How to Measure and Analyze Tryptophan Fluorescence in Membranes Properly, and Why Bother? *Anal Biochem* **2000**, *285* (2), 235–245, https://doi.org/10.1006/abio.2000.4773.

(33) Yu, Z.; Cao, Y.; Tian, Y.; Ji, W.; Chen, K.-E.; Wang, Z.; Ren, J.; Xiao, H.; Zhang, L.; Liu, W.; Fan, L.; Zhang, Q.; Cao, C. Real-Time and Quantitative Protein Detection via Polyacrylamide Gel Electrophoresis and Online Intrinsic Fluorescence Imaging. *Anal Chim Acta* **2024**, *1291*, 342219, https://doi.org/10.1016/j.aca.2024.342219.

(34) Szabo, A. G.; Rayner, D. M. Fluorescence Decay of Tryptophan Conformers in Aqueous Solution. *J Am Chem Soc* **1980**, *102* (2), 554–563, https://doi.org/10.1021/ja00522a020.

(35) René Albani, J. Fluorescence Lifetimes of Tryptophan: Structural Origin and Relation with So → 1Lb and So → 1La Transitions. *J Fluoresc* **2009**, *19* (6), 1061–1071, https://doi.org/10.1007/s10895-009-0506-7.

(36) Osysko, A. P.; Muíño, P. L. Fluorescence Quenching of Tryptophan and Tryptophanyl Dipeptides in Solution. *Journal of Biophysical Chemistry* **2011**, *02* (03), 316–321, https://doi.org/10.4236/jbpc.2011.23036.

(37) Gudgin, E.; Lopez-Delgado, R.; Ware, W. R. Photophysics of Tryptophan in Water, Deuterium Oxide and in Nonaqueous Solvents. *J Phys Chem* **1983**, *87* (9), 1559–1565, https://doi.org/10.1021/j100232a021.

(38) Campbell, E. A.; Korzheva, N.; Mustaev, A.; Murakami, K.; Nair, S.; Goldfarb, A.; Darst, S. A. Structural Mechanism for Rifampicin Inhibition of Bacterial RNA Polymerase. *Cell* **2001**, *104* (6), 901–912, https://doi.org/10.1016/S0092-8674(01)00286-0.

(39) McClure, W. R.; Cech, C. L. On the Mechanism of Rifampicin Inhibition of RNA Synthesis. *Journal of Biological Chemistry* **1978**, *253* (24), 8949–8956, https://doi.org/10.1016/s0021-9258(17)34269-2.

(40) Aono, A.; Murase, Y.; Minegishi, M.; Ohtawa, S.; Yano, M.; Chikamatsu, K.; Shimomura, Y.; Hosoya, M.; Igarashi, Y.; Morishige, Y.; Yamada, H.; Takaki, A.; Togashi, K.; Hiura, M.; Mitarai, S. Clinical Evaluation of the Cobas® MTB-RIF/INH Reagent and the Cobas® 6800 for the Detection of Isoniazid and Rifampicin Resistance. *Tuberculosis* **2022**, *134*, 102199, https://doi.org/10.1016/j.tube.2022.102199.

(41) Ahsan Imam, M.; Fatima, N.; Shameem, M.; Ahmed, S. Evaluation of the Genexpert Mycobacterium Tuberculosis/Rifampicin Assay for Early Detection of Extrapulmonary Tuberculosis and Rifampicin Resistance in Aligarh Region of Northern India. *CHRISMED Journal of Health and Research* **2023**, *10* (1), 44, https://doi.org/10.4103/cjhr.cjhr_45_22.

(42) Prahl, J. B.; Lundqvist, M.; Bahl, J. M. C.; Johansen, I. S.; Andersen, Å. B.; Frimodt-Møller, N.; Cohen, A. S. Simultaneous Quantification of Isoniazid, Rifampicin, Ethambutol and Pyrazinamide by Liquid Chromatography/Tandem Mass Spectrometry. *APMIS* **2016**, *124* (11), 1004–1015, https://doi.org/10.1111/apm.12590.

(43) Acocella, G. Clinical Pharmacokinetics of Rifampicin. *Clin Pharmacokinet* **1978**, *3* (2), 108–127, https://doi.org/10.2165/00003088-197803020-00002.

(44) Holstege, C. P. Rifampin. In *Encyclopedia of Toxicology: Third Edition*; Elsevier, 2014; pp 134–136, https://doi.org/10.1016/B978-0-12-386454-3.00781-8.

(45) *SciFinder.* https://scifinder-n.cas.org/search/substance/6631538c9ab018107a85046f/1 (accessed 2024-04-30).

(46) Pyrazinamide/Rifampicin. *Reactions Weekly* **2022**, *1925* (1), 439–439, https://doi.org/10.1007/s40278-022-24216-5.

(47) Amusengeri, A.; Khan, A.; Tastan Bishop, Ö. The Structural Basis of Mycobacterium Tuberculosis RpoB Drug-Resistant Clinical Mutations on Rifampicin Drug Binding. *Molecules* **2022**, *27* (3), https://doi.org/10.3390/molecules27030885.

(48) Elmorsy, E.; Attalla, S.; Fikry, E.; Kocon, A.; Turner, R.; Christie, D.; Warren, A.; Nwidu, L.; Carter, W. Adverse Effects of Anti-Tuberculosis Drugs on HepG2 Cell Bioenergetics. *Hum Exp Toxicol* **2017**, *36* (6), 616–625, https://doi.org/10.1177/0960327116660751.

(49) Agarwal, A.; Sharma, S.; Bansal, R.; Meena, M.; Airun, M. Near Fatal Poisoning by Isoniazid and Rifampicin. *J Assoc Physicians India* **2016**, *64* (12), 88–89.

(50) Wang, W. H.; Takeuchi, R.; Jain, S. H.; Jiang, Y. H.; Watanuki, S.; Ohtaki, Y.; Nakaishi, K.; Watabe, S.; Lu, P. L.; Ito, E. A Novel, Rapid (within Hours) Culture-Free Diagnostic Method for Detecting Live Mycobacterium Tuberculosis with High Sensitivity. *EBioMedicine* **2020**, *60,* https://doi.org/10.1016/j.ebiom.2020.103007.

(51) Iha, K.; Inada, M.; Kawada, N.; Nakaishi, K.; Watabe, S.; Tan, Y. H.; Shen, C.; Ke, L.-Y.; Yoshimura, T.; Ito, E. Ultrasensitive ELISA Developed for Diagnosis. *Diagnostics* **2019**, *9* (3), 78, https://doi.org/10.3390/diagnostics9030078.

(52) Allanson, A. L.; Cotton, M. M.; Tettey, J. N. A.; Boyter, A. C. Determination of Rifampicin in Human Plasma and Blood Spots by High Performance Liquid Chromatography with UV Detection: A Potential Method for Therapeutic Drug Monitoring. *J Pharm Biomed Anal* **2007**, *44* (4), 963–969, https://doi.org/10.1016/j.jpba.2007.04.007.

(53) Fox, D.; O'Connor, R.; Mallon, P.; McMahon, G. Simultaneous Determination of Efavirenz, Rifampicin and Its Metabolite Desacetyl Rifampicin Levels in Human Plasma. *J Pharm Biomed Anal* **2011**, *56* (4), 785–791, https://doi.org/10.1016/j.jpba.2011.07.041.

(54) Aqil, Mohd.; Bishnoi, M.; Chauhan, M. K. Swift and Precise Determination of Rifampicin by RP-HPLC Technology Development in Pharmaceuticals. *Iranian Journal of Science* **2023**, *47* (4), 1137–1144, https://doi.org/10.1007/s40995-023-01471-1.

(55) Srivastava, A.; Waterhouse, D.; Ardrey, A.; Ward, S. A. Quantification of Rifampicin in Human Plasma and Cerebrospinal Fluid by a Highly Sensitive and Rapid Liquid Chromatographic–Tandem Mass Spectrometric Method. *J Pharm Biomed Anal* **2012**, *70,* 523–528, https://doi.org/10.1016/j.jpba.2012.05.028.

(56) Prahl, J. B.; Lundqvist, M.; Bahl, J. M. C.; Johansen, I. S.; Andersen, Å. B.; Frimodt-Møller, N.; Cohen, A. S. Simultaneous Quantification of Isoniazid, Rifampicin, Ethambutol and Pyrazinamide by Liquid Chromatography/Tandem Mass Spectrometry. *APMIS* **2016**, *124* (11), 1004–1015, https://doi.org/10.1111/apm.12590.

(57) Blakemore, R.; Story, E.; Helb, D.; Kop, J.; Banada, P.; Owens, M. R.; Chakravorty, S.; Jones, M.; Alland, D. Evaluation of the Analytical Performance of the Xpert MTB/RIF Assay. *J Clin Microbiol* **2010**, *48* (7), 2495–2501, https://doi.org/10.1128/JCM.00128-10.

(58) Gotham, D.; McKenna, L.; Deborggraeve, S.; Madoori, S.; Branigan, D. Public Investments in the Development of GeneXpert Molecular Diagnostic Technology. *PLoS One* **2021**, *16* (8), e0256883, https://doi.org/10.1371/journal.pone.0256883.

(59) Chakravorty, S.; Simmons, A. M.; Rowneki, M.; Parmar, H.; Cao, Y.; Ryan, J.; Banada, P. P.; Deshpande, S.; Shenai, S.; Gall, A.; Glass, J.; Krieswirth, B.; Schumacher, S. G.; Nabeta, P.; Tukvadze, N.; Rodrigues, C.; Skrahina, A.; Tagliani, E.; Cirillo, D. M.; Davidow, A.; Denkinger, C. M.; Persing, D.; Kwiatkowski, R.; Jones, M.; Alland, D. The New Xpert MTB/RIF Ultra: Improving Detection of *Mycobacterium Tuberculosis* and Resistance to Rifampin in an Assay Suitable for Point-of-Care Testing. *mBio* **2017**, *8* (4), https://doi.org/10.1128/mBio.00812-17.

(60) Patel, V. B.; Connolly, C.; Singh, R.; Lenders, L.; Matinyenya, B.; Theron, G.; Ndung'u, T.; Dheda, K. Comparison of Amplicor and GeneXpert MTB/RIF Tests for Diagnosis of Tuberculous Meningitis. *J Clin Microbiol* **2014**, *52* (10), 3777–3780, https://doi.org/10.1128/JCM.01235-14.

(61) Messelhäusser, U.; Kämpf, P.; Hörmansdorfer, S.; Wagner, B.; Schalch, B.; Busch, U.; Höller, C.; Wallner, P.; Barth, G.; Rampp, A. Culture and Molecular Method for Detection of Mycobacterium Tuberculosis Complex and Mycobacterium Avium Subsp. Paratuberculosis in Milk and Dairy Products. *Appl Environ Microbiol* **2012**, *78* (1), 295–297, https://doi.org/10.1128/AEM.06322-11.

(62) Campbell, E. A.; Korzheva, N.; Mustaev, A.; Murakami, K.; Nair, S.; Goldfarb, A.; Darst, S. A. Structural Mechanism for Rifampicin Inhibition of Bacterial RNA Polymerase. *Cell* **2001**, *104* (6), 901–912, https://doi.org/10.1016/S0092-8674(01)00286-0.

(63) Mitchison, D. A.; Allen, B. W.; Miller, A. B. Detection of Rifampicin in Urine by a Simple Microbiological Assay. *Tubercle* **1970**, *51* (3), 300–304, https://doi.org/10.1016/0041-3879(70)90023-1.

(64) Do, P. C.; Assefa, Y. A.; Batikawai, S. M.; Reid, S. A. Strengthening Antimicrobial Resistance Surveillance Systems: A Scoping Review. *BMC Infect Dis* **2023**, *23* (1), 593, https://doi.org/10.1186/s12879-023-08585-2.

(65) Bilgin, K.; Yanik, K.; Karadag, A.; Odabasi, H.; Tas, H.; Gunaydin, M. Comparison of a Real-Time Polymerase Chain Reaction-Based System and Erlich–Ziehl–Neelsen Method with Culture in the Identification of Mycobacterium Tuberculosis. *Turk J Med Sci* **2016**, *46*, 203–206, https://doi.org/10.3906/sag-1411-34.

(66) Stoltenburg, R.; Schubert, T.; Strehlitz, B. In Vitro Selection and Interaction Studies of a DNA Aptamer Targeting Protein A. *PLoS One* **2015**, *10* (7), e0134403, https://doi.org/10.1371/journal.pone.0134403.

(67) Gómez-Arango, C.; Gorostiza, I.; Úcar, E.; García-Vivar, M. L.; Pérez, C. E.; De Dios, J. R.; Alvarez, B.; Ruibal-Escribano, A.; Stoye, C.; Vasques, M.; Belzunegui, J.; Escobar, A.; Trancho, Z.; Ruiz del Agua, A.; Del Rio, L.; Jorquera, C.; Diez, E.; Martínez, A.; Nagore, D. Cost-Effectiveness of Therapeutic Drug Monitoring-Guided Adalimumab Therapy in Rheumatic Diseases: A Prospective, Pragmatic Trial. *Rheumatol Ther* **2021**, *8* (3), 1323–1339, https://doi.org/10.1007/s40744-021-00345-5.

(68) Fang, Z.; Zhang, H.; Guo, J.; Guo, J. Overview of Therapeutic Drug Monitoring and Clinical Practice. *Talanta* **2024**, *266*, 124996, https://doi.org/10.1016/j.talanta.2023.124996.

(69) Duhme, D. W. Reduction of Digoxin Toxicity Associated with Measurement of Serum Levels. *Ann Intern Med* **1974**, *80* (4), 516, https://doi.org/10.7326/0003-4819-80-4-516.

(70) Naji, K. M.; Al-Khatib, B. Y.; Al-Haj, N. S.; D'souza, M. R. Hepatoprotective Activity of Melittin on Isoniazid- and Rifampicin-Induced Liver Injuries in Male Albino Rats. *BMC Pharmacol Toxicol* **2021**, *22* (1), 39, https://doi.org/10.1186/s40360-021-00507-9.

(71) Aljohani, M. M.; Cialla-May, D.; Popp, J.; Chinnappan, R.; Al-Kattan, K.; Zourob, M. Aptamers: Potential Diagnostic and Therapeutic Agents for Blood Diseases. *Molecules* **2022**, *27* (2), https://doi.org/10.3390/molecules27020383.

(72) Ku, T. H.; Zhang, T.; Luo, H.; Yen, T. M.; Chen, P. W.; Han, Y.; Lo, Y. H. Nucleic Acid Aptamers: An Emerging Tool for Biotechnology and Biomedical Sensing. *Sensors (Switzerland)*. MDPI AG July 6, 2015, pp 16281–16313, https://doi.org/10.3390/s150716281.

(74) Tuerk, C.; Gold, L. Systematic Evolution of Ligands by Exponential Enrichment: RNA Ligands Tobacteriophage T4 DNA Polymerase. *Science (1979)* **1990**, *249*, 505–510.

(75) Wiedman, G. R.; Zhao, Y.; Mustaev, A.; Ping, J.; Vishnubhotla, R.; Johnson, A. T. C.; Perlin, D. S. An Aptamer-Based Biosensor for the Azole Class of Antifungal Drugs. *mSphere* **2017**, *2* (4), https://doi.org/10.1128/mSphere.00274-17.

(76) Bachu, V.; Barman, K.; Goswami, P. Analysis on the In-Silico Ensemble Methods for 3D Modelling of SsDNA Aptamers. *Biophys Chem* **2023**, *303*, https://doi.org/10.1016/j.bpc.2023.107111.

(77) Craig Tuerk; Larry Gold. Systematic Evolution of Ligands by Exponential Enrichment: RNA Ligands to Bacteriophage T4 DNA Polymerase. *Science (1979)* **1990**, *249* (4968), 505–510.

(78) DeRosa, M. C.; Lin, A.; Mallikaratchy, P.; McConnell, E. M.; McKeague, M.; Patel, R.; Shigdar, S. In Vitro Selection of Aptamers and Their Applications. *Nature Reviews Methods Primers* **2023**, *3* (1), 54, https://doi.org/10.1038/s43586-023-00238-7.

(79) Zhou, Q.; Xu, Z.; Liu, Z. Molecularly Imprinting–Aptamer Techniques and Their Applications in Molecular Recognition. *Biosensors (Basel)* **2022**, *12* (8), https://doi.org/10.3390/bios12080576.

(80) Keefe, A. D.; Pai, S.; Ellington, A. Aptamers as Therapeutics. *Nature Reviews Drug Discovery*. **2010**, pp 537–550, https://doi.org/10.1038/nrd3141.

(81) Kalra, P.; Dhiman, A.; Cho, W. C.; Bruno, J. G.; Sharma, T. K. Simple Methods and Rational Design for Enhancing Aptamer Sensitivity and Specificity. *Front Mol Biosci* **2018**, *5*, https://doi.org/10.3389/fmolb.2018.00041.

(82) Hamula, C. L. A.; Peng, H.; Wang, Z.; Tyrrell, G. J.; Li, X.-F.; Le, X. C. An Improved SELEX Technique for Selection of DNA Aptamers Binding to M-Type 11 of Streptococcus Pyogenes. *Methods* **2016**, *97*, 51–57, https://doi.org/10.1016/j.ymeth.2015.12.005.

(83) Kalra, P.; Dhiman, A.; Cho, W. C.; Bruno, J. G.; Sharma, T. K. Simple Methods and Rational Design for Enhancing Aptamer Sensitivity and Specificity. *Front Mol Biosci* **2018**, *5*, https://doi.org/10.3389/fmolb.2018.00041.

(84) *DNA structures prediction*. https://rna.urmc.rochester.edu/RNAstructureWeb/Servers/Predict1/Predict1.html (accessed 2019-05-18).

(85) SantaLucia, J.; Hicks, D. The Thermodynamics of DNA Structural Motifs. *Annu Rev Biophys Biomol Struct* **2004**, *33* (1), 415–440, https://doi.org/10.1146/annurev.biophys.32.110601.141800.

(86) Jeddi, I.; Saiz, L. Three-Dimensional Modeling of Single Stranded DNA Hairpins for Aptamer-Based Biosensors. *Sci Rep* **2017**, *7* (1), 1178, https://doi.org/10.1038/s41598-017-01348-5.

(87) Binet, T.; Padiolleau-Lefèvre, S.; Octave, S.; Avalle, B.; Maffucci, I. Comparative Study of Single-Stranded Oligonucleotides Secondary Structure Prediction Tools. *BMC Bioinformatics* **2023**, *24* (1), 422, https://doi.org/10.1186/s12859-023-05532-5.

(88) Chen, C.; Zhao, J.; Jiang, J.; Yu, R. A Novel Exonuclease III-Aided Amplification Assay for Lysozyme Based on Graphene Oxide Platform. *Talanta* **2012**, *101*, 357–361, https://doi.org/10.1016/j.talanta.2012.09.041.

(89) Wu, M.; Kempaiah, R.; Huang, P.-J. J.; Maheshwari, V.; Liu, J. Adsorption and Desorption of DNA on Graphene Oxide Studied by Fluorescently Labeled Oligonucleotides. *Langmuir* **2011**, *27* (6), 2731–2738, https://doi.org/10.1021/la1037926.

(90) Gray, D. M.; Wen, J.; Gray, C. W.; Repges, R.; Repges, C.; Raabe, G.; Fleischhauer, J. Measured and Calculated CD Spectra of G-quartets Stacked with the Same or Opposite Polarities. *Chirality* **2008**, *20* (3–4), 431–440, https://doi.org/10.1002/chir.20455.

(91) Kumar, G. S.; Neckers, D. C. Photochemistry of Azobenzene-Containing Polymers. *Chem Rev* **1989**, *89* (8), 1915–1925, https://doi.org/10.1021/cr00098a012.

(92) Song, X.; Perlstein, J.; Whitten, D. G. Supramolecular Aggregates of Azobenzene Phospholipids and Related Compounds in Bilayer Assemblies and Other Microheterogeneous Media: Structure, Properties, and Photoreactivity [1]. *J Am Chem Soc* **1997**, *119* (39), 9144–9159, https://doi.org/10.1021/ja971291n.

(93) Das, G.; Prakasam, T.; Addicoat, M. A.; Sharma, S. K.; Ravaux, F.; Mathew, R.; Baias, M.; Jagannathan, R.; Olson, M. A.; Trabolsi, A. Azobenzene-Equipped Covalent Organic

Framework: Light-Operated Reservoir. *J Am Chem Soc* **2019**, *141* (48), 19078–19087, https://doi.org/10.1021/jacs.9b09643.

(94) Ventura, C. R.; Wiedman, G. R. Substituting Azobenzene for Proline in Melittin to Create Photomelittin: A Light-Controlled Membrane Active Peptide. *Biochimica et Biophysica Acta (BBA) - Biomembranes* **2021**, *1863* (12), 183759, https://doi.org/10.1016/j.bbamem.2021.183759.

(95) Bandara, H. M. D.; Burdette, S. C. Photoisomerization in Different Classes of Azobenzene. *Chem. Soc. Rev.* **2012**, *41* (5), 1809–1825, https://doi.org/10.1039/C1CS15179G.

(96) Frederic, C.; Wiedman, G. R. Investigating the Interaction of Azobenzene Moiety on the Aromatic Amino Acid Tryptophan. *Peptide Science* **2023,** https://doi.org/10.1002/pep2.24334.

(97) Kumar, A.; Singh, S.; Singh Mudahar, G.; Singh Thind, K. Molar Extinction Coefficients of Some Commonly Used Solvents. *Radiation Physics and Chemistry* **2006**, *75* (7), 737–740, https://doi.org/10.1016/j.radphyschem.2005.12.035.

(98) Li, P.; Wu, G. Important Roles of Amino Acids in Immune Responses. *British Journal of Nutrition* **2022**, *127* (3), 398–402, https://doi.org/10.1017/S0007114521004566.

(99) Richard, D. M.; Dawes, M. A.; Mathias, C. W.; Acheson, A.; Hill-Kapturczak, N.; Dougherty, D. M. *L* -Tryptophan: Basic Metabolic Functions, Behavioral Research and Therapeutic Indications. *International Journal of Tryptophan Research* **2009**, *2*, IJTR.S2129, https://doi.org/10.4137/IJTR.S2129.

(100) Kanova, M.; Kohout, P. Tryptophan: A Unique Role in the Critically Ill. *Int J Mol Sci* **2021**, *22* (21), 11714, https://doi.org/10.3390/ijms222111714.

(101) Kelly, B.; Pearce, E. L. Amino Assets: How Amino Acids Support Immunity. *Cell Metab* **2020**, *32* (2), 154–175, https://doi.org/10.1016/j.cmet.2020.06.010.

(102) Beharry, A. A.; Woolley, G. A. Azobenzene Photoswitches for Biomolecules. *Chem Soc Rev* **2011**, *40* (8), 4422, https://doi.org/10.1039/c1cs15023e.

(103) Abendroth, J. M.; Bushuyev, O. S.; Weiss, P. S.; Barrett, C. J. Controlling Motion at the Nanoscale: Rise of the Molecular Machines. *ACS Nano* **2015**, *9* (8), 7746–7768, https://doi.org/10.1021/acsnano.5b03367.

(104) Aemissegger, A.; Hilvert, D. Synthesis and Application of an Azobenzene Amino Acid as a Light-Switchable Turn Element in Polypeptides. *Nat Protoc* **2007**, *2* (1), 161–167, https://doi.org/10.1038/nprot.2006.488.

(105) Hood, C. A.; Fuentes, G.; Patel, H.; Page, K.; Menakuru, M.; Park, J. H. Fast Conventional Fmoc Solid-phase Peptide Synthesis with HCTU. *Journal of Peptide Science* **2008**, *14* (1), 97–101, https://doi.org/10.1002/psc.921.

(106) Behrendt, R.; White, P.; Offer, J. Advances in Fmoc Solid-phase Peptide Synthesis. *Journal of Peptide Science* **2016**, *22* (1), 4–27, https://doi.org/10.1002/psc.2836.

(107) Dokić, J.; Gothe, M.; Wirth, J.; Peters, M. V.; Schwarz, J.; Hecht, S.; Saalfrank, P. Quantum Chemical Investigation of Thermal Cis-to-Trans Isomerization of Azobenzene Derivatives: Substituent Effects, Solvent Effects, and Comparison to Experimental Data. *Journal of Physical Chemistry A* **2009**, *113* (24), https://doi.org/10.1021/jp9021344.

(108) Fedele, C.; Ruoko, T. P.; Kuntze, K.; Virkki, M.; Priimagi, A. New Tricks and Emerging Applications from Contemporary Azobenzene Research. *Photochemical and Photobiological Sciences* **2022**, *21* (10), https://doi.org/10.1007/s43630-022-00262-8.

(109) Beharry, A. A.; Woolley, G. A. Azobenzene Photoswitches for Biomolecules. *Chem Soc Rev* **2011**, *40* (8), 4422–4437, https://doi.org/10.1039/c1cs15023e.

(110) Song, X.; Perlstein, J.; Whitten, D. G. Supramolecular Aggregates of Azobenzene Phospholipids and Related Compounds in Bilayer Assemblies and Other Microheterogeneous Media: Structure, Properties, and Photoreactivity. *J Am Chem Soc* **1997**, *119* (39), https://doi.org/10.1021/ja971291n.

(111) Mach, H.; Middaugh, C. R.; Lewis, R. V. Statistical Determination of the Average Values of the Extinction Coefficients of Tryptophan and Tyrosine in Native Proteins. *Anal Biochem* **1992**, *200* (1), https://doi.org/10.1016/0003-2697(92)90279-G.

(112) Lu, H.; Zheng, Y.; Zhao, X.; Wang, L.; Ma, S.; Han, X.; Xu, B.; Tian, W.; Gao, H. Highly Efficient Far Red/Near-Infrared Solid Fluorophores: Aggregation-Induced Emission, Intramolecular Charge Transfer, Twisted Molecular Conformation, and Bioimaging Applications. *Angewandte Chemie - International Edition* **2016**, *55* (1), https://doi.org/10.1002/anie.201507031.

(113) Zhu, M.; Zhou, H. Azobenzene-Based Small Molecular Photoswitches for Protein Modulation. *Org Biomol Chem* **2018**, *16* (44), 8434–8445, https://doi.org/10.1039/C8OB02157K.

(114) Más-Montoya, M.; García Alcaraz, A.; Espinosa Ferao, A.; Bautista, D.; Curiel, D. Insight into the Stokes Shift, Divergent Solvatochromism and Aggregation-Induced Emission of Boron Complexes with Locked and Unlocked Benzophenanthridine Ligands. *Dyes and Pigments* **2023**, *209*, https://doi.org/10.1016/j.dyepig.2022.110924.

(115) Liu, D. R.; Magliery, T. J.; Pastrnak, M.; Schultz, P. G. Engineering a TRNA and Aminoacyl-TRNA Synthetase for the Site-Specific Incorporation of Unnatural Amino Acids into Proteins in Vivo. *Proc Natl Acad Sci U S A* **1997**, *94* (19), 10092–10097, https://doi.org/10.1073/pnas.94.19.10092.

(116) Sungwienwong, I.; Hostetler, Z. M.; Blizzard, R. J.; Porter, J. J.; Driggers, C. M.; Mbengi, L. Z.; Villegas, J. A.; Speight, L. C.; Saven, J. G.; Perona, J. J.; Kohli, R. M.; Mehl, R. A.; Petersson, E. J. Improving Target Amino Acid Selectivity in a Permissive Aminoacyl

TRNA Synthetase through Counter-Selection. *Org Biomol Chem* **2017**, *15* (17), https://doi.org/10.1039/c7ob00582b.

(117) Lee, J.; Lee, H.; Kim, C. Stimuli-Responsive Conformational Transformation of Antimicrobial Peptides Stapled with an Azobenzene Unit. *New Journal of Chemistry* **2020**, *44* (35), https://doi.org/10.1039/d0nj03409f.

(118) Aemissegger, A.; Hilvert, D. Synthesis and Application of an Azobenzene Amino Acid as a Light-Switchable Turn Element in Polypeptides. *Nat Protoc* **2007**, *2* (1), 161–167, https://doi.org/10.1038/nprot.2006.488.

(119) Ferris, D. P.; Zhao, Y. L.; Khashab, N. M.; Khatib, H. A.; Stoddart, J. F.; Zink, J. I. Light-Operated Mechanized Nanoparticles. *J Am Chem Soc* **2009**, *131* (5), https://doi.org/10.1021/ja807798g.

(120) Rijcken, C. J. F.; Soga, O.; Hennink, W. E.; Nostrum, C. F. van. Triggered Destabilisation of Polymeric Micelles and Vesicles by Changing Polymers Polarity: An Attractive Tool for Drug Delivery. *Journal of Controlled Release*. 2007, https://doi.org/10.1016/j.jconrel.2007.03.023.

(121) Tomatsu, I.; Peng, K.; Kros, A. Photoresponsive Hydrogels for Biomedical Applications. *Advanced Drug Delivery Reviews*. 2011, https://doi.org/10.1016/j.addr.2011.06.009.

(122) Wu, Y. X.; Kwon, Y. J. Aptamers: The "Evolution" of SELEX. *Methods* **2016**, *106*, 21–28, https://doi.org/10.1016/j.ymeth.2016.04.020.

(123) William J. Jaremko, Z. H. W. W. A. W. N. K. L. N. One Aptamer, Two Functions: The Full-Length Aptamer Inhibits AMPA Receptors, While the Short One Inhibits Both AMPA and Kainate Receptors. *RNA & DISEASE* **2017,** https://doi.org/10.14800/rd.1560.

(124) *SciFinder. https://scifinder-n.cas.org/search/substance/663153b99ab018107a850618/1* (accessed 2024-04-30).

(125) Atta ur-Rahman; M, C. *Applications of NMR Spectroscopy. Bentham Science Publishers Ltd*; Shāriqah, United Arab Emirates, **2021**; Vol. 9.

Appendix A. SELEX Data

Background

Despite the potential applications for aptamers, their effective use has been hindered by several challenges. These include the time-consuming procedures involved in their selection and synthesis, the consumption of resources such as time, materials, and expertise, and the constraint of a limited variety of nucleobases available. These factors impede the adoption and utilization of aptamers across various fields and industries [122]. In the context of this research, the aptamers did not demonstrate high selectivity for Rifampicin compared to Amphotericin B. Consequently, a new experiment with rifampicin was initiated to validate the reproducibility of the initial results obtained.

The SELEX process was carried out for rifabutin. In contrast to Rifampicin, rifabutin features a secondary amine in addition to the amide group, as illustrated in Figure A 1[124]. The aim of conducting the SELEX process for rifabutin, an antibiotic commonly employed against mycobacterial infections, was to generate labeled beads with enhanced affinity for the secondary amine and identify new aptamers specific to this antibiotic. Therefore, running the SELEX process for both Rifampicin and Rifabutin could produce potential aptamers with high affinity and selectivity to optimize simpler TDM.

Samples and Discussions

The labeled and unlabeled (Counter SELEX) for Rifampicin and Rifabutin were prepared for a total of four (4) samples. The SELEX process was followed for seven (7) rounds. The SELEX rounds are depicted in Figures A 2 through A 11, while the summary table is presented in Table A

1. To validate the PCR process after each SELEX round, the non-specific N40-mer sample was

prepared and amplified as well.

Absolute stereochemistry shown
E/Z labels describe double bond geometry
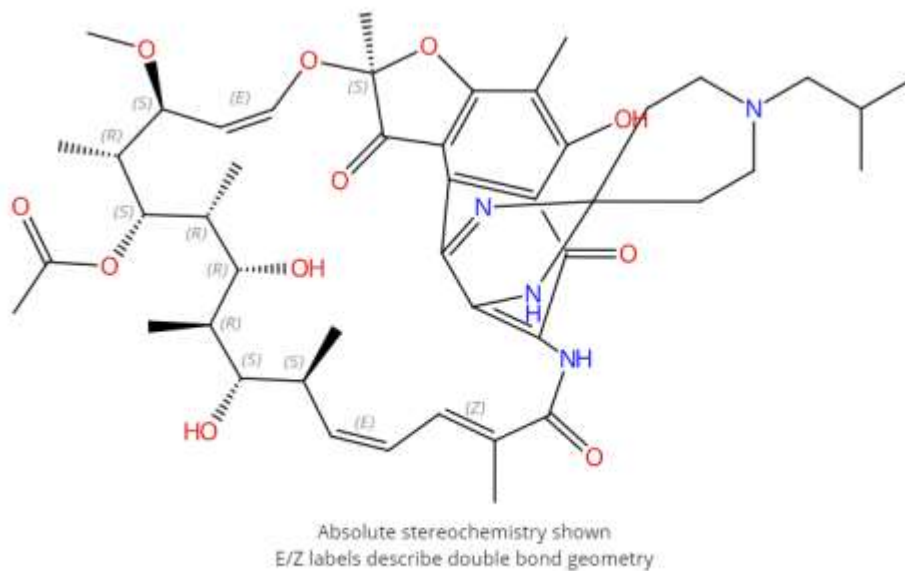
Figure A 1. Rifabutin structure generated using SciFinder
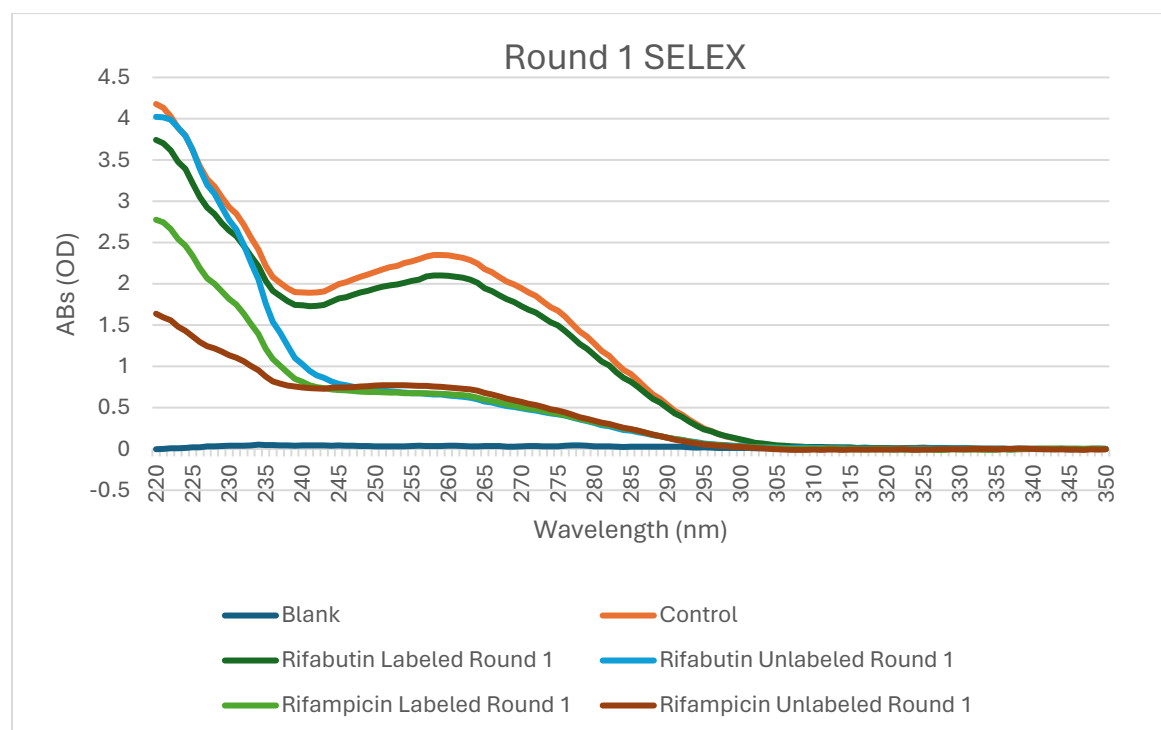
Figure A 2. Round 1 of SELEX process for labeled and unlabeled (Counter SELEX) of Rifampicin and Rifabutin, along with the amplified 40-mer control.
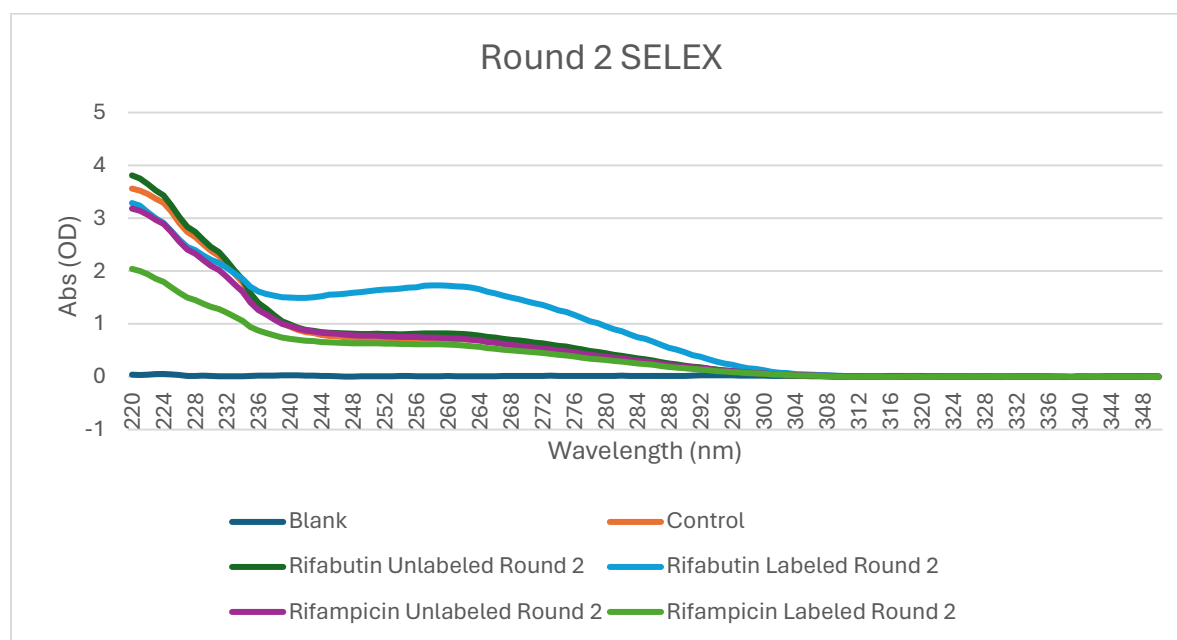
Figure A 3. Round 2 of SELEX process for labeled and unlabeled (Counter SELEX) of Rifampicin and Rifabutin, along with the amplified 40-mer
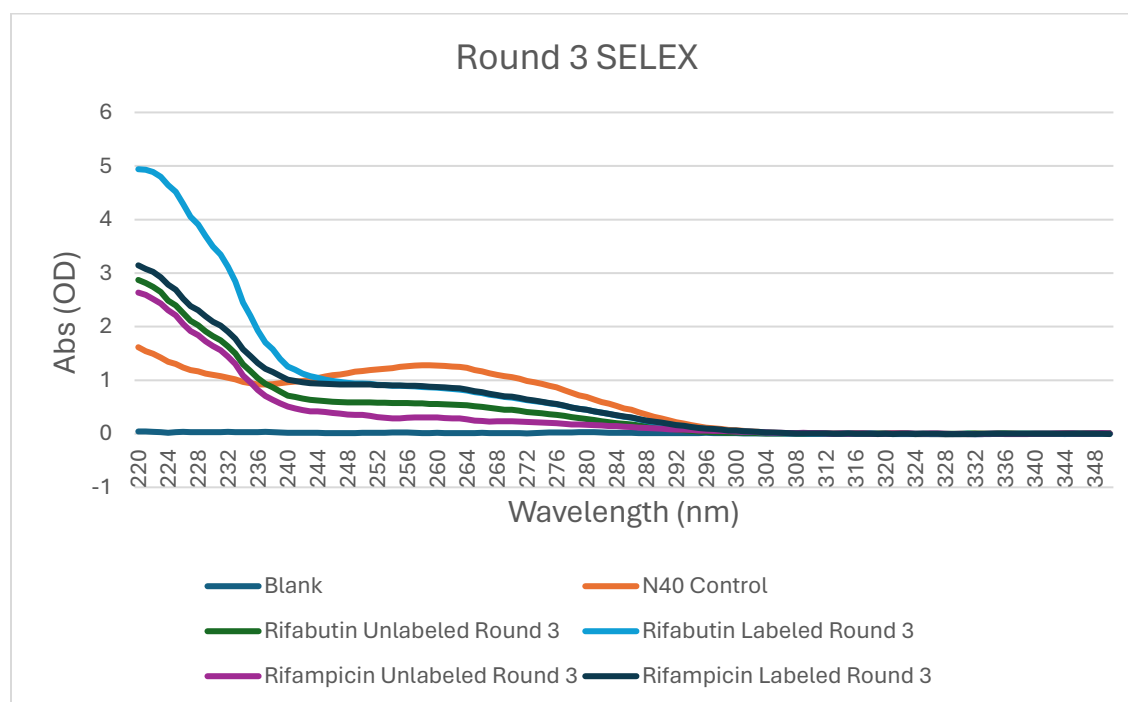
Figure A 4. Round 3 of SELEX process for labeled and unlabeled (Counter SELEX) of Rifampicin and Rifabutin, along with the amplified 40-mer control.
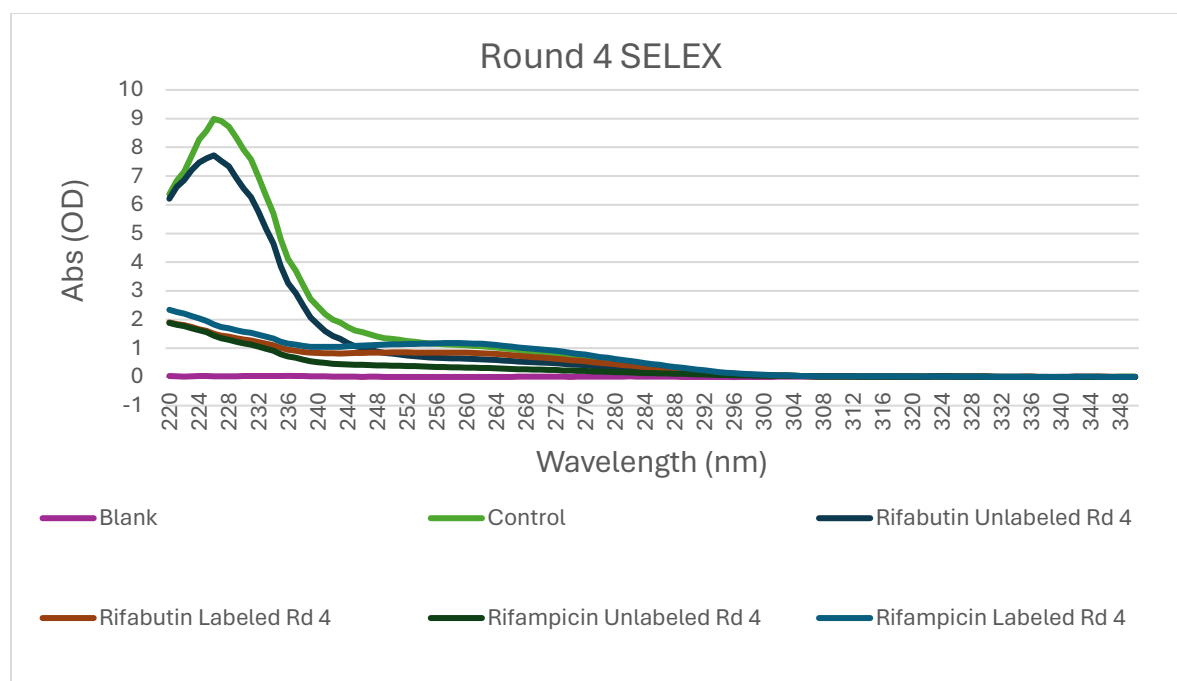
Figure A 5. Round 4 of SELEX process for labeled and unlabeled (Counter SELEX) of Rifampicin and Rifabutin, along with the amplified 40-mer control.
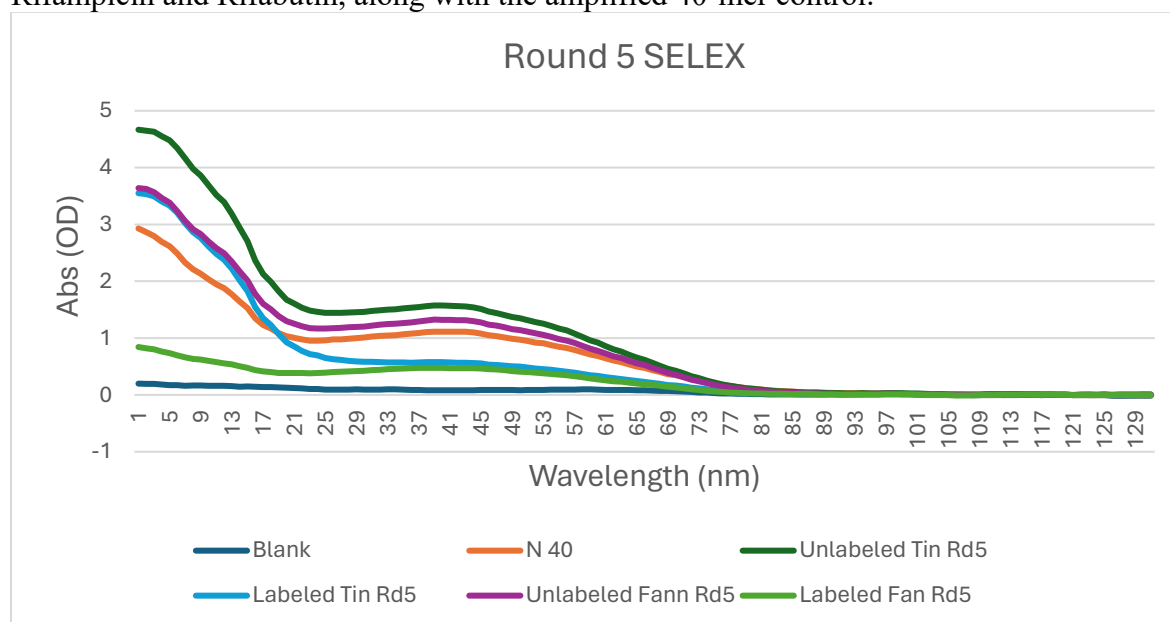
Figure A 6. Round 5 of SELEX process for labeled and unlabeled (Counter SELEX) of Rifampicin and Rifabutin, along with the amplified 40-mer control.
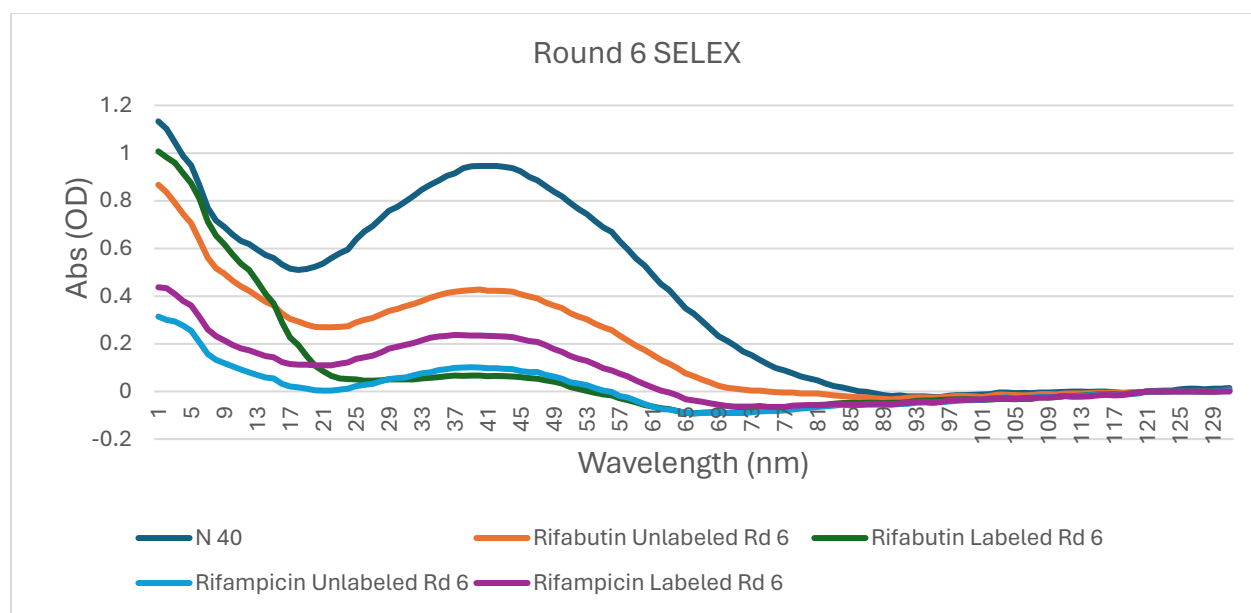
Figure A 7. Round 6 of SELEX process for labeled and unlabeled (Counter SELEX) of Rifampicin and Rifabutin, along with the amplified 40-mer control.
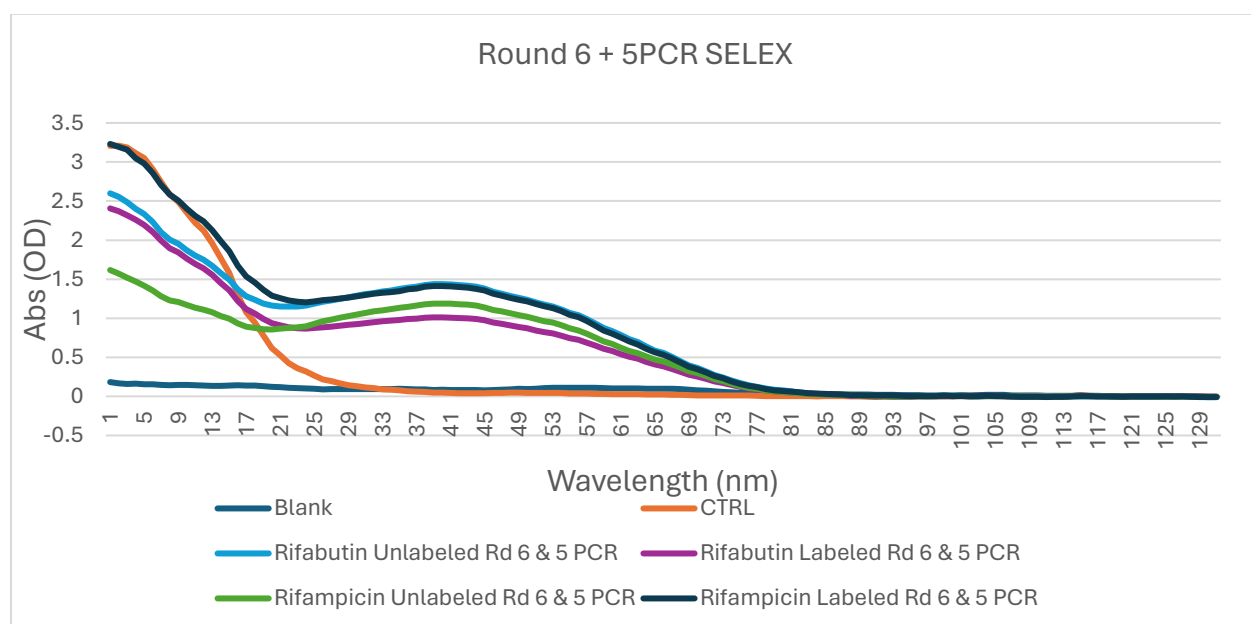
Figure A 8. Round 6 of the SELEX process plus 5 rounds of PCR amplification for labeled and unlabeled (Counter SELEX) Rifampicin and Rifabutin, along with the amplified 40-mer control.
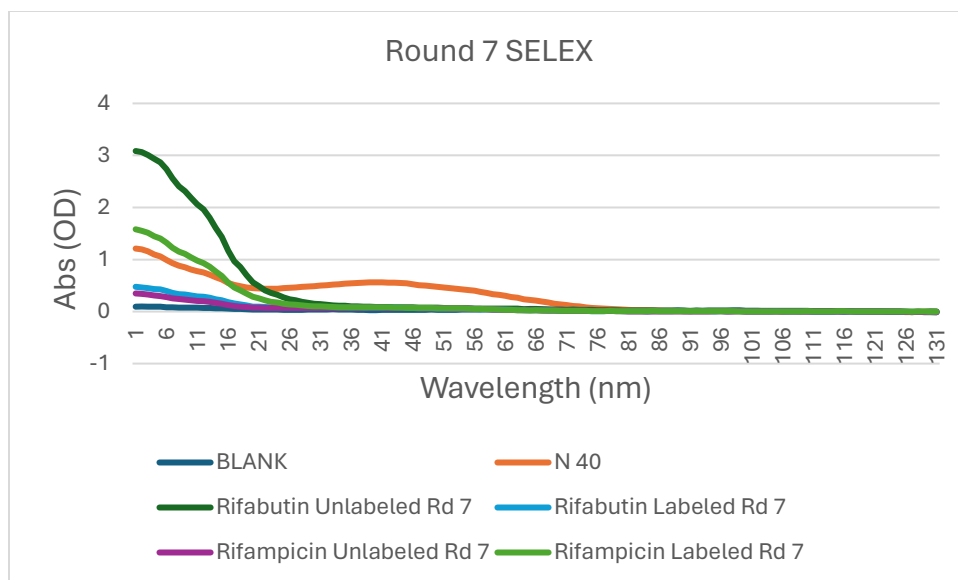
Figure A 9. Round 7 of SELEX process for labeled and unlabeled (Counter SELEX) of Rifampicin and Rifabutin, along with the amplified 40-mer control.
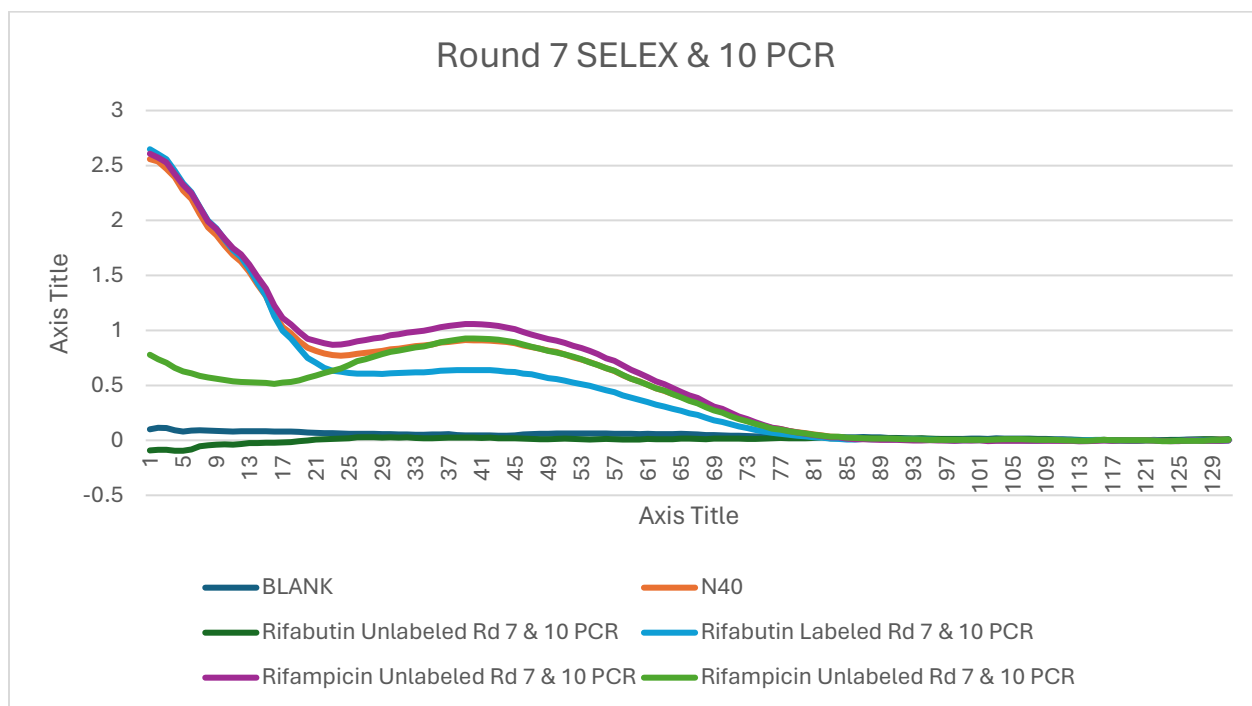
Figure A 10. Round 7 of the SELEX process plus 10 rounds of PCR amplification for labeled and unlabeled (Counter SELEX) Rifampicin and Rifabutin, along with the amplified 40-mer control.
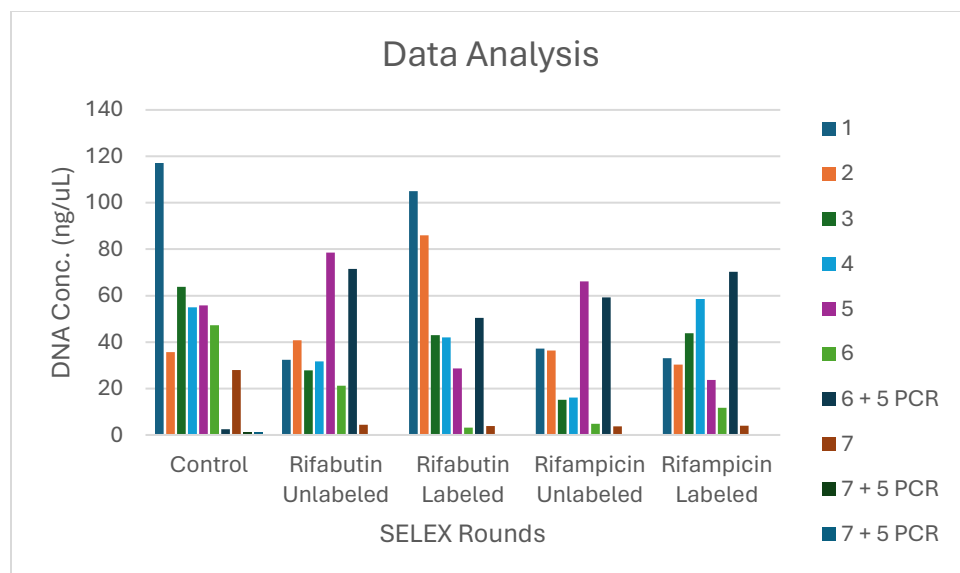
Figure A 11. SELEX rounds were conducted for various conditions, including Control, Rifampicin Labeled and Unlabeled, and Rifabutin Labeled and Unlabeled.

Table A 1. A breakdown of DNA concentrations for each SELEX round. If the DNA concentration is less than 10 ng/μL, the samples were amplified for an additional 5 to 10 PCR rounds.

Control (ng/μL)	Rifabutin Unlabeled (ng/μL)	Rifabutin Labeled (ng/μL)	Rifampicin Unlabeled (ng/μL)	Rifampicin Labeled (ng/μL)	Rounds
117.2	32.42	104.94	37.18	33.08	1
35.71	40.85	86.05	36.43	30.34	2
63.74	27.83	43.01	15.16	43.75	3
54.98	31.66	42.08	16.17	58.52	4
55.74	78.56	28.64	66.08	23.67	5
47.28	21.15	3.21	4.85	11.66	6
2.44	71.56	50.41	59.29	70.33	6 + 5 PCR
27.97	4.43	3.83	3.69	4.02	7
45.47	65.1	31.91	52.72	46.13	7 + 10 PCR

Conclusion

The series of seven SELEX rounds conducted under varying conditions, encompassing

Control, Rifampicin Labeled and Unlabeled, and Rifabutin Labeled and Unlabeled settings, has

yielded insights on the reproducibility of the PCR assay. We have gained a deeper understanding

of the molecules and target interactions. These findings pave the way for future research aimed at refining and optimizing selection processes, as well as potentially uncovering novel applications for these molecules. Overall, this experimentation has contributed to the advancement of the SELEX method and holds promise for further advancements in aptamer development.

Appendix B. Additional peptides

Background

When subjected to UV light irradiation, the combination of tryptophan (W) and azobenzene (Z), synthesized through solid-phase peptide synthesis (SPPS), displayed a visibly red-shift in fluorescence. The red shift in fluorescence emission indicates a change in the electronic structure or environmental conditions surrounding the fluorophore. A range of compounds were synthesized to explore the influence of the aromatic ring in tryptophan on the photoswitchable properties of the molecule azobenzene. These synthesized compounds integrated alanine as a spacer between the W and Z moieties. The aim was to explore the influence of the aromatic ring moiety. Remarkably, it was noted that peptides containing as many as six alanine residues still demonstrated visible fluorescence, characterized by a red-shift, upon exposure to UV light irradiation. Furthermore, the impact of Solid-Phase Peptide Synthesis (SPPS) was investigated by preparing individual compounds at a concentration of 1 mg/mL. Interestingly, these compounds did not exhibit visible fluorescence upon irradiation with UV light.

Samples and Discussion

A series of samples were prepared: FMOC-tryptophan, L-tryptophan, FMOC-tryptophan & azobenzene, and L-tryptophan & azobenzene. All the samples shown in Figure B 1 were prepared using 50% of 200 Proof ethanol at a 1 mg/mL concentration. Azobenzene and tryptophan were prepared at a concentration of 0.5 mM, and 1000 μL of each reagent was combined and subsequently analyzed using the nanodrop spectrophotometer. The samples were irradiated for 80 minutes and analyzed. According to the data, there was no change in absorbance observed when tryptophan (W) was irradiated with UV light. However, both azobenzene (Z) and the combination

of both (W + Z) exhibited a change in absorbance without displaying visible fluorescence or red-shifted emission, as illustrated in Figures B 2 to B 6.
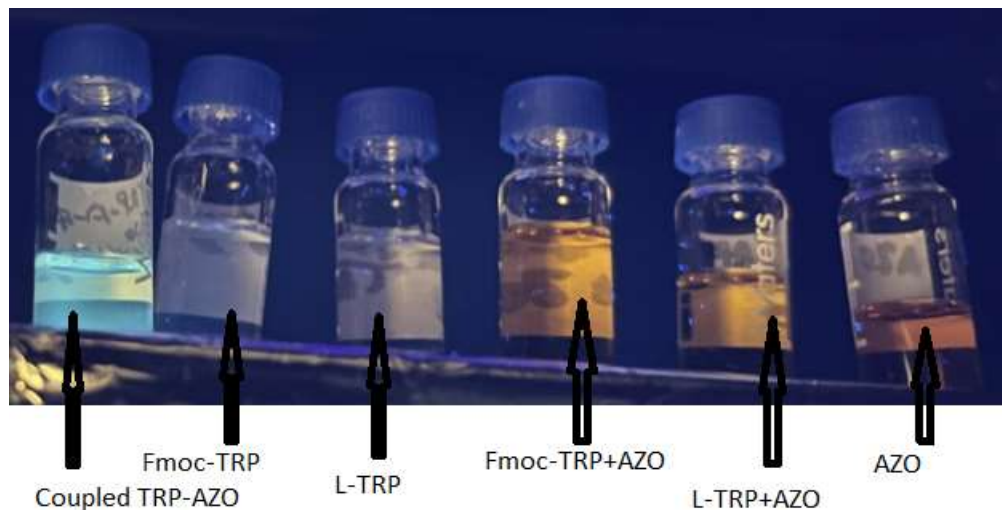
Figure B 1. FMOC-tryptophan, L-tryptophan, FMOC-tryptophan & azobenzene, and L-tryptophan & azobenzene did not exhibit visible fluorescence, unlike the WZ produced by SPPS.
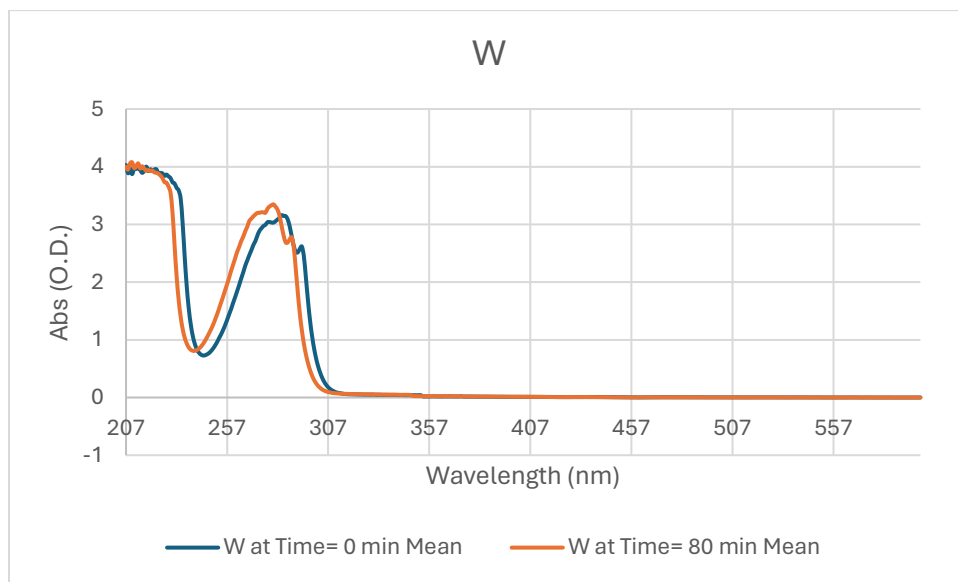
Figure B 2. Scan wavelength versus absorbance of Tryptophan (w) at 1 mg/mL, measured at an initial time, 0 minute, and after UV light irradiation at 80 minutes, n=3.
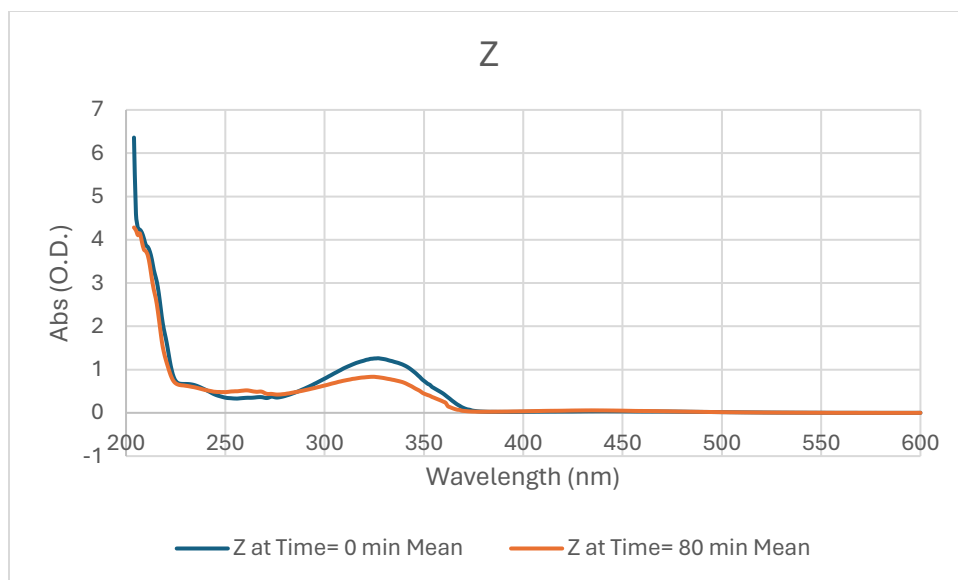
Figure B 3. Scan wavelength versus absorbance of Azobenzene (z) at 1 mg/mL, measured at an initial time, 0 minute, and after UV light irradiation at 80 minutes, n=3.
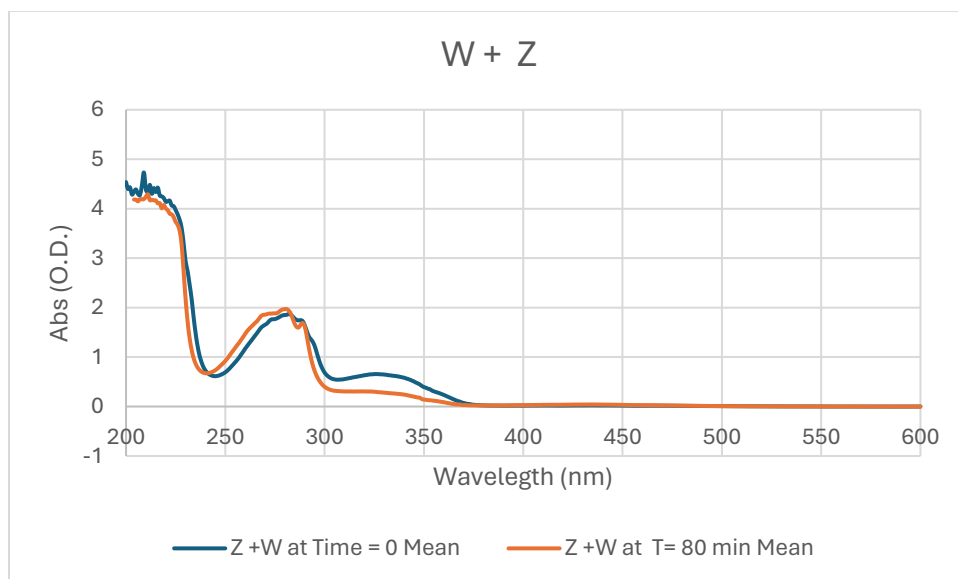
Figure B 4. Scan wavelength versus absorbance of combined W + Z at 1 mg/mL, measured at an initial time, 0 minute, and after UV light irradiation at 80 minutes, n=3.
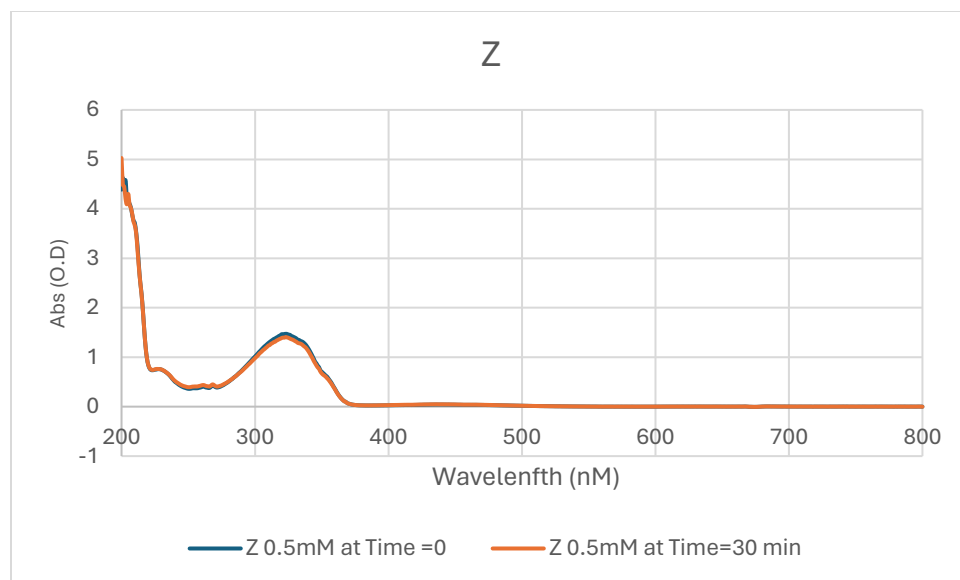
Figure B 5. Additional experiment of Scan wavelength versus absorbance of Azobenzene (z) measured at an initial time, 0 minute, and after UV light irradiation at 30 minutes.
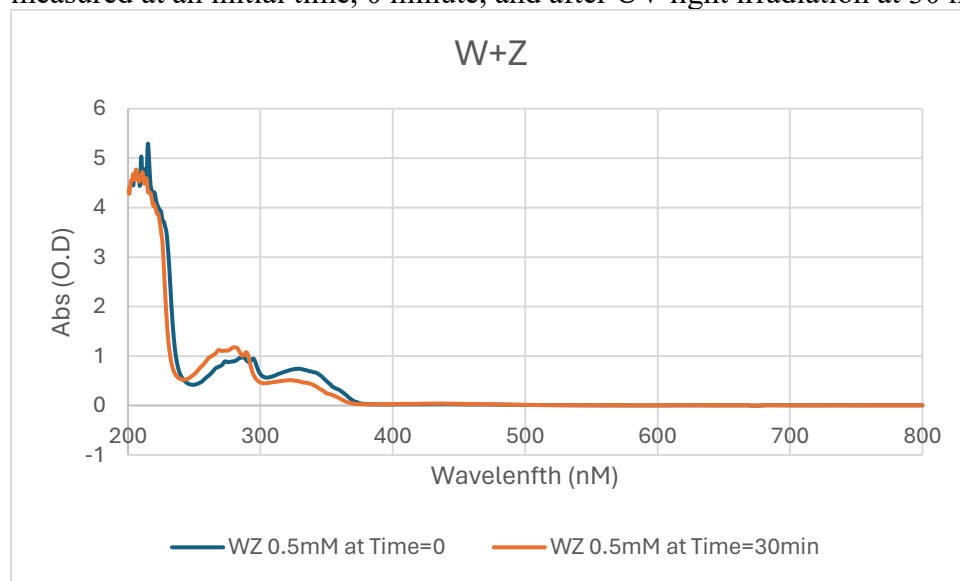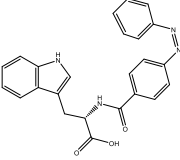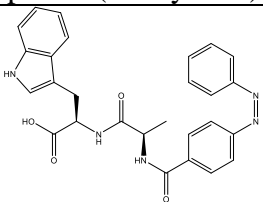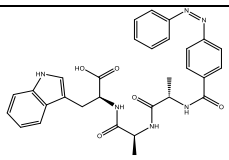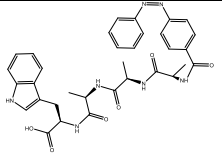
Figure B 6. Additional experiment of Scan wavelength versus absorbance of combined W + Z measured at an initial time, 0 minute, and after UV light irradiation at 30 minutes.
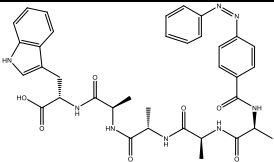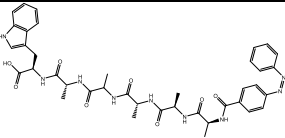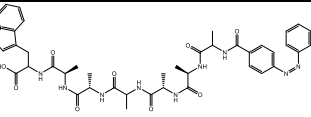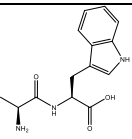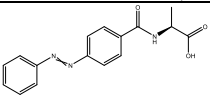
Under the same conditions, exposure to UV light, Azobenzene, and L-tryptophan remained unchanged. However, a shift in Förster Resonance Energy Transfer (FRET) was observed during the trans-to-cis isomerization of the Azobenzene and Tryptophan solution when irradiated with UV light. Additionally, in the combined solution, the peak intensity for Azobenzene decreased while

that of Tryptophan increased, suggesting alterations in fluorescence properties induced by their interaction.

Table B 1 presents the molecular structures, masses, and fluorescence states of the nine (9) peptides produced using Solid-Phase Peptide Synthesis (SPPS). Correspondingly, Figure B 7 illustrates the samples when irradiated with UV light, providing a visual representation of their fluorescence properties.

Table B 1. The molecular structures, masses, and fluorescence states of the nine (9) peptides synthesized utilizing SPPS.

#	Peptides Structure	Mass (g/mol)	Fluorescent When irradiated with UV light (Yes/No)
a.	Tryptophan-4(PhenylAzo)benzoic Acid (WZ)	412.15	Yes
b.	Tryptophan- Alanine-4(PhenylAzo)benzoic Acid (WAZ)	483.19	Yes
c.	Tryptophan- Alanine-Alanine-4(PhenylAzo)benzoic Acid (WAAZ)	554.23	Yes
d.	Tryptophan- Alanine-Alanine- Alanine-4(PhenylAzo)benzoic Acid (WAAAZ)	625.26	Yes

e.	 Tryptophan- Alanine-Alanine- Alanine- Alanine-4(PhenylAzo)benzoic Acid (WAAAAZ)	696.30	Yes
f.	 Tryptophan- Alanine-Alanine- Alanine- Alanine-Alanine-4(PhenylAzo)benzoic Acid (WAAAAAZ_	739.32	Yes
g.	 Tryptophan- Alanine-Alanine- Alanine- Alanine-Alanine- Alanine-4(PhenylAzo)benzoic Acid (WAAAAAAZ	838.38	Yes
h.	 Tryptophan-Alanine (WA)	275.13	No
i.	 Alanine-4(PhenylAzo)benzoic Acid (AZ)	297.11	No
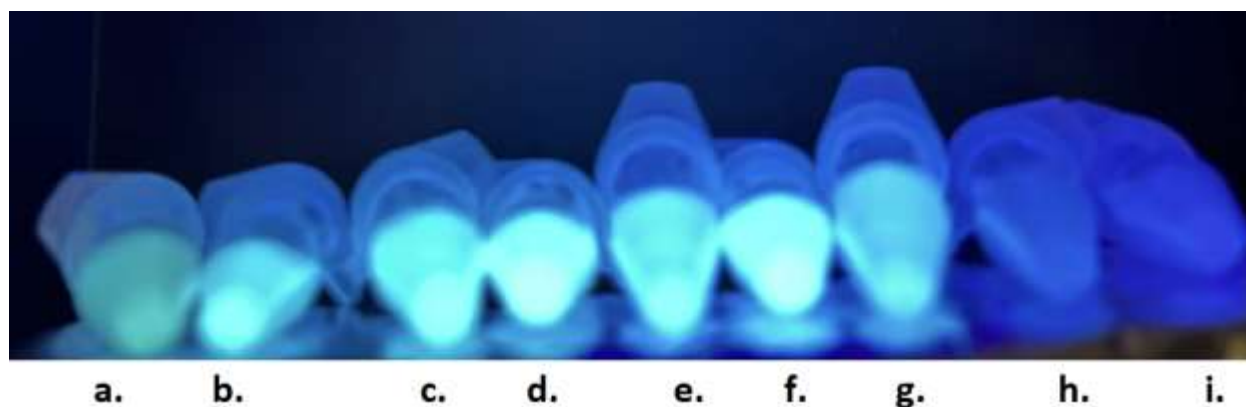
Figure B 7. Samples a. to i. correlate with the samples in Table B 1. This represents the fluorescence properties of the samples when irradiated with UV light.

Figure B 8. Additional images showcasing peptides WZ and WAZ under UV light for enhanced visualization.

Table B 2. Spectrofluorometer Parameters used to generate results for the peptides.

Plate area		A1-A11;B1-B12;C1-C6;C8
Mode	Fluorescence Intensity Scan Top Reading	
Name	Amino Acid Azo Study 071622	
Scan selection		Emission Scan
Excitation		Monochromator
Excitation wavelength		280 nm
Excitation bandwidth		7.5 nm
Emission wavelength start		300 nm
Emission wavelength end		500 nm
Emission wavelength step size		2 nm
Emission scan number		101
Emission bandwidth		5 nm
Gain		100 Manual
Mirror		Automatic (50% Mirror)
Number of flashes		30
Integration time		40 µs
Lag time		0 µs
Settle time		0 ms
Z-Position		34324 µm
Z-Position mode		Manual
Part of Plate		A1-A11;B1-B12;C1-C6;C8
Start Time		2022-07-16 12:34:10
Temperature		23.9 °C
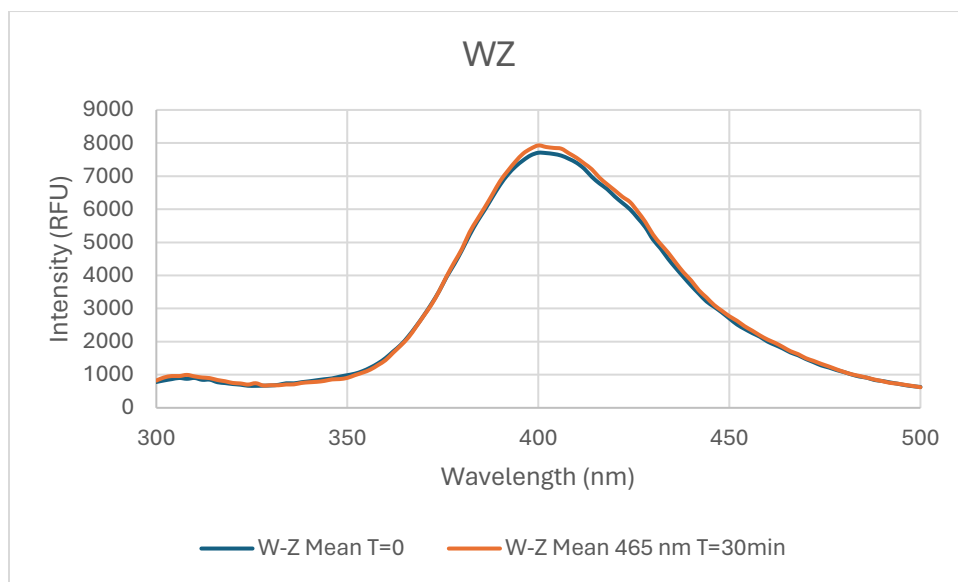
Figure B 9. Spectrofluorometer results: Scan wavelength versus Intensity, Relative Fluorescence Unit (RFU) of WZ peptide measured at initial time, 0 minute, and after incubate with blue light (466 nm) at 30 minutes, n=3.
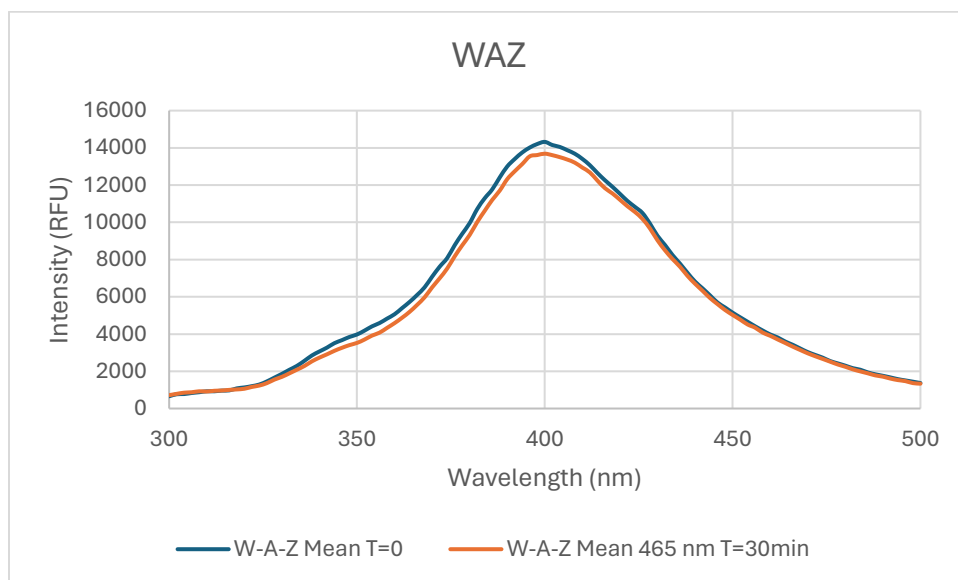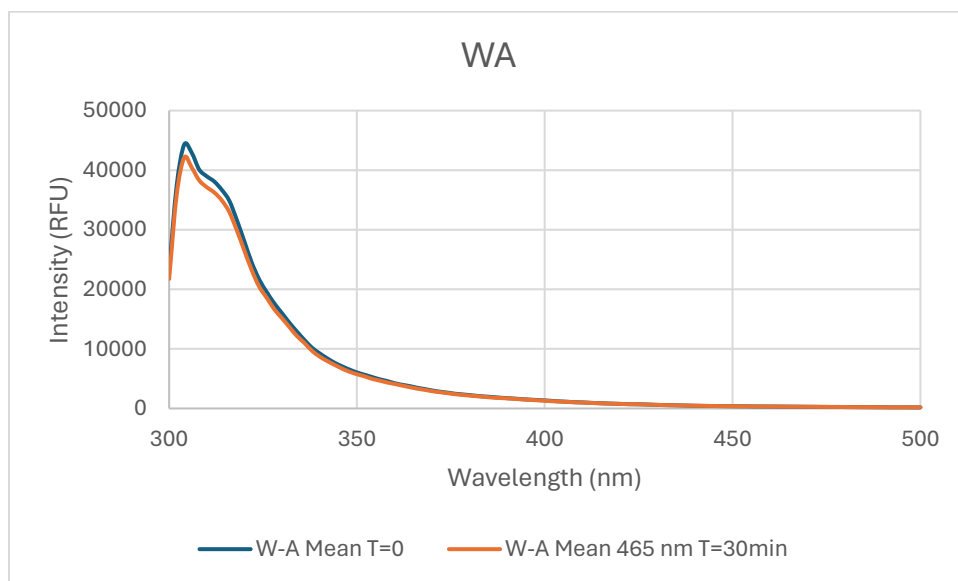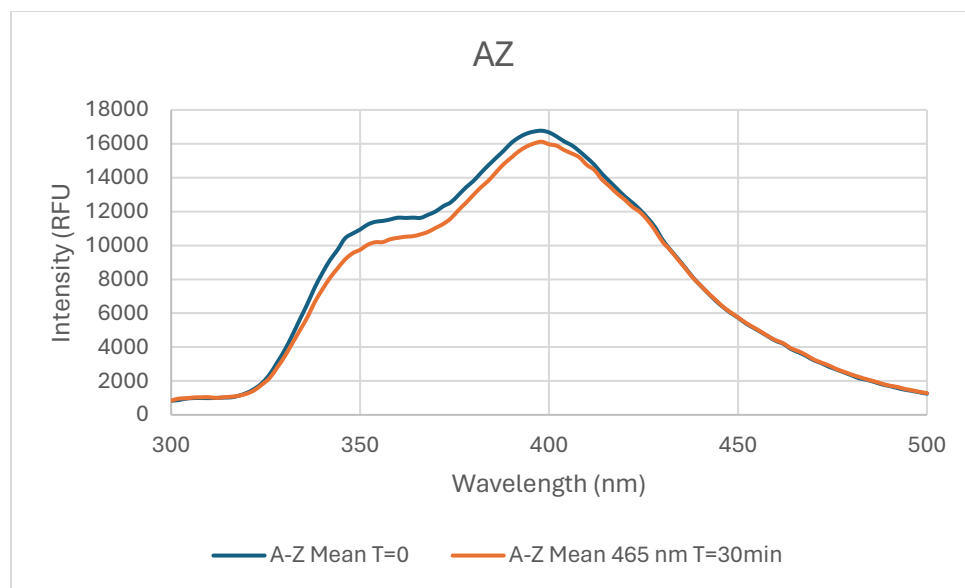

Figure B 10. Spectrofluorometer results: Scan wavelength versus Intensity, Relative Fluorescence Unit (RFU) of WAZ peptide measured at initial time, 0 minute, and after incubate with blue light (466 nm) at 30 minutes, n=3.
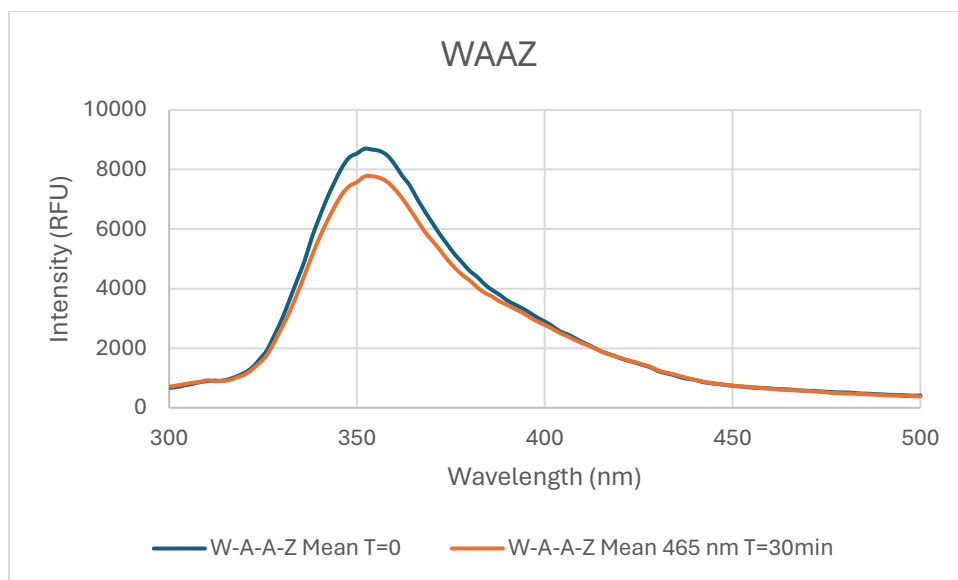
Figure B 11. Spectrofluorometer results: Scan wavelength versus Intensity, Relative Fluorescence Unit (RFU) of WAAZ peptide measured at initial time, 0 minute, and after incubate with blue light (466 nm) at 30 minutes, n=3.
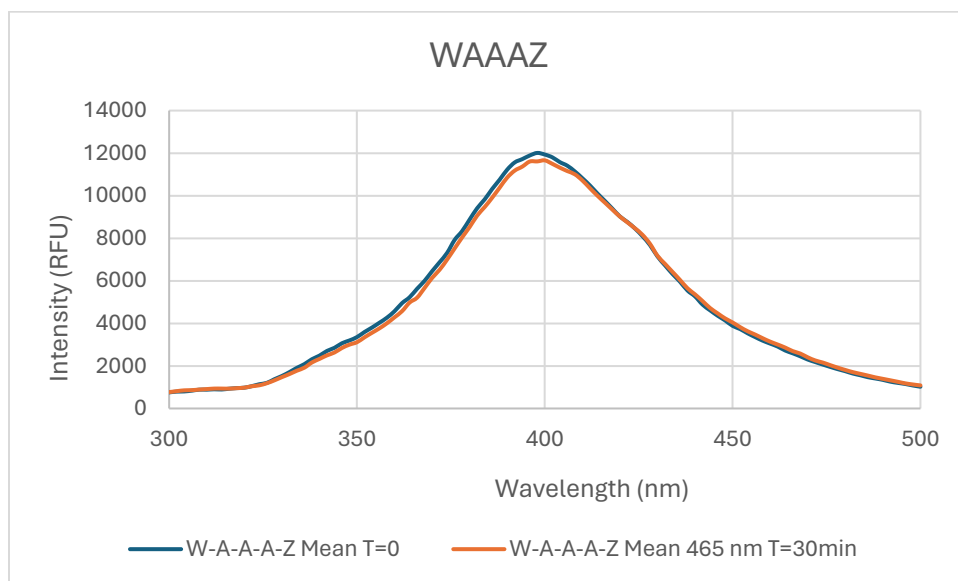
Figure B 12. Spectrofluorometer results: Scan wavelength versus Intensity, Relative Fluorescence Unit (RFU) of WAAAZ peptide measured at initial time, 0 minute, and after incubate with blue light (466 nm) at 30 minutes, n=3.
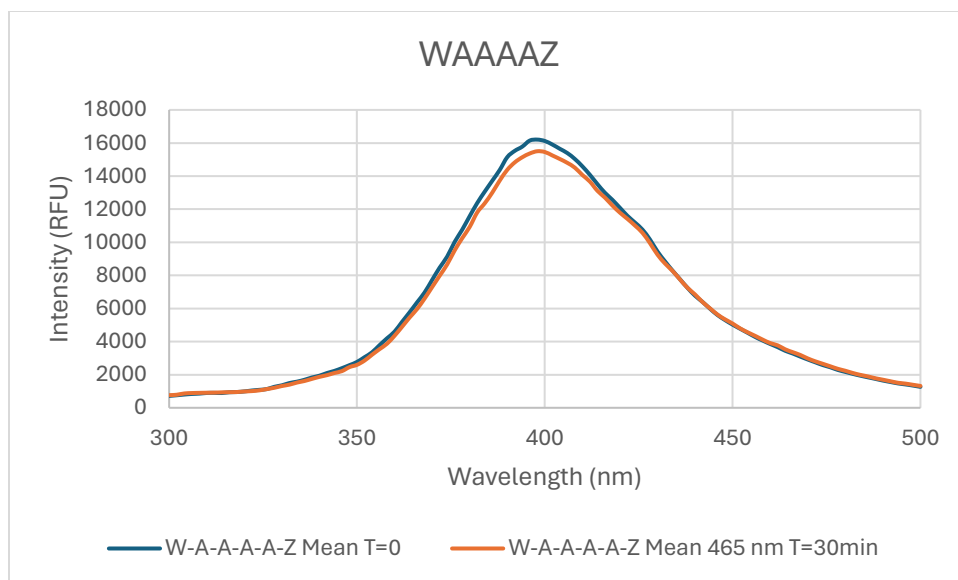
Figure B 13. Spectrofluorometer results: Scan wavelength versus Intensity, Relative Fluorescence Unit (RFU) of WAAAAZ peptide measured at initial time, 0 minute, and after incubate with blue light (466 nm) at 30 minutes, n=3.
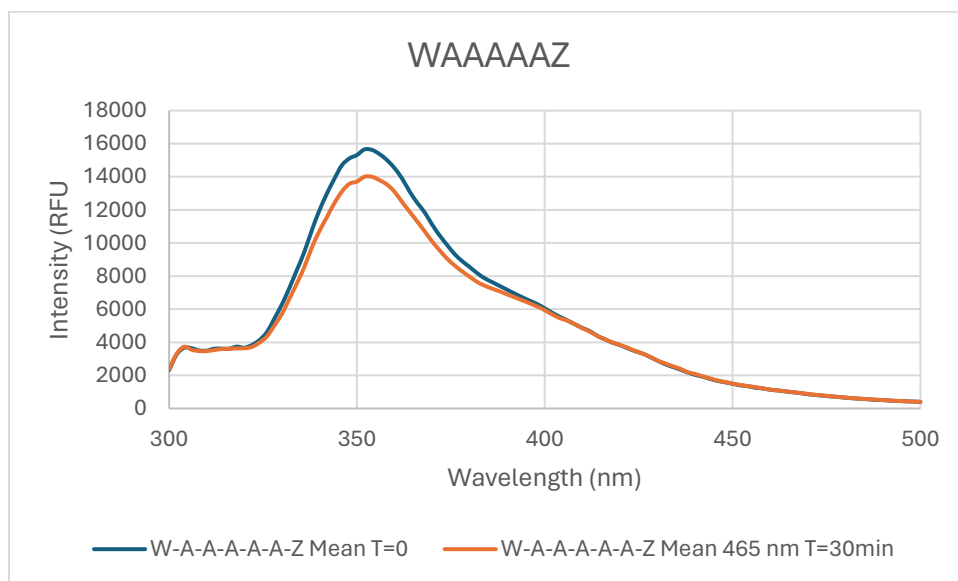
Figure B 14. Spectrofluorometer results: Scan wavelength versus Intensity, Relative Fluorescence Unit (RFU) of WAAAAAZ peptide measured at initial time, 0 minute, and after incubate with blue light (466 nm) at 30 minutes, n=3.
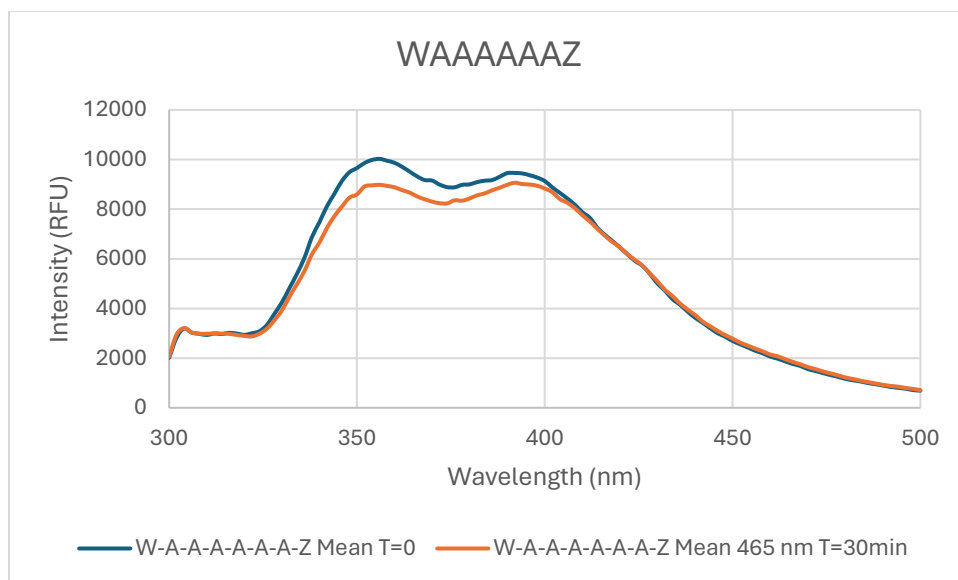
Figure B 15. Spectrofluorometer results: Scan wavelength versus Intensity, Relative Fluorescence Unit (RFU) of WAAAAAAZ peptide measured at initial time, 0 minute, and after incubate with blue light (466 nm) at 30 minutes, n=3.

Figure B 16. Spectrofluorometer results: Scan wavelength versus Intensity, Relative Fluorescence Unit (RFU) of WA peptide measured at initial time, 0 minute, and after incubate with blue light (466 nm) at 30 minutes, n=3.

Figure B 17. Spectrofluorometer results: Scan wavelength versus Intensity, Relative Fluorescence Unit (RFU) of AZ peptide measured at initial time, 0 minute, and after incubate with blue light (466 nm) at 30 minutes, n=3.
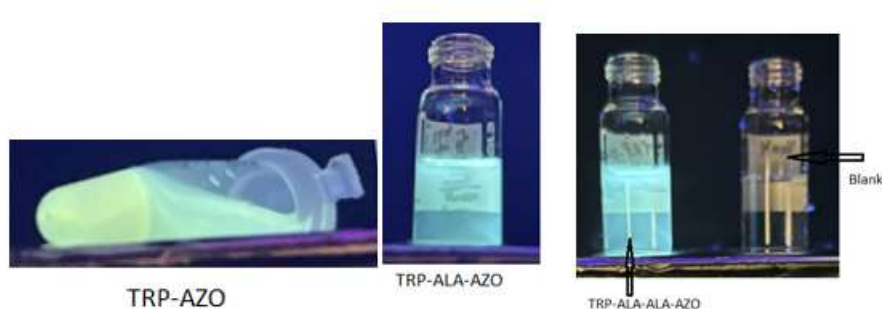
Figure B 18. Additional pictures of the samples produced from SPPS compared to blank sample.

These samples were analyzed using a plate reader, with an excitation wavelength of 280 nm and emission scanned from 300 nm to 500 nm, alongside other parameters detailed in Table B 2. Subsequently, the plate was incubated at 465 nm for 10 minutes, and subsequent analysis was performed using the same parameters, as shown in Figures B 9 to B 18. These experiments provided insights into the photo-switching behavior of the synthesized compounds and their potential applications in various fields.

HPLC Data

The analytical HPLC system, Shimadzu Nexera-i LC2040c, equipped with a photodiode array detector (PDA), utilized a Phenomenex Hypersil 5 μm ODS (C18) 120Å, 125 x 4 mm LC Column as the stationary phase was used to assess the purity of the peptides. Peptide concentrations of 1 mg/mL were diluted in a solvent mixture of 50% acetonitrile containing 0.1% formic acid (FA) and 50% water containing 0.1% FA. Experiments were conducted at a flow rate of 1 mL/min with injection volumes of 10 μL. A gradient elution method was employed, ranging from 5% to 95% of water containing 0.1% FA and acetonitrile containing 0.1% FA. Chromatographic data were collected using the PDA detector over a spectral range of 200 to 456 nm. The chromatograms were specifically analyzed at 220 nm, 280 nm, and 320 nm. The chromatograms in the Figures are displayed at 220 nm since tryptophan, an aromatic amino acid with a conjugated ring system, displays distinctive absorption around this wavelength owing to its intrinsic UV-absorbing properties. The data are depicted in Figures B 19 to B 27.
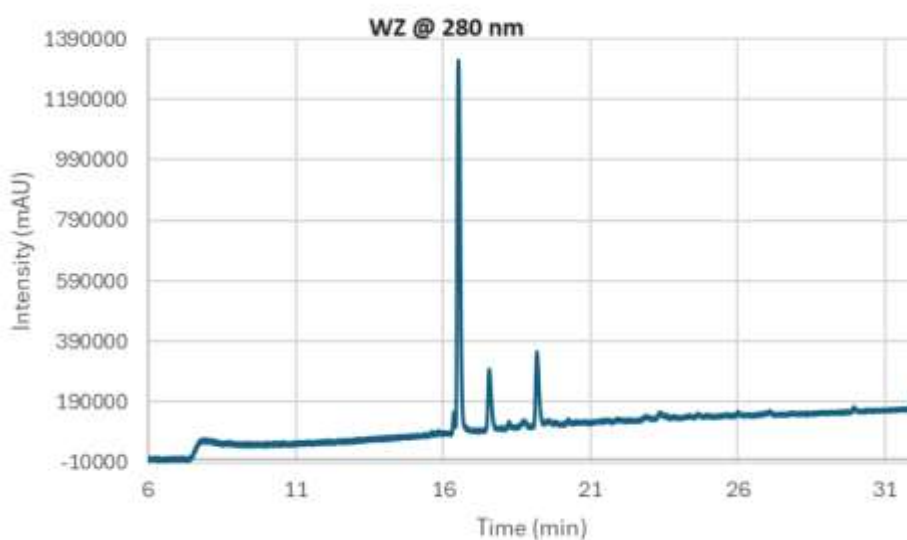
Figure B 19. Chromatogram of the WZ peptide at 280 nm
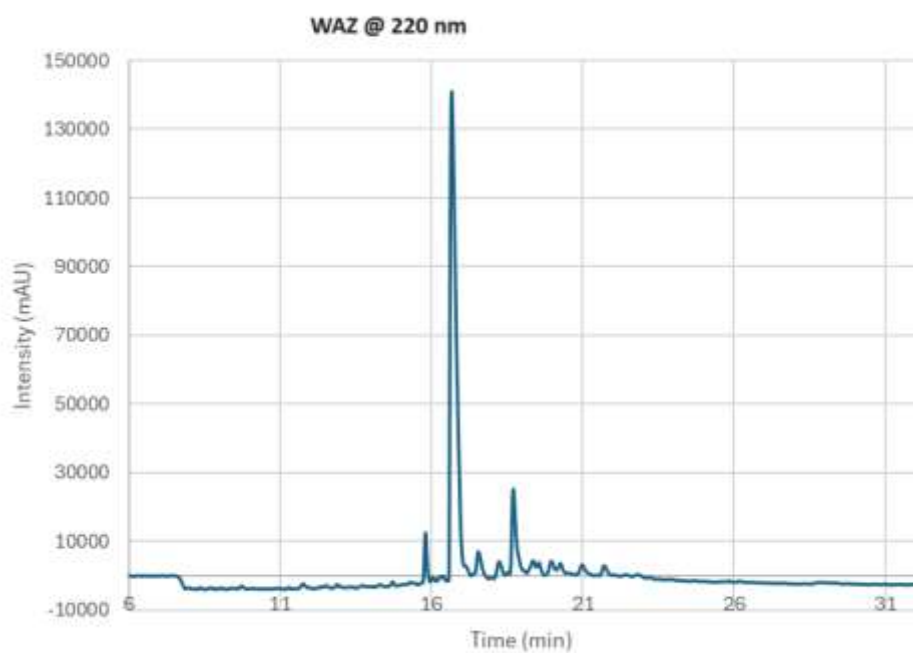
Figure B 20. Chromatogram of the WAZ peptide at 220 nm
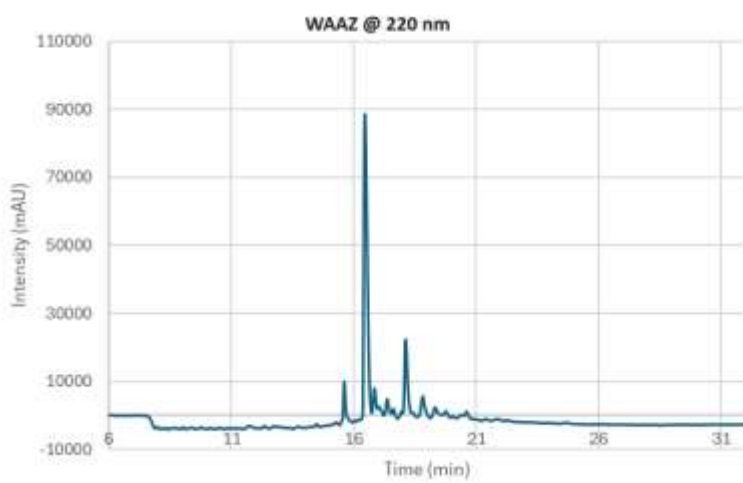
Figure B 21. Chromatogram of the WAAZ peptide at 220 nm
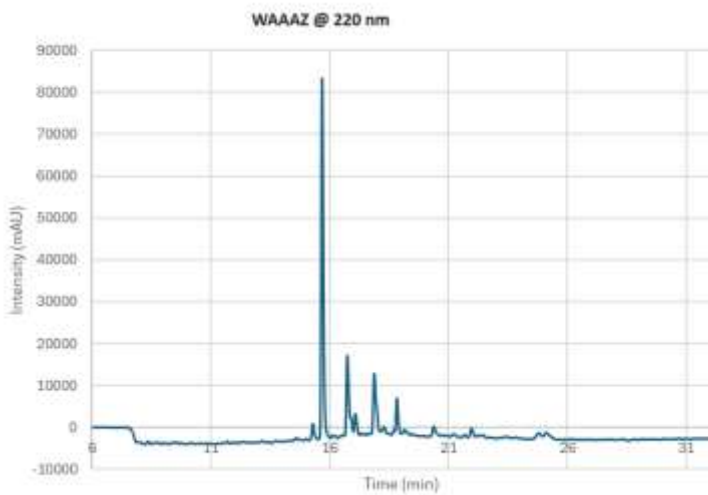
Figure B 22. Chromatogram of the WAAAZ peptide at 220 nm
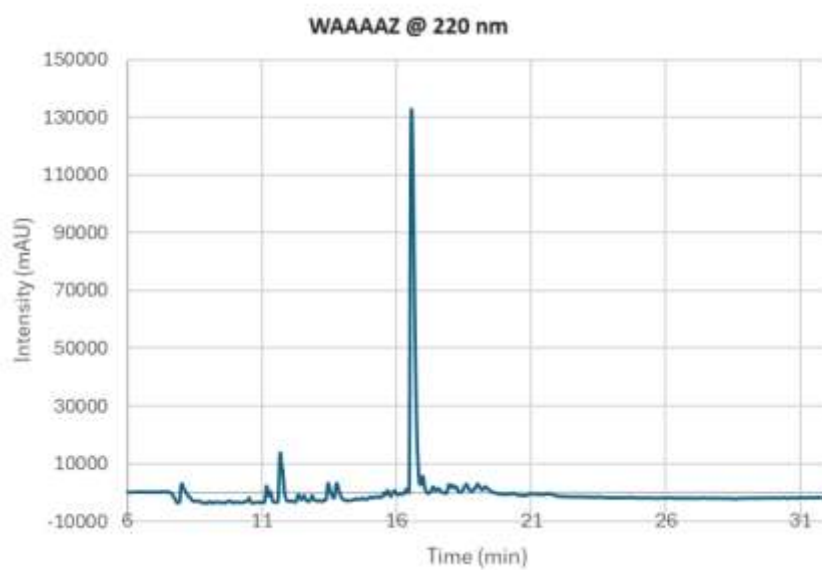
Figure B 23. Chromatogram of the WAAAAZ peptide at 220 nm
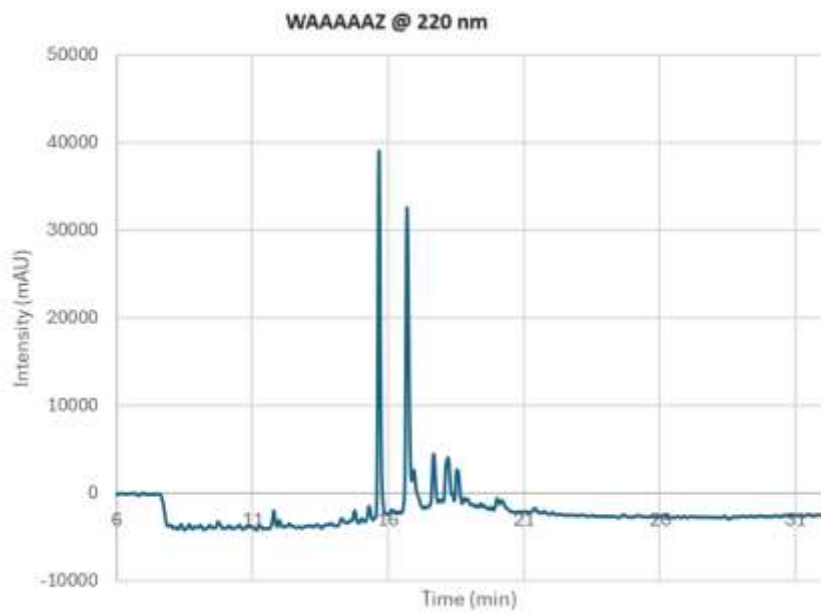
Figure B 24. Chromatogram of the WAAAAAZ peptide at 220 nm
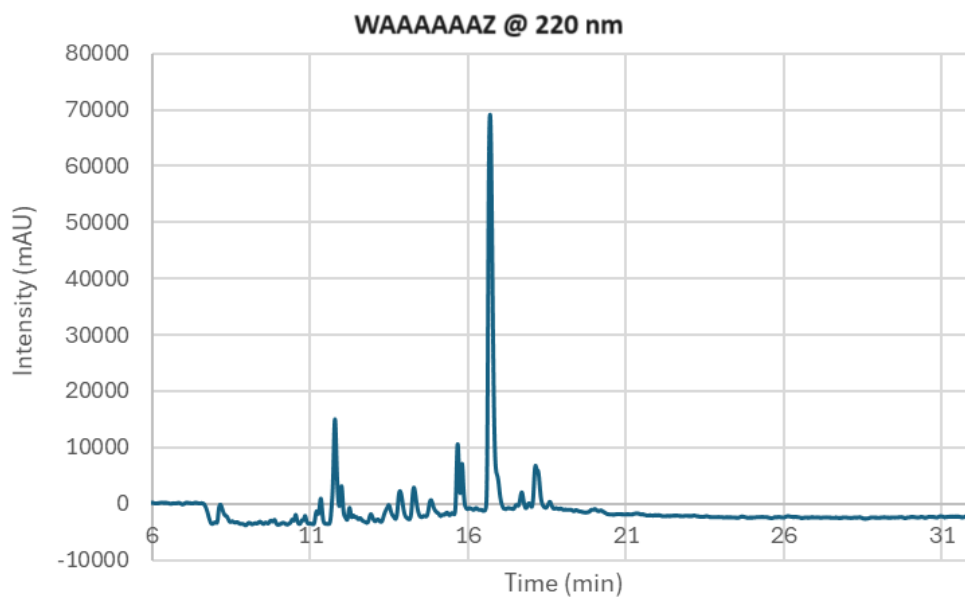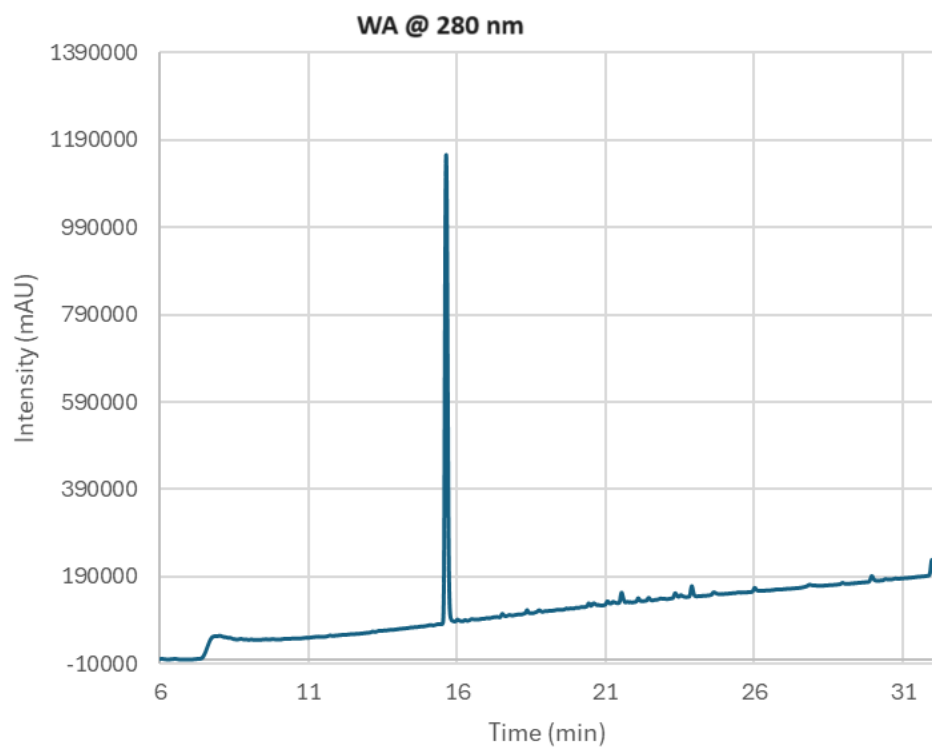

Figure B 25. Chromatogram of the WAAAAAAZ peptide at 220 nm
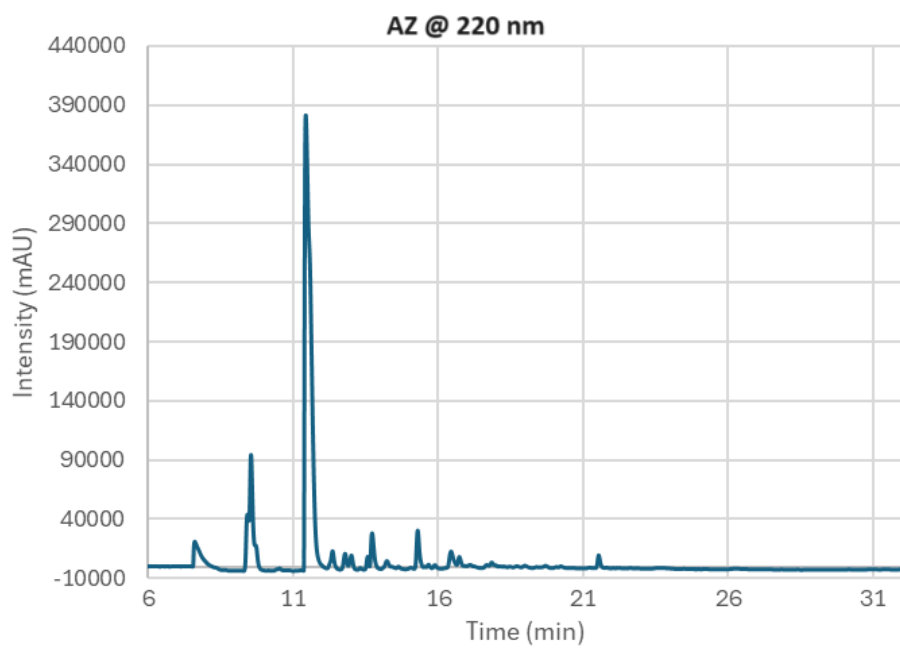
Figure B 26. Chromatogram of the WA peptide at 280 nm

Figure B 27. Chromatogram of the AZ peptide at 220 nm

The Hewlett Packard 1100 MSD Electrospray Mass Spectrometer was employed for analysis. Peptides were prepared at a concentration of 1 mg/mL, diluted in a solvent mixture of 50% acetonitrile containing 0.1% formic acid (FA) and 50% water containing 0.1% FA. Direct injections of 10 μL were performed at flow rates of 0.5 mL/min. Peak deconvolution was carried out using the Chemstation software. The mass analyzer separates ions perpendicular to their primary motion axis according to their mass-to-charge ratio (m/z), facilitated by the interaction of the ions with a magnetic field. The data are shown in Figures B 28 to B 35.
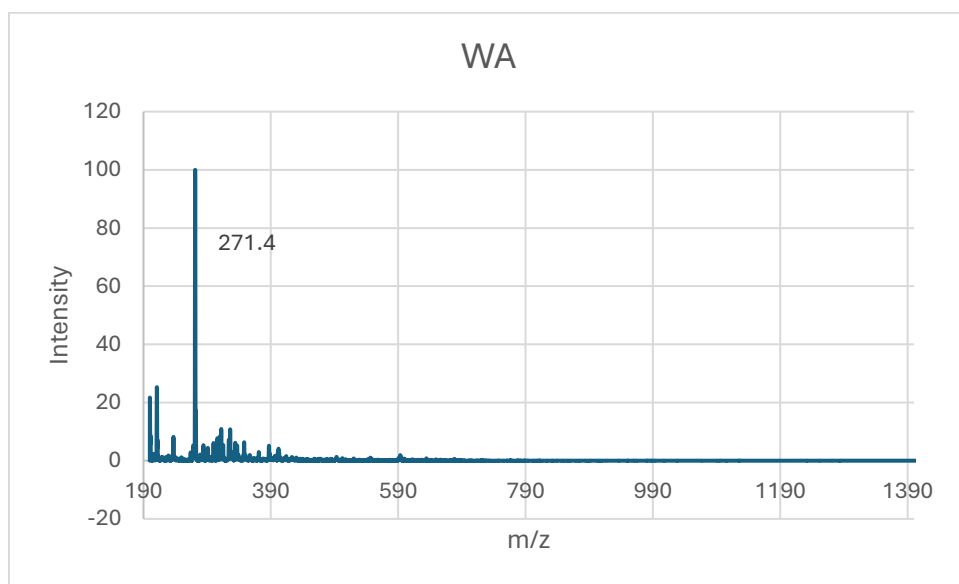
Figure B 28. Mass spectrometry analysis of the WA peptide
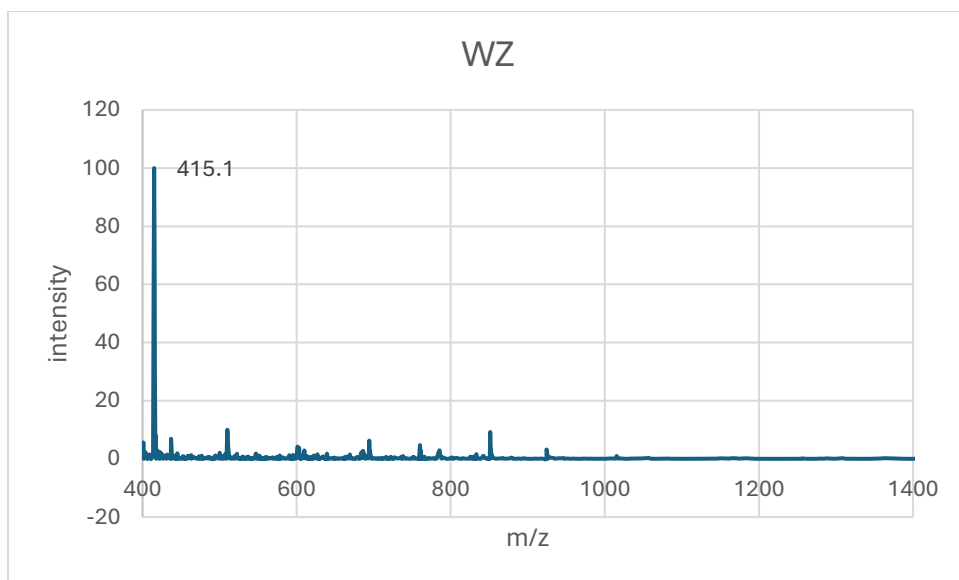
Figure B 29. Mass spectrometry analysis of the WZ peptide
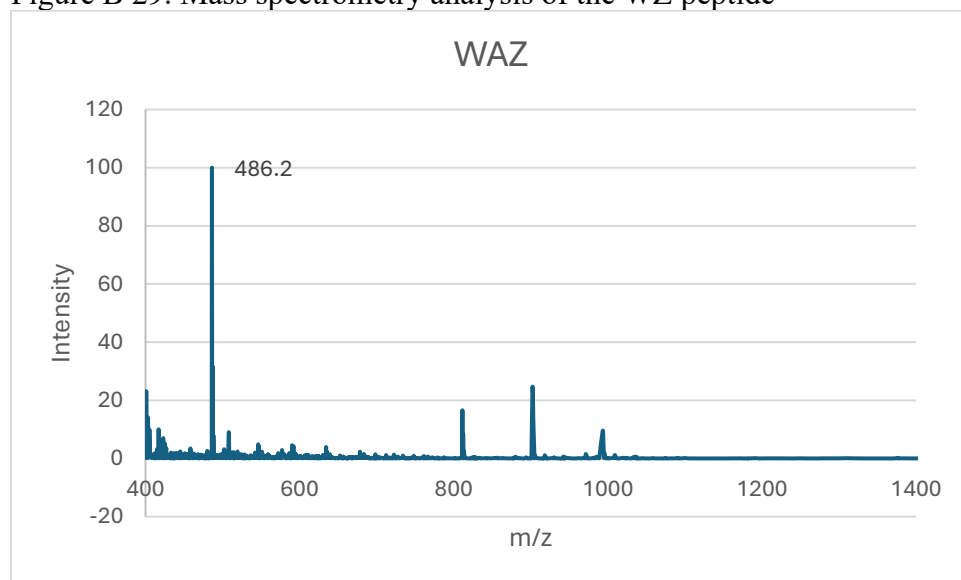
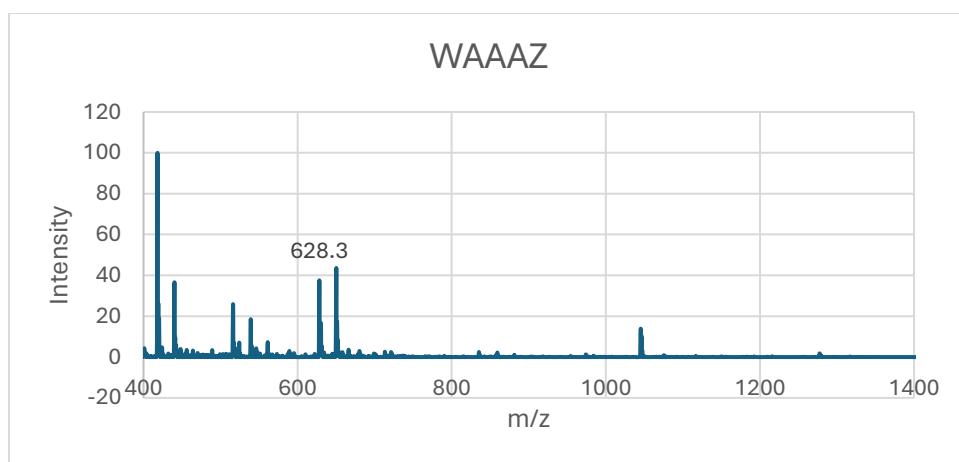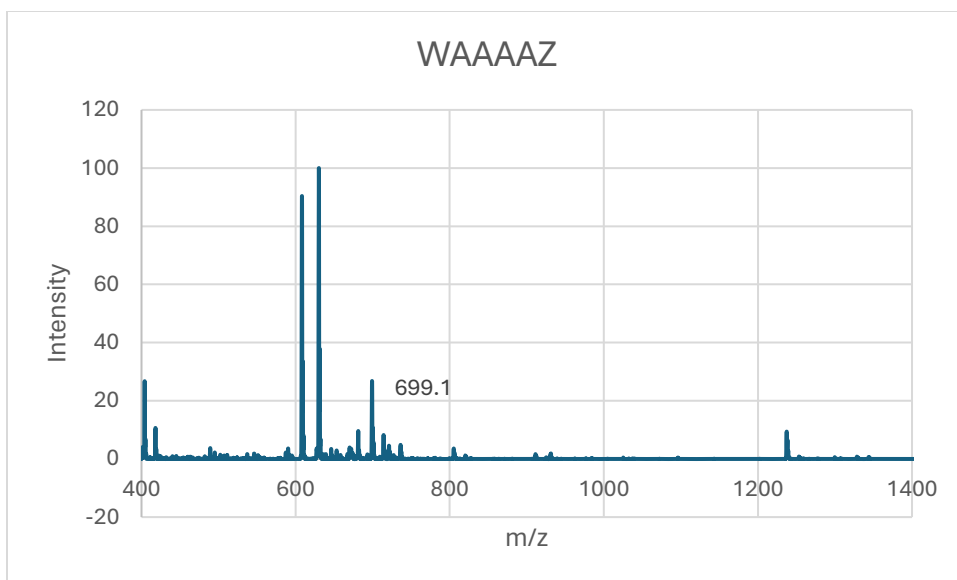**Figure B 30.** Mass spectrometry analysis of the WAZ peptide
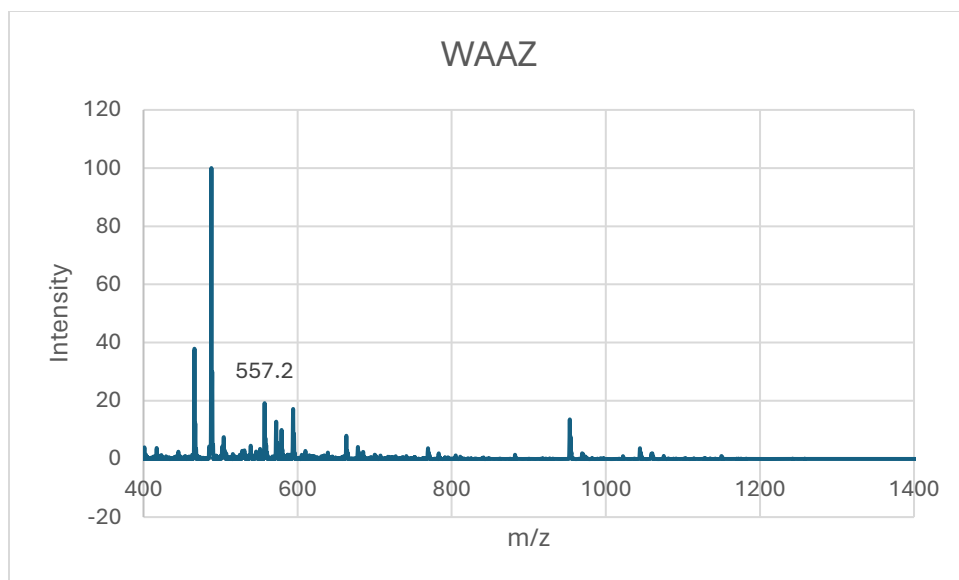
Figure B 31. Mass spectrometry analysis of the WAAZ peptide

Figure B 32. Mass spectrometry analysis of the WAAAZ peptide
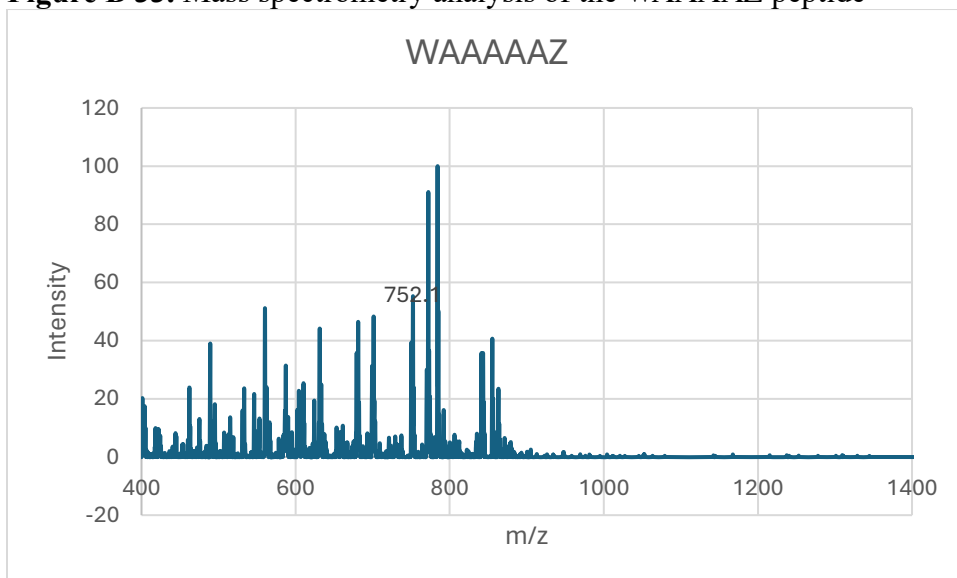
Figure B 33. Mass spectrometry analysis of the WAAAAZ peptide

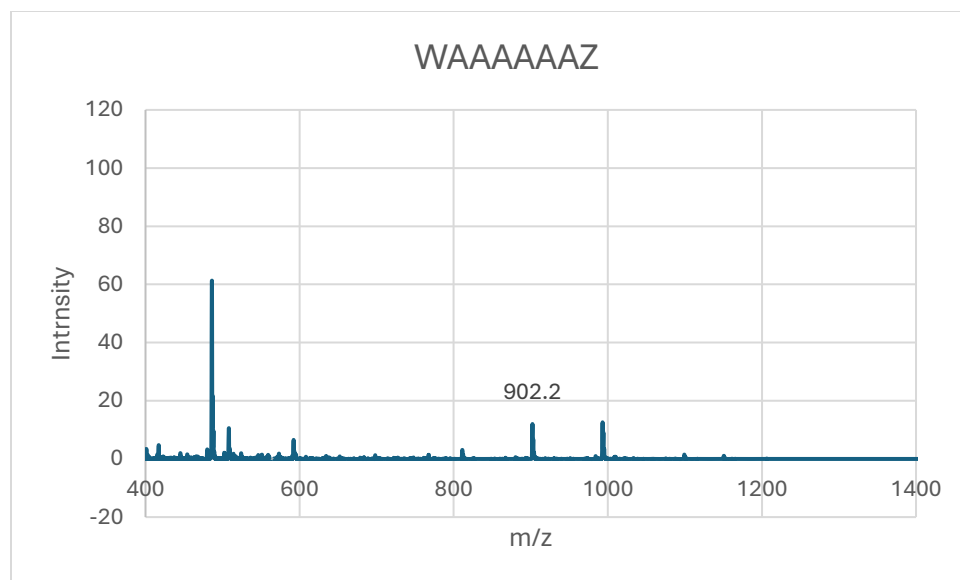**Figure B 34.** Mass spectrometry analysis of the WAAAAAZ peptide

Figure B 35. Mass spectrometry analysis of the WAAAAAAZ peptide

Nuclear Magnetic Resonance (NMR) spectroscopy is the analytical technique utilized to study molecular structure, dynamics, and interactions. It relies on the principle of nuclear spin alignment in a magnetic field and the subsequent absorption and emission of electromagnetic radiation by atomic nuclei, particularly hydrogen (^{1}H) and carbon (^{13}C) nuclei, which are prevalent in organic molecules[125]. In the context of peptides, NMR spectroscopy offers insights into their structural characteristics, including conformation, folding patterns, and interactions with other molecules. By observing the chemical shifts and coupling patterns of H nuclei within the peptide backbone and side chains, NMR provides information about the spatial arrangement of atoms and the flexibility of the peptide structure. The peptides, WZ and WAZ were subjected to NMR analysis, focusing on the behavior of hydrogen nuclei within the peptides.

Sample

For NMR spectroscopy experiments, the lyophilized peptides WZ and WAZ were dissolved in deuterated dimethyl sulfoxide (DMSO-d6), sourced from Acros Organics, with a purity of 99.9%. The data are depicted in Figures B 36 to B 39.
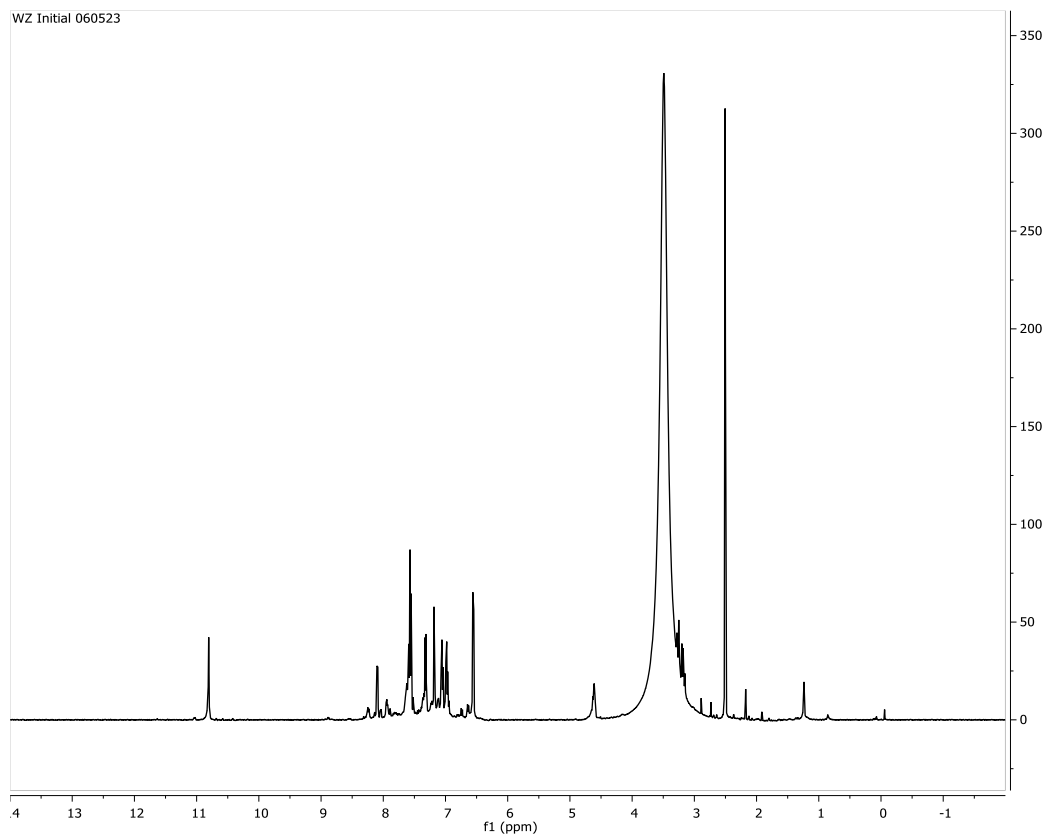

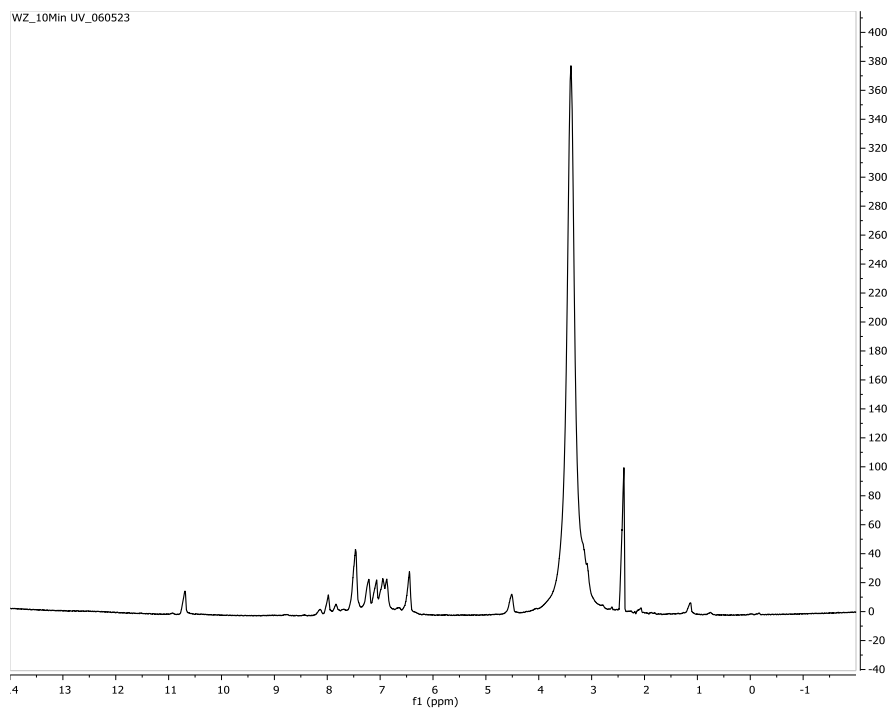**Figure B 36.** Initial condition ^{1}H NMR spectrum of the WZ peptide

Figure B 37. ^{1}H NMR spectrum of the WZ peptide, irradiated with UV light for10 minutes
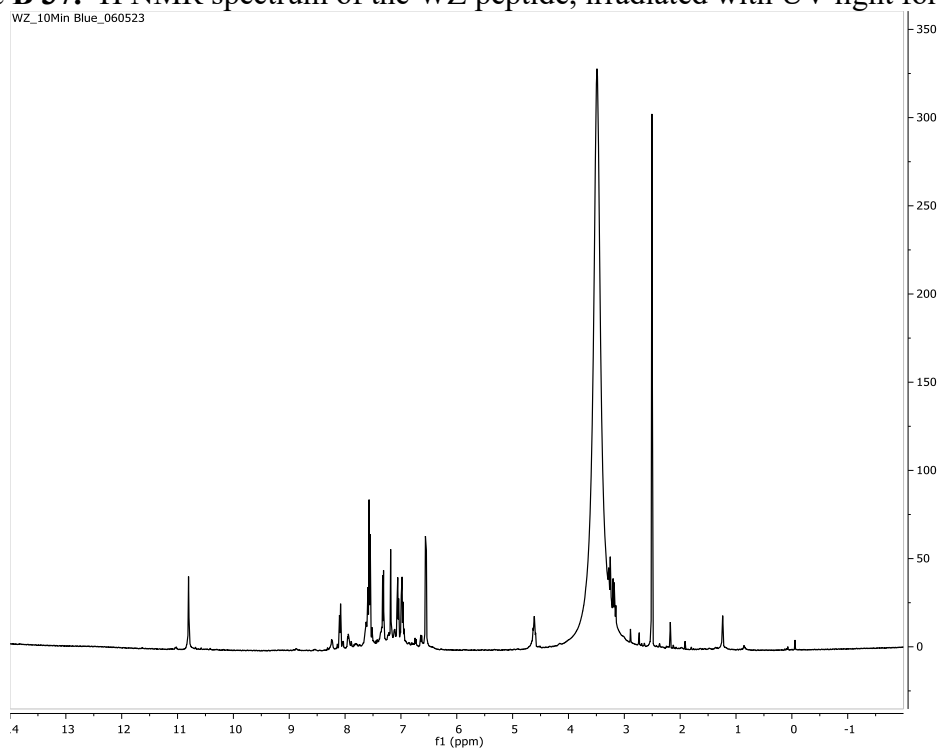

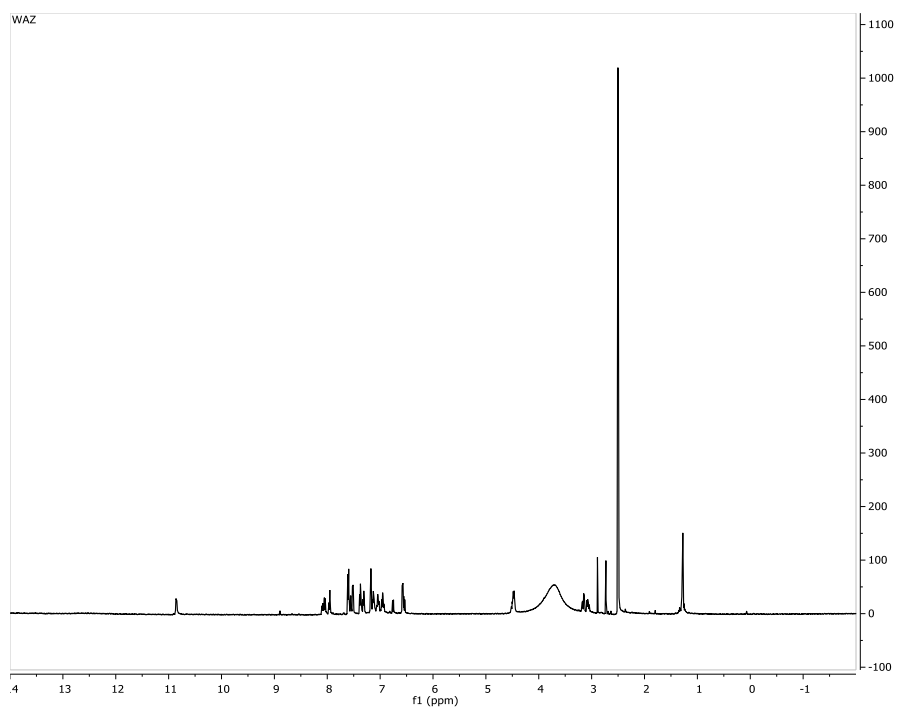**Figure B 38.** ^{1}H NMR spectrum of the WZ peptide, incubated with blue light (465 nm) for10 minutes

Figure B 39. ^{1}H NMR spectrum of the WAZ peptide